


5-2015

PHOSPHOTRANSACETYLASE AND XYLULOSE 5-PHOSPHATE/FRUCTOSE 6-PHOSPHATE PHOSPHOKETOLASE: TWO EUKARYOTIC PARTNERS OF ACETATE KINASE

Tonya Taylor
Clemson University, tonyaj@g.clemson.edu

Follow this and additional works at: https://tigerprints.clemson.edu/all_dissertations

 Part of the [Biochemistry Commons](#), [Genetics and Genomics Commons](#), and the [Microbiology Commons](#)

Recommended Citation

Taylor, Tonya, "PHOSPHOTRANSACETYLASE AND XYLULOSE 5-PHOSPHATE/FRUCTOSE 6-PHOSPHATE PHOSPHOKETOLASE: TWO EUKARYOTIC PARTNERS OF ACETATE KINASE" (2015). *All Dissertations*. 1523.
https://tigerprints.clemson.edu/all_dissertations/1523

This Dissertation is brought to you for free and open access by the Dissertations at TigerPrints. It has been accepted for inclusion in All Dissertations by an authorized administrator of TigerPrints. For more information, please contact kokeefe@clemson.edu.

PHOSPHOTRANSACETYLASE AND XYLULOSE 5-PHOSPHATE/FRUCTOSE 6-
PHOSPHATE PHOSPHOKETOLASE: TWO EUKARYOTIC PARTNERS OF
ACETATE KINASE

A Dissertation
Presented to
the Graduate School of
Clemson University

In Partial Fulfillment
of the Requirements for the Degree
Doctor of Philosophy
Biochemistry and Molecular Biology

by
Tonya Lanae Taylor
May 2015

Accepted by:
Kerry S. Smith, Committee Chair
William R. Marcotte, Jr.
James C. Morris
Meredith T. Morris
Lukasz Kozubowski

ABSTRACT

Although acetate is a predominant metabolite produced by many eukaryotic microbes, far less attention has been given to acetate metabolism in eukaryotes than in bacteria and archaea. Acetate kinase (Ack), which catalyzes the reversible phosphorylation of acetate from ATP, is a key enzyme in bacterial acetate metabolism. Ack primarily partners with phosphotransacetylase (Pta), which catalyzes the generation of acetyl phosphate from acetyl-CoA, but can also partner with xylulose 5-phosphate/fructose 6-phosphate phosphoketolase (Xfp), which produces acetyl phosphate from either xylulose 5-phosphate or fructose 6-phosphate. The Ack-Pta pathway, found primarily in bacteria, is also present in lower eukaryotes such as the green algae *Chlamydomonas reinhardtii* and the oomycete, *Phytophthora*. The Ack-Xfp pathway, which forms a modified pentose phosphoketolase pathway in heterofermentative bacteria, has been found in a number of ascomycete and basidiomycete fungi. Although bacterial and eukaryotic microbes possess these pathways, humans, animals and plants lack these enzymes, making this pathway a potential drug target in eukaryotic pathogens.

Two types of Ptas have previously been identified: Pta^I and Pta^{II}. Pta^{II} enzymes have an N-terminal regulatory domain that the Pta^I enzymes lack. Through sequence analysis, we identified four subtypes, IIa, IIb, IIc, and IId, of the Pta^{II} enzymes based on the presence or absence of two N-terminal subdomains. Here we describe the first biochemical characterization of a eukaryotic Pta, the *Phytophthora ramorum* Type IIa Pta1 (PrPta1^{IIa}). Although the N-terminus of PrPta1^{IIa} shares only 19% amino acid identity with the N-terminus of the bacterial *Escherichia coli* and *Salmonella enterica* Pta^{IIa} enzymes, the effector molecules, ATP, NADH, PEP, and pyruvate, inhibit all three enzymes in the acetyl-CoA-forming direction; whereas, AMP differentially regulates PrPta1^{IIa} compared to SePta^{IIa}.

We hypothesize that Xfp-Ack would function as a modified pentose phosphoketolase pathway to produce acetate and ATP in the opportunistic, fungal pathogen *Cryptococcus neoformans*, which has two open reading frames, designated as Xfp1 and Xfp2, with sequence identity to Xfp. To investigate the metabolic and physiological role of the Ack-Xfp pathway in *C. neoformans*, we have generated single *XFP1*, *XFP2* and *ACK* knockouts, as well as a *XFP1/XFP2* double knockout. Our results indicate both Xfp1 and Xfp2 play a role in the survival of *C. neoformans* within macrophages, and that Ack and Xfp2 most likely partner together under low glucose and possibly low iron environments.

DEDICATION

I would like to dedicate this dissertation to my family:

Ian – I could have never accomplished this without you. Thank you for enduring the ups and downs of graduate school and life with me, and for the constant love and support.

Daddy and Momma: You have always taught me that hard work and dedication is the key to success. You also encouraged me to be different and to stand out among the crowd.

Although those two life lessons essentially drove me to get my Ph.D, the most important life lesson I learned from you two was that God has a plan and purpose for my life! I love you both very much and am blessed to have you as parents.

ACKNOWLEDGMENTS

I would like to begin by thanking Dr. Kerry Smith for the opportunity to work in his lab, and for his guidance, patience and encouragement over the years. I would also like to thank Dr. Cheryl Ingram-Smith for her insight and advice throughout my graduate career.

In addition, I would like to thank my dissertation committee, Dr. William Marcotte, Dr. Meredith Morris, Dr. Lukasz Kozubowski, and Dr. James Morris. They have provided a wealth of advice on the direction of my project, insight into problems that have arose during my experiments, and knowledge into techniques that were new to our lab.

I would also like to acknowledge present and past Smith and Ingram-Smith lab members for their contributions towards my project, which included helpful discussions, technical support, and assistance with experiments. I would particularly like to thank Dr. Katie Glenn, Grace Kisirkoi, Cheryl Jones, Thanh Dang, Chris Nguyen, Taylor Luckie, Ben Arnson, and Ann Guggisberg. Without you all, I would have repeated many more experiments, stressed out a little more than normal, and not laughed nearly as much! I want to give a huge thank you to Dr. Katie Glenn, who began this journey with me 4.5 years ago and is one of the best lab mates, friends, and bridesmaids I could have asked for.

Furthermore, the faculty and the graduate students of the Genetics and Biochemistry Department and the Eukaryotic Pathogens Innovation Center have provided valuable suggestions and thought-provoking questions, which have been crucial in the completion of my degree.

Finally, I'm so very thankful for my loving family and sweet friends who have encouraged and supported me through this adventure.

TABLE OF CONTENTS

	Page
TITLE PAGE	i
ABSTRACT	ii
DEDICATION	iv
ACKNOWLEDGMENTS	v
LIST OF TABLES	viii
LIST OF FIGURES	ix
CHAPTER	
I. Literature Review of Acetate Metabolism in Bacterial and Eukaryotic Microbes	1
Introduction	1
Acetate Metabolism in Bacteria	2
Acetate Production in Eukaryotes	12
<i>Phytophthora ramorum</i>	18
<i>Cryptococcus neoformans</i>	19
References	26
II. Biochemical and Kinetic Characterization of the Eukaryotic Phosphotransacetylase Type IIa Enzyme from <i>Phytophthora ramorum</i>	47
Abstract	47
Introduction	49
Materials and Methods	52
Results	57
Discussion	63
Acknowledgments	67
References	68
III. Biolistic Transformation of a Fluorescent Tagged Gene into the Opportunistic Fungal Pathogen <i>Cryptococcus neoformans</i>	83

Table of Contents (Continued)

	Page
Abstract.....	83
Introduction.....	84
Materials and Methods.....	86
Representative Results.....	94
Discussion.....	96
Acknowledgments.....	98
References.....	99
IV. The Investigation into the Metabolic and Physiological Role of the Ack-Xfp Pathway in <i>Cryptococcus neoformans</i>	109
Abstract.....	109
Introduction.....	111
Materials and Methods.....	114
Results.....	121
Discussion.....	127
Acknowledgments.....	134
References.....	135
V. Conclusions.....	164
APPENDICES.....	170
A: Fungal Ack Structures Possess a Loop that is Non- Existent in Other Ack Enzymes.....	170

LIST OF TABLES

Table		Page
2.1	Kinetic Parameters for PrPta ^{II} Wild Type and the G ³⁰⁰ D Variant in the Acetyl-CoA-forming Direction.....	74
2.2	IC ₅₀ Values for Pta ^{II} Enzymes in the Acetyl-CoA Direction	75
3.1	PCR and RT-PCR Primers	101
4.1	Primers Used in Creating the Deletion Constructs	141
4.2	PCR and RT-PCR Confirmation Primers	142
4.3	The Effect of Fluconazole Determined Through Etest.....	143

LIST OF FIGURES

Figure	Page
1.1	Main Acetate Metabolism Pathways in Bacteria 38
1.2	Acetyl Phosphate Producing Enzymes in Bacteria 39
1.3	Structure of <i>M. thermophila</i> Pta 40
1.4	Dark, Anoxic Conditions Indicate Ack1 and Pat2 are Important in the Chloroplast 41
1.5	Phylogenetic Analysis of Bacterial and Eukaryotic Phosphoketolases
1.6	<i>Phytophthora ramorum</i> Asexual Life Cycle 43
1.7	AIDS-related Cryptococcosis Kills Approximately 504,000 Individuals in Sub-Saharan Africa 44
1.8	The Infection Cycle of <i>Cryptococcus neoformans</i> 45
1.9	Survival and Replication of <i>C. neoformans</i> Within the Macrophage 46
2.1	The Phylogeny of Pta Family 76
2.2	Subdomain Structure of Pta ^I and Pta ^{II} Classes 78
2.3a	The Regulation of PrPta1 ^{II} by Allosteric Effectors 79
2.3b	The Regulation of PrPta1 ^{II} by Allosteric Effectors 79
2.4a	The Effect of NADP on CoASH 80
2.4b	The Effect of NADP on Acetyl Phosphate 80
2.5	SePTA Displays Unusual Response to AMP 81
2.6	Pyruvate Effect on WT versus the G300D Variant 82
3.1	Protocol Scheme 102

List of Figures (Continued)

Figure	Page
3.2a DNA-coated Gold Beads Successfully Shot Onto a YPD + 1M Sorbitol Plate	103
3.2b Transforming 2 µg of DNA Results in 20-30 Colonies per Plate.....	104
3.3a Schematic of the ACK:mCherry:Neo Construct and Primer Design.....	105
3.3b PCR Used to Confirm Successful Homologous Recombination.....	106
3.3c RT-PCR Confirmation of Expression of the mCherry Tag	107
3.4 Fluorescence of the mCherry tagged Ack.....	108
4.1 A Model Demonstrating Putative Acetate Producing Pathways in <i>C. neoformans</i>	144
4.2 <i>XFP1</i> , <i>XFP2</i> , and <i>ACK</i> Deletion Strategy	145
4.3a $\Delta xfp1$ KN99 α Knockout Mutant gDNA Confirmation	146
4.3b $\Delta xfp2$ KN99 α Knockout Mutant gDNA Confirmation.....	147
4.4a $\Delta xfp1$ KN99 α Knockout Mutant RT-PCR Confirmation	149
4.4b $\Delta xfp2$ KN99 α Knockout Mutant RT-PCR Confirmation	149
4.4c Actin RNA controls	149
4.5 Knockouts Lack a Growth Phenotype on All Carbon Sources Tested	150
4.6 Growth Differences Observed With the Knockouts When Grown in Low Glucose.....	151
4.7a The Effect of the <i>ACK</i> and <i>XFP</i> Mutants on Virulence Factors.....	153
4.7b The Effect of the <i>ACK</i> and <i>XFP</i> Mutants on Virulence Factors.....	153
4.8 Knockouts Lack a Stress Response Phenotype on All Compounds Tested.....	154

List of Figures (Continued)

Figures	Page
4.9 A Representation of the Fluconazole Etest.....	155
4.10 No Difference in Virulence Between the WT and Knockouts in <i>Galleria mellonella</i> Model.....	156
4.11 Xfp1 and Xfp2 May Play a Role in the Survival of <i>C. neoformans</i> in Macrophages	157
4.12 Full Length AckmCherry Detected in Cell Lysate	158
4.13 AckmCherry Confocal Microscopy	159
4.14 The Localization of Ackmcherry is Not Within the Vacuolar Membrane or the Nucleus	160
4.15 Ackmcherry Does Not Appear To Co-Localize With the Mitotracker	161
4.16 AckmCherry Does Not Appear to Co-localize with FM1-43	162
4.17 AckmCherry Does Not Appear to Co-localize with the ER-tracker	163
A-1 The <i>E. histolytica</i> Ack (A) and <i>C. neoformans</i> Ack (B) Crystal Structures	170
A-2 Sequence Alignment of Ack Sequences	171

CHAPTER ONE

Literature Review of Acetate Metabolism in Bacterial and Eukaryotic Microbes

I. Introduction

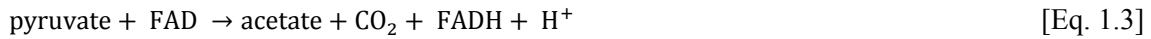
Numerous studies have focused on enzymes in acetate assimilation and dissimilation pathways in bacteria. Although acetate is an important end product of energy metabolism in fungi and protists (1-3), few investigations into acetate production have been reported in eukaryotic microbes. The main acetate metabolism pathways in bacteria include acetate kinase (Ack), that functions with phosphotransacetylase (Pta) to interconvert acetate and acetyl-CoA (4). Although primarily identified as a bacterial pathway, a number of eukaryotic microbes have the Ack-Pta pathway (5). Eucaryote and basidiomycete fungi lack an open reading frame (ORF) with identity to Pta, but instead possess a xylulose 5-phosphate/fructose 6-phosphate phosphoketolase (Xfp) to convert either xylulose 5-phosphate or fructose 6-phosphate to acetyl phosphate and either glyceraldehyde 3-phosphate or erythrose 4-phosphate, which resembles heterofermentative bacteria, which uses this pathway as a modified pentose phosphate pathway (6). While missing in plants and animals, both of these pathways exist and are utilized in eukaryotic microbes; however, little is known about both the biochemistry of the enzymes and the roles these two pathways play in physiology and metabolism of eukaryotic pathogens. Thus, both the Ack-Pta and Ack-Xfp pathways may be potential targets for the development of treatments.

This chapter is a comprehensive review of acetate dissimilation and assimilation in bacteria and the physiological roles of Pta and Xfp in both bacterial and eukaryotic microbes. The main focus of this chapter encompasses published studies on the metabolism of acetate in eukaryotic pathogens. The focus of this dissertation is to begin to unravel the role acetate, as well

as Pta and Xfp, may play in the virulence of eukaryotic pathogens, and if these roles differ from that found in bacteria.

II. Acetate Metabolism in Bacteria

Acetate metabolism, which includes both dissimilation and assimilation, is well studied in bacteria, such as *E. coli*. The study of *E. coli* growth on multiple acetogenic carbon sources, has led to the observation that a “switch” occurs that allows the cells to adapt to their varying nutritional status; when acetate evolution and activation come to equilibrium with one another, bacterial cells execute what is known as the “acetate switch” (4, 7). This “switch” allows the cell to detect the external and internal environment and to activate the expression of genes that constitute the cellular processes responsible for altering the acetate metabolism of the cell [Figure 1.1] (4). In order to regenerate NAD^+ , to recycle CoA and to limit the induction of the full TCA cycle, which increases the rate of cell growth, the cell must excrete acetate (4, 8). During acetate evolution, the TCA cycle operates through a branched route, which provides precursor metabolites but lacks the production of high-energy molecules. Therefore, in *E. coli*, ATP pools regenerate through glycolysis or through the Ack [EC 2.7.2.1; Eq. 1.1] - Pta [EC 2.3.1.8; Eq. 1.2] pathway that converts acetyl-CoA to acetate, which is excreted outside of the cell (9, 10). Another pathway in *E. coli* that produces acetate directly from pyruvate under both aerobic and microaerophilic conditions is pyruvate oxidase [PoxB; EC 1.2.5.1; Eq. 1.3], which also generates FADH_2 that provides two electrons for oxidative phosphorylation (4). The Ack-Pta pathway is active during exponential, aerobic and anaerobic growth, while maximal activity of Pox is seen during late exponential and stationary phase under aerobic conditions (11-13).

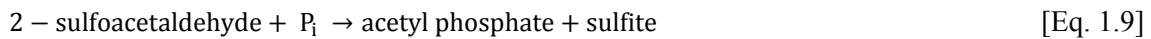
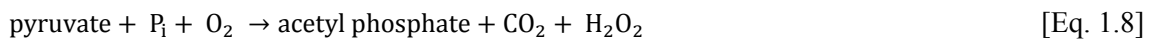
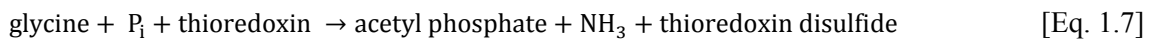
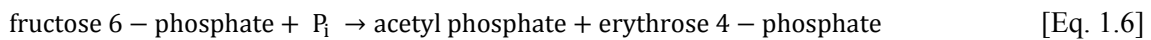
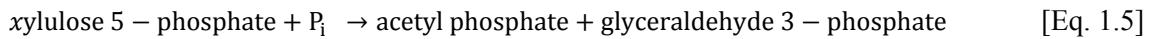


While the Ack-Pta pathway is the primary pathway for acetate dissimilation, AMP-forming acetyl-CoA synthetase [Acs; EC 6.2.1.1; Eq. 1.4] is the main acetate assimilation pathway in bacteria (4), where it functions under low acetate concentrations (9, 14). However, during growth on high concentrations of acetate, the Ack-Pta pathway can activate acetate as this pathway is reversible.



Several other enzymes that produce acetyl phosphate, can partner with Ack in bacteria as an alternative pathway to produce acetate [**Figure 1.2**] (4). Phosphoketolase (PK) enzymes convert the sugars xylulose 5-phosphate [X5P; EC 4.1.2.9; Eq. 1.5] and fructose 6-phosphate to acetyl-phosphate [F6P; EC 4.1.2.22; Eq. 1.6], and are found in heterofermentative lactobacilli (15, 16). Gram-positive bacteria such as *Clostridium* and *Eubacterium* species use glycine reductase [GR; EC 1.2.1.4.2; Eq. 1.7] to catalyze the production of acetyl phosphate from glycine (17, 18). Unlike PoxB in *E. coli*, an acetyl phosphate forming pyruvate oxidase [APF-Pox; EC 1.2.3.3; Eq. 1.8] is found in lactobacilli that converts pyruvate to acetyl phosphate under aerobic conditions, and may be the main contributor to the acetyl phosphate pool in *Streptococcus pneumoniae* (19). Lastly, the sulfoacetaldehyde acetyltransferase [Xsc; EC 2.3.3.15; Eq. 1.9] is

found across the *Bacteria*, although missing in *E. coli*, and is responsible for producing acetyl phosphate and sulfite from sulfoacetaldehyde (20).



In most organisms, ORFs with sequence identity to either Pta and/or Ack are found in microbes along with the following enzymes listed in Eq. 1.5-1.9, and the encoding genes are often expressed together in operons (4). Therefore, these enzymes can partner with Pta and/or Ack to produce acetyl phosphate as a global signal to activate response regulatory pathways, to convert acetyl phosphate to acetate for dissimilation purposes, or to generate acetyl-CoA that feeds back into the TCA cycle or for fatty acid synthesis (4). Not only is acetyl phosphate an important metabolic intermediate produced in all Ack pathways, it also can donate phosphate groups to signal transduction pathways that regulate responsive processes such as stress, pathogenesis, and chemotaxis (21).

Pta, the Primary Bacterial and Archaeal Partner of Ack

The isolation and analysis of mutants resistant to fluoroacetate, a toxic analogue of acetate, assisted in delineating the role of Ack and Pta in *E. coli* metabolism. These studies established that Ack-Pta works primarily in acetate dissimilation, but that this pathway can play a role in acetate assimilation under high acetate concentrations (9). When the cells were grown with

labeled acetate and glucose as carbon sources, neither the Δ ack nor Δ pta mutants incorporated the labeled acetate. However, when the same experiment used glycerol, both mutants were able to take up and incorporate the labeled acetate (9). Additionally, when adding glucose to cells growing on glycerol, little effect was observed for the uptake of the labeled acetate or the incorporation with either mutant, suggesting that glucose transcriptionally represses the Ack-Pta pathway without inhibiting the enzymes (9). Acs is the high affinity pathway, which can explain the incorporation of labeled acetate in the absence of both Ack and Pta, since Acs acts as a scavenger under low acetate concentrations. When Δ ack mutants were grown on acetate as the sole carbon source, the cells doubled in growth within 6 hours, whereas Δ pta mutants took 15 hours for the same amount of growth. Unlike WT cells and Δ ack cells, Δ pta cells were unable to excrete acetate into the growth medium when grown on glucose (9). This study indicates that Pta, not Ack, is essential for excretion of acetate through the formation of acetyl phosphate, which can be hydrolyzed non-enzymatically to acetate without the need for Ack (9).

Another study in *Salmonella enterica* planned to use the inactivation of the enzyme isocitrate lyase to specify if *S. enterica* virulence was affected by its ability to use acetate as both a carbon and energy source (22). Since an earlier study showed that a double knockout of both ack and pta lacked an affect on virulence in a mouse model, this study planned on using Pta as a control. Therefore, the knockouts of both isocitrate lyase and Pta were made in unison; however, the pta knockout not isocitrate lyase, was avirulent in the mouse model (22). Compared to wild type, the complemented strain was as virulent; therefore, this experiment indicates that Pta is essential for growth and/or invasion of *S. enterica* in the mammalian host.

Experimental studies with both *Vibrio cholera* (23) and *Listeria monocytogenes* (24) show that Pta plays an important role in colonization and motility. In all of these examples, they speculate that the acetyl phosphate pools are changing, which may manipulate the

phosphorylation of certain response regulators or provide another mechanism of acetate excretion that is unknown (9, 22).

Enzymology

Kaplan et al. (25) jointly confirmed Ack and Pta activities in *E. coli* cell extracts in 1948; however, Ack and Pta were not purified and characterized until the mid-1950's (10, 26). Rose et al. (10) determined that the enzymatic role of Ack is to reversibly phosphorylate acetate to acetyl phosphate [Eq. 1.1] utilizing the γ - phosphoryl group of ATP. The enzymatic mechanism of Ack operates through a direct in-line transfer of the phosphate group of ATP to acetate (27). Pta was initially partially purified from extracts of *Clostridium kluyveri* (26). These experiments established that the enzymatic rate of Pta was directly proportional to the amount of CoA in the reaction, and that the CoA-enzyme complex was highly dissociable due to the inability to saturate Pta with CoA (26). Stadtman also demonstrated a requirement for both KCl and NH₄Cl and an optimal pH of 7.4-8.2 (26).

Sequencing of bacterial genomes reveals two types of Pta: Pta^I and Pta^{II} (28-30). Pta^I enzymes have been thoroughly characterized, and there are a number of solved crystal structures (31-36). Only two Pta^{II} enzymes, one from *E. coli* (EcPta^{II}) and one from *S. enterica* (SePta^{II}), have been fully characterized and a structure is unavailable (29, 30). Comprised of only a catalytic subunit, the Pta^I enzyme is approximately 350 amino acids long. In addition to possessing a catalytic C-terminal domain, Pta^{II} enzymes have a N-terminal regulatory domain of roughly 350 amino acids (29, 30). The regulatory domain of Pta^{II} contains two recognizable subdomains: the P-loop containing NTPase and the DRTGG domains (30). The P-loop NTPase domain includes a conserved nucleotide tri-phosphate-binding motif, and exists in enzymes involved in multiple cellular processes (37). The DRTGG domain has an unknown function and

is identifiable by some of the most conserved residues found in the domain. This domain is associated with the cystathione-beta-synthase domain (CBS) that exists in both membrane-bound and cytosolic proteins, and known to function in all three domains of life (38).

Little is known about the N-terminal domain of Pta^{II} and its regulatory function, except from the closely related (96.1% identity) EcPta^{II} and SePta^{II} enzymes. The EcPta^{II} operates in both the acetyl-CoA-forming direction, as well as the acetyl phosphate forming direction, although the k_{cat} is 8-fold lower in this direction. In the acetyl-CoA – forming direction, EcPta^{II} displays positive cooperativity in regards to CoA, but not with acetyl phosphate, and in the acetyl phosphate – forming direction, a sigmoidal response for acetyl-CoA, but not with P_i, is observed (30). Truncations of the N-terminal region of EcPta^{II} reveal that the regulation of the enzyme is through metabolic effector molecules. The P-loop domain is required for the effect of NADH, ATP, PEP and pyruvate, and the DRTGG subdomain is vital for the sigmoidal response observed in allosteric enzymes (30).

Like the EcPta^{II} enzyme, the SePta^{II} enzyme also catalyzes the acetyl-CoA and acetyl phosphate forming directions of the Pta pathway and is also an allosteric enzyme (29). However, unlike EcPta^{II}, the SePta^{II} enzyme displays positive cooperativity for acetyl phosphate, not CoA, in the acetyl-CoA forming direction, and is reported to lack a sigmoidal response in the acetyl phosphate-forming direction. Although the SePta^{II} kinetics indicate a lack of cooperativity with either substrate in the acetyl phosphate-forming direction, the authors still tested NADH and pyruvate as metabolic effectors only in this direction (29). Both the EcPta^{II} and SePta^{II} enzymes were inhibited by NADH and activated by pyruvate in the acetyl phosphate forming direction (29, 30).

Structure

The Ack-Pta pathway is also present in one genus of methane-producing archaea. *Methanosarcina* species utilize this pathway to activate acetate to acetyl-CoA for use as a carbon and/or energy source (33, 39, 40). However, the pathway can also function in the opposite direction for energy conservation during growth on carbon monoxide (41, 42). Pta follows a ternary catalytic mechanism that lacks an order in the binding of both substrates (31). However, the mechanism is base-catalyzed with an important Asp-316 residue interacting with the thiol group of CoA, forming a nucleophile that readily attacks acetyl phosphate. Acetyl-CoA is produced, along with the PO_4^{3-} ion; this ion removes the proton from Asp-316 that is abstracted from CoA, regenerating Asp-316 for the next round of catalysis (32). The Pta structure from *M. thermophila* forms a homodimer [**Figure 1.3A**], and each elongated monomer contains two domains [**Figure 1.3B**] (36). Domain one consists of a sheet of β_3 , β_2 , β_1 , β_4 , and β_{11} in parallel, encompassed by four major alpha helices. Domain two includes β_{10} , β_5 , β_6 , β_9 , β_7 , and β_8 in both parallel and anti-parallel, with five major helices surrounding the mixed sheet. This crystal structure of Pta (36) confirmed the 1976 suggested ternary mechanism suggested by Henkin et al. (36, 43).

Xfp, an Enzyme Partner for Ack in Heterofermentative Bacteria.

Lactic acid bacteria are Gram positive, non-sporulating bacteria that produce lactate as the main fermentation product. Homofermentative bacteria produce fermentation products that consist of 100% lactate, and use glycolysis as the sole method to metabolize hexose sugars (44). Whereas heterofermentative bacteria produce fermentation products that include approximately 50% lactate, with other products such as acetate, ethanol, and CO_2 , and break down hexose sugars through both glycolysis and the pentose phosphate pathway (44). Phosphoketolases constitute a

modified form of the pentose phosphate pathway that converts either fructose 6-phosphate [Eq. 1.6] from glycolysis or xylulose 5-phosphate [Eq. 1.5] from the pentose phosphate pathway to acetyl phosphate. Within this enzymatic family, there are either dual substrate specific enzymes, xylulose 5-phosphate/fructose 6-phosphate phosphoketolases (Xfp), or single substrate specific enzymes, fructose 6-phosphate phosphoketolases (F6ppk) (45).

Physiological Significance

The biochemical characterization of the recombinant *Lactobacillus pentosus* Xfp and the investigation into the metabolic and physiological role of this enzyme indicates that it is necessary for the fermentation of pentose sugars and gluconate (46). The Δ xfp mutant is unable to grow on arabinose, xylose, ribose or gluconate, and the observation of maximal activity of Xfp in cell extracts occurs during growth on xylose and gluconate, not on glucose and fructose. Further confirmation that Xfp is active under certain growth conditions results from a western blot in which Xfp was only detected from cells grown on pentoses and gluconate, and not on glucose or fructose (46).

Another study indicates that Xfp in *Clostridium acetobutylicum* could possibly use both the pentose phosphate pathway and the Ack-Xfp pathway for the metabolism of both arabinose and xylose (47). *C. acetobutylicum* Xfp is a dual substrate specific enzyme, with a slight preference for X5P, and expression is 6.7x higher when cells are grown in arabinose versus xylose. Although this bacterium can ferment both substrates, it grows 3.5x better on arabinose than xylose, indicating that the pentose phosphate pathway in *C. acetobutylicum* is unable to metabolize sugars swiftly due to two possible reasons: the lack of proper amounts of transaldolase or an inefficient system of transporting xylose (47). Therefore, the physiological role of the Ack-Xfp pathway could be to metabolize pentose and hexose sugars and sugar alcohols as a modified

pentose phosphate pathway to provide for the nutrient status of the cell under conditions when the cells are unable to use the pentose phosphate pathway fully. Another possible role would be to connect the oxidative portion of the pentose phosphate pathway with the lower part of glycolysis (46, 47).

Enzymology

Several bacterial phosphoketolase enzymes have been kinetically characterized, with *Bifidobacterium lactis* and *Lactobacillus plantarum* being one of the most thorough of the investigations (15, 16, 48-50). Most lactic acid bacteria have two ORFs with sequence identity to phosphoketolases, and *B. lactis* and *L. plantarum* are no exception (15, 16). Both phosphoketolase enzymes from *B. lactis* had activity in crude extract, and phosphoketolase assays provided evidence that one was an Xfp and the other was an F6ppk (15). Characterization of the Xfp uncovered a slight preference for F6P over X5P, the requirement for thiamine pyrophosphate (TPP), and the production of a 92,000 Da subunit (15).

With *L. plantarum*, both phosphoketolase enzymes are Xfps; however, only Xfp2 was further characterized. Unlike *B. lactis*, *L. plantarum* Xfp2 has a slight preference for X5P over F6P (16). Yevenes et al. (16) established that the *L. plantarum* Xfp2 enzyme follows a ping-pong kinetic mechanism (16). The kinetic mechanism for *L. plantarum* Xfp2 indicates that F6P binds to the TPP bound Xfp enzyme to form the enzyme bound DHETPP (2-(α,β -dihydroxyethylidene)-thiamine pyrophosphate) intermediate; this also releases E4P. Dehydration of the DHETPP, creates the enzyme bound AcTPP (2-acetyl-thiamine pyrophosphate) intermediate. Once P_i binds to the enzyme and accepts the acetyl group from AcTPP, acetyl phosphate is released (16). Recently, the *L. plantarum* Xfp2 was reported to be allosterically regulated by PEP, OAA and glyoxylate. Unlike the eukaryotic Xfp2 from *C. neoformans*,

mentioned later in this chapter, ATP and AMP have no effect on *L. plantarum* Xfp2 (51). This study indicates that allosteric regulation is not only a eukaryotic adaptation, but spans across both the *Bacteria* and *Eukarya*.

The cyanobacteria *Anabaena* species has three ORFs with sequence identity to phosphoketolases; however, when recombinantly produced and purified, only All1483 and All2567 had phosphoketolase activity (52). These two enzymes utilize both X5P and F6P as substrates, and display positive cooperativity for F6P and negative cooperativity for P_i. Although the other putative phosphoketolase, Alr1850, lacked phosphoketolase activity and sequence similarity with the other two Xfp enzymes, BLAST searches indicate that all three enzymes have a TPP-binding domain within the N-terminus. Therefore, Alr1850 is a TPP-dependent enzyme, which may catalyze reactions with different substrates (52).

Structure

Structures of the *Bifidobacterium breve* and *Bifidobacterium longum* Xfps were solved in 2010 (53, 54). Gel filtration studies, with both bacterial Xfps, confirmed a homohexameric peak with the simplest functional unit being a dimer. Each Xfp subunit consisted of an N-terminal, middle and C-terminal domain, with the active site located between the middle and N-terminal domains (53, 54). Although the overall bacterial Xfp structure resembles the TPP-dependent transketolase (TK) from *Saccharomyces cerevisiae*, which plays a role in the pentose phosphate pathway also utilizing X5P as a substrate, *B.breve* and *B.longum* only share 15% and 17.1% amino acid identity, respectively, with the TK enzyme (53, 54). However, histidine residues found in the active site and other residues that play a role in the binding of TPP are conserved between both the Xfp and TK enzymes. One particular residue, Glu-479, plays an active role in the initial binding of TPP and forming the TPP bound enzyme. Altering this residue to alanine in

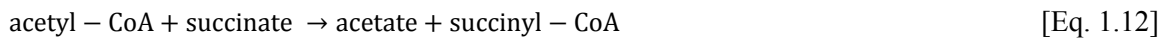
B. breve or aspartate in *B. longum* eliminated all activity, further confirming the relation of both bacterial Xfp enzymes to other TPP-dependent enzymes (53, 54). Although similar to TK, there are some major differences that make Xfp a phosphoketolase and not a transketolase. These include the dehydration of DHETPP in the absence of P_i, and the nucleophilic attack of AcTPP by P_i. Through NMR studies, Suzuki et al. (53) showed that the active site of the transketolase lacks any form of dehydration, but that this dehydration reaction is more like enolase, the glycolytic enzyme that produces PEP.

III. Acetate Production in Eukaryotes

The foundation of energy metabolism is glycolysis, which supplies ATP and balances the cells redox equivalents. However, fermentation allows for the production of ATP in the presence of glucose but in the absence of oxygen. A highly diverse group of eukaryotic microbes have evolved ways to produce acetate as a metabolic end product when supplied glucose but little oxygen through anaerobic metabolism (55). Multiple studies have focused on eukaryotic energy metabolism at the molecular level; however, there is a necessity for further detail on acetate production and the enzymes that catalyze the acetate producing reactions.

The metabolism of pyruvate, β -oxidation of fatty acids, and the catabolism of amino acids produce acetyl-CoA (55). Acetyl-CoA conversion to acetate occurs in eukaryotes through six different pathways. Although previously thought to be only a bacterial and archaeal pathway, Ack and Pta [Eq. 1.1 & 1.2] are in green algae and in the *Phytophthora* species (5). In 1975, Reeves et al. (56) identified the ADP-forming acetyl-CoA synthetase [AcS; EC 6.2.1.13; Eq. 1.10] in *Entamoeba histolytica*, which is also conserved in *Giardia lamblia* and the *Plasmodium* species (57). Acetyl-CoA hydrolase [Ach1; EC 3.1.2.1; Eq. 1.11] is fairly universal, and found in a number of microbes, including the kinetoplastids, such as *Trypanosoma brucei*, along with

acetate:succinate CoA transferase [Asct; EC 2.8.3.8; Eq. 1.12] (55). Acetate formation occurs through Asct in the model organism *Saccharomyces cerevisiae* as well, (58) and in a number of parasites, including the parasitic helminth, *Fasciola hepatica* (59).



Acetyl-CoA is not the only source for acetate dissimilation in eukaryotes. Pyruvate, in addition to acetyl-CoA, is able to act as electron acceptor during fermentation in eukaryotic microbes (59). In yeast such as *S. cerevisiae*, only one acetate production pathway originates from pyruvate, which involves the pyruvate dehydrogenase complex through the enzymes pyruvate decarboxylase [Pdc; EC 4.1.1.1; Eq. 1.13] and acetaldehyde dehydrogenase [Ald; EC 1.2.1.5; Eq. 1.14] (55). Euascomycete and basidiomycete fungi have another pathway for acetate production, Xfp-Ack, [Eq. 1.1, 1.5, & 1.6] which is primarily found in bacteria (5). However, this pathway does not use pyruvate or acetyl-CoA as a precursor for acetate, but uses five and six carbon sugars such as xylulose 5-phosphate and fructose 6-phosphate.



Role of Acetate in Pathogenic Eukaryotic Microbes

During invasion and other stages of infection, the availability of oxygen for a pathogen may be limiting. Therefore, under hypoxic and anoxic conditions, acetate production from

glucose is an important metabolic end product (55). Acetate formation is a main part of energy metabolism in eukaryotic pathogens but not in mammalian hosts; therefore, this portion of energy metabolism could be focused on as a novel therapeutic target (55). *F. hepatica* is a parasitic liver fluke that infects mainly cattle and sheep; however, it can infect humans. Both the liver and bile duct are invaded by this parasite, but the level of oxygen in both of these organs differs. The oxygen level decreases from the liver to the bile duct, which alters acetate metabolism. In the bile duct, the production of acetate provides ATP for the parasite under anaerobic conditions via Asct (59, 60).

E. histolytica and *G. lamblia* are amitochondriate protists that rely primarily on glycolysis for all metabolite and ATP production; two main metabolic products created by these two organisms are acetate and ethanol (57, 61). To conserve energy, Acd, found in both parasitic protozoa, converts acetyl-CoA to acetate; however, in *E. histolytica*, Acd also functions to convert acetate to acetyl-CoA, which could be explained as playing a role in the survival and growth of the parasite within the intestine, where bacteria produce high concentrations of acetate and glucose levels are low (2, 57, 61, 62). Unlike *G. lamblia*, *E. histolytica* also has an Ack that catalyzes the production of acetyl phosphate from acetate; the Ack enzyme identified in *E. histolytica* is the only known Ack enzyme that uses pyrophosphate and inorganic phosphate instead of ATP and ADP (63). The role of Ack could possibly be to produce PP_i for glycolysis, and the acetate that is produced may be converted by Acd to acetyl CoA (62).

Multiple studies of *T. brucei*, the causative agent of sleeping sickness, focus on acetate metabolism throughout the parasite's life cycle. This organism possesses enzymes involved in acetate metabolism such as Acs, Ach, and Asct (64). Acs functions in the acetyl-CoA forming direction in *T. brucei* where de novo biosynthesis of lipids occurs though this enzyme. RNAi

experiments of Acs resulted in a 20-fold reduction of labeled glucose or acetate into fatty acid synthesis and indicated that Acs is essential for growth.

Although this parasite produces acetyl-CoA through Acs, both Ach and Asct produce acetate from acetyl-CoA (64). The overexpression of Asct in *T. brucei* resulted in increased activity, as well as increased acetate excretion, whereas the knockout of Asct led to lower levels of both acetate and succinate (65). However, gene deletion of Asct does not prevent all acetate production (65). *T. brucei* does have an ORF with sequence identity to Ach which is likely the other source of acetate production (55).

Acetate Kinase-Phosphotransacetylase Pathway in Eukaryotes

Using *M. thermophila* ACK as the query search, BLAST searches identified the first eukaryotic ACK sequences in a number of eukaryotic microbes, including *Chlamydomonas reinhardtii*, *Entamoeba histolytica*, the oomycete genus *Phytophthora*, and fungi from the phyla Ascomycota, Chytridiomycota, and Basidiomycota (5). Similar to many bacteria, both *C. reinhardtii* and *Phytophthora* have ORFs that have sequence identity to Pta. Most species of *Phytophthora* have one Ack and two Ptas, but *C. reinhardtii* has two Acks and two Ptas. This suggests that *Phytophthora* and *Chlamydomonas* utilize different Ack-Pta pathways for acetate assimilation and acetate dissimilation (5).

Photosynthetic organisms experience levels of little to no oxygen when light is limiting and respiration has increased, and during these periods, it is unknown what mechanisms are regulated that allows these organisms to respond to the changing environment (66). *C. reinhardtii* is a unicellular green algae that experiences levels of anoxia, generally under dark conditions. Mus et al. (66) examined transcript levels under anoxia in dark environments to attempt to elucidate cellular metabolism and gene expression during this rapid environmental change. Pat1

and Ack2 localize to the mitochondria, whereas Pat2 and Ack1 localize to the chloroplast (67-70) (Note: Pta is defined as Pat in *Chlamydomonas*). *PAT1*, *PAT2*, *ACK1* and *ACK2* transcript levels increased when cells were grown in the dark and under anoxia. Levels were two to three-fold higher for *PAT2* and *ACK1* compared to *PAT1* and *ACK2* at 30 minutes, and approximately six fold higher for *ACK1* and 16 fold higher for *PAT2* at two hours (66). The upregulation of fermentative pathways occur to produce energy under these conditions.

Yang et al. (70) generated Ack1, Ack2 and Pat2 mutants to further study the role these enzymes play in producing acetate and ATP under dark, anoxic conditions *in vivo* [Figure 1.4]. Viability assays conducted on the Δ ack1, Δ ack2, Δ pat2, Δ ack1 Δ ack2, and Δ pat2 Δ ack2 indicated that the Δ ack1 and Δ pat2 mutants were more susceptible to killing under anoxic conditions. This suggests that acetate and/or ATP plays an important role in the chloroplast under conditions of low oxygen (70). The Δ ack2 mutant, found in the mitochondria, appeared similar to the WT. Although there was a two to seven fold reduction in the levels of intracellular acetate for all of the mutants, acetate excretion still occurred; indicating, the Ack-Pta pathway contributes to the main population of acetate in both the chloroplast and mitochondria, but is not the only source, as Ach is present and may be responsible (70). Acs has been thought to be the primary pathway for acetate assimilation in eukaryotic microbes, but W. Yang et al. has recently demonstrated that Ack1-Pat2 is primary pathway for acetate assimilation under dark oxic conditions and Acs is the primary pathway under light oxic conditions (W. Yang and A. Grossman, personal communication).

Acetate Kinase-Xylulose 5-Phosphate/Fructose 6-Phosphate

Phosphoketolase Pathway in Fungi

ACK sequences have previously been identified in both euscomycete and basidiomycete fungi; however, these fungal genomes lack an ORF with identity to *PTA*, the primary partner to *ACK* (5). However, they do have at least one ORF with identity to *XFP*, and in most cases two (5). Of the 650 bacterial and eukaryotic genomes that Sanchez et al. (71) screened for putative *XFP* genes, 110 contained at least one phosphoketolase gene. Out of the 57 Eukarya genomes screened, only 20 genomes, which were from the Ascomycota and Basidiomycota fungal Phyla, included at least one *XFP* sequence; these fungal *XFP* sequences separate into two distinct clades designated as *XFP1* and *XFP2* (71). The authors hypothesized from their phylogenetic analysis [Figure 1.5] that the *XFP2* sequences are of bacterial origin due to the Xfp2 monophyletic cluster branching out from a group of sequences from bacteria. In addition, the *XFP1* sequences are closely related to the marine bacteria *Shewanella*, although the direction of transfer, whether of bacterial descent, is debatable. Nevertheless, it is clear the evolution or acquisition of Xfp1 occurred before the separation of the Ascomycota and Basidiomycota fungal phyla (71). The putative *XFP* genes identified were extremely variable hindering any possibility of understanding the evolutionary history of these genes, or the ability to identify the substrates these enzymes catalyze by the phylogenetic relationships observed through this analysis (71).

All fungi that have at least one *XFP* open reading frame also have *ACK* with the exception of *Schizosaccharomyces* species, which has one *XFP* belonging to the Xfp1 family (5). As in heterofermentative bacteria, Ack and Xfp could partner together within fungi to form a modified pentose phosphate pathway. When grown on xylose and glucose, cell growth diminished, indicating the phosphoketolase pathway as an alternative pathway for the metabolism of these carbon sources (72). Most *Aspergillus* species have two *XFP* genes, but *Aspergillus*

nidulans has only one belonging to the Xfp1 sub-family. Through the use of a constitutive promoter, Panagiotou et al. (73) overexpressed *A. nidulans* Xfp, which resulted in both higher growth rates and biomass yields when grown on xylose, ethanol and glycerol. Incorporation of iodoacetate led to a 6-fold increase in the production of acetyl-CoA, which is a result of the flux through the phosphoketolase pathway (73). These studies provide evidence that central carbon metabolism may rely on the Xfp-Ack pathway to supply flexibility.

In addition to the *Aspergillus* species relying on the Xfp-Ack pathway to provide flexibility to central metabolism, the insect pathogenic fungus *Metarhizium anisopliae* requires this pathway for pathogenesis (74). *Metarhizium anisopliae* has one *XFP* gene identified as *MPK1* that belongs to the Xfp2 sub-family. Culturing the fungus in insect haemolymph resulted in elevated transcript levels of *MPK1*, and gene deletion studies indicate that *MPK1* is required for full virulence against insects (74). The generation of an *ACK* mutant was not reported.

IV. Phytophthora ramorum

Some of the most devastating species of plant pathogens that impact the agriculture and forest ecosystems come from the genus *Phytophthora*, whose name derives from the Greek meaning “plant-destroyer (75). There are more than eighty known different species of *Phytophthora*, and most are plant pathogens. This genus produces progeny sexually and asexually. Oospores are the sexual progeny, which are durable and survive within harsh conditions, allowing the cells to re-infect other plants and continue the asexual life cycle. The asexual life cycle allows the cell to differentiate into other forms, such as the zoospore that initiates infection [Figure 1.6] (76). The dispersal of progeny spores occurs over wide ranges through rain, wind, rivers, streams, and human and animal activities (77). Unlike fungi with genomes that average approximately 37 Mb, oomycetes all have genomes larger than 40 Mb and

are diploid, indicating diversity in their biology and evolution compared to fungi, as well as the genes used to infect host organisms (78).

Unlike other *Phytophthora* species, *Phytophthora ramorum*, which causes Sudden Oak Death (SOD), can infect a broad range of host plants, up to 109 different species (76). *P. ramorum* grows optimally at 20°C, reproduces sexually, and has a 65 Mb genome. This species is only found in North America and Europe, and studies indicate that the populations are from three distinct lineages (79).

The two main diseases of *P. ramorum* infection are Sudden oak death, which occurs on oak trees within the United States, and Ramorum blight, which is found in both Europe and North America within the forest, nursery and garden environments (79). With Sudden oak death, the features consist of stem cankers and bleeding cankers found normally in Coast live oak, tanoak, and European Beech. With Ramorum blight, the symptoms found include leaf blight, tip and shoot dieback, and foliar and twig blight in a wide list of host including rhododendron, lilac, Douglas fir, and California bay laurel (79). When found in the forest, populations are cut down and eliminated through burning or through containment and preventative measures to slow down the infection process. Established protocols for nurseries include good sanitary practices, quarantine procedures, and eradication methods during outbreaks (79). Although there are containment and preventative measures, *P. ramorum* is a quarantined plant pathogen to reduce further introduction and propagation.

V. Cryptococcus neoformans

Cryptococcus neoformans, an invasive opportunistic pathogen of the central nervous system, is the most frequent cause of fungal meningitis worldwide (80). *C. neoformans* infects approximately one million individuals worldwide each year (CDC Report, 2009), and kills

approximately 650,000 people globally. The majority of those individuals are found in sub-Saharan Africa **[Figure 1.7]** and Asia (80-83). Although first isolated 120 years ago in fermented peach juice, it was during the AIDS epidemic when this yeast-like basidiomycete gained prominence, as 5-10% of individuals with AIDS also developed life-threatening cryptococcosis (84). This encapsulated fungus is spherical in structure and 5-10 μm in size. It gains access into the respiratory tract through inhalation of its spores, which are encountered throughout the environment (80, 84). Individuals with an intact immune system can clear the infection; however, for those who are immunocompromised, the fungus can either lay dormant reoccurring later on in the individual's life or establish a pulmonary infection through the production of cryptococcomas. Once pulmonary cryptococcosis is established, *C. neoformans* can disseminate throughout the body, causing systemic disease, including life-threatening meningitis **[Figure 1.8]** (80, 85). The fungus disseminates quickly, having a predilection to the central nervous system, and is the third most frequent neurological complication in AIDS patients.

The treatment for cryptococcosis is unsatisfactory due to harmful side effects and growing resistance, and the treatment goals are different between those patients who are infected versus those who have developed meningitis. Fluconazole, amphotericin B, and flucytosine are the three primary drugs available. Fluconazole inhibits the synthesis of ergosterol in the fungal cell membrane by inactivating 14- α -demethylase that plays a role in its production. Amphotericin B binds to ergosterol causing a transmembrane channel within the cell membrane; these pores formed by amphotericin B allow ion leakage, which eventually causes cell death. Both amphotericin B and flucytosine, a pyrimidine analogue that disrupts nucleic acid biosynthesis, are fairly toxic to humans (81, 82). Those infected with *C. neoformans* but with an unaffected central nervous system, are given fluconazole. Individuals who have AIDS or have meningitis are given a regimen of amphotericin B and flucytosine (81, 82).

Virulence

C. neoformans is grouped within the Order Tremellales, which includes a large number of mycoparasitic fungi. This indicates that *C. neoformans* may be a pathogen to the heterologous hosts that it has been isolated from, such as amoebae, insects and mites (80). As a soil fungus, *C. neoformans* evolutionarily adapted to its surroundings to survive, and in turn, became an intracellular pathogen. Some of the organisms that this fungus co-exists and interacts with could have stimulated virulence of *C. neoformans* by the toxins they excrete or the anti-cryptococcal activity they have gained (80).

C. neoformans does not require a human host during its life cycle, but it does infect humans and other mammals. Mammals have multilayered defense mechanisms to fight off infection, and thus life inside the mammalian host is a hostile environment. *C. neoformans* has three well-defined traits that increase pathogenicity: a polysaccharide capsule, melanin production, and growth at mammalian body temperature (84, 86). The polysaccharide capsule consists of glucuronoxylomannan and galactoxylomannan polysaccharides, and when cell-associated, can provide protection from phagocytosis through concealment of components found on the cell wall. This capsule can also be shed, which results in reduced leukocyte migration, and as a result, diminishes the inflammatory response (84, 87). *C. neoformans* also deposits melanin into the cell wall. This provides protection against free radicals and phagocytosis by stabilizing the cell wall. Cells producing melanin are also less susceptible to killing by amphotericin B (84, 86, 88). Clinical isolates of *C. neoformans* can grow at 37°C, which is required to cause disease in the mammalian host; the ability to grow at this temperature is a rare trait within the fungal community because it is estimated that only 0.01% of soil fungi are able to grow at 37°C. (84). Enzymes important for virulence include phospholipase B that aids in dissemination across the blood brain barrier, possibly through the destruction of the host cell membranes, urease that

produces ammonia and carbamate through the hydrolysis of urea, to increase the local pH and aid in transversal across the blood brain barrier, and an array of reductases, permeases, and siderophores that aid in iron acquisition (84, 86, 89).

An important adaptation to the host environment is the ability of *C. neoformans* to survive and replicate within the macrophage [Figure 1.9] (90, 91). Once phagocytosed by macrophages, *Cryptococcal* cells become enclosed within lysosomes and get exposed to a low pH. Most pathogenic microbes evolve ways to manipulate the phagolysosomal fusion, and therefore, avoid the environmental acidification. *C. neoformans* does not inhibit this phagolysosomal fusion, and not only survives in the low pH of the macrophage, but prospers in the acidic environments (90). In addition to being able to survive the acidic environment within macrophages, *C. neoformans* also causes macrophage dysfunction by shedding the capsule components within the lysosome vesicles (92). Persistence of *C. neoformans* within the macrophage has been described as a mode of dissemination for the fungus, including a way to transverse the blood brain barrier defined as the Trojan horse method (93).

A Model Organism and the Gene Tools Created to Unravel Its Biology

Cryptococcus neoformans was previously grouped into 3 varieties and 4 serotypes: *Cryptococcus neoformans* var. *grubii* (serotype A), *Cryptococcus neoformans* var. *neoformans* (serotype D), and *Cryptococcus neoformans* var. *gattii*, now known just as *Cryptococcus gattii* (serotypes B and C) (84). The life cycle of each of these species includes the survival of haploid types, either α or a , that mate with either the opposite mating type to produce a dikaryon or with the same mating type to produce a monokaryon (94). The different mating types are characterized by the MAT locus, which is the same size and contains the same genes in each, but the difference is within the arrangement of the genes within this locus for either α or a cells. This distinction

allowed for the creation of congenic strain pairs in serotype A and D, which has aided in the development of genome wide analysis tools, that made *C. neoformans* a model organism (84, 94-96).

The ability of this organism to survive as both a haploid and a diploid provides a mechanism where essential genes in *C. neoformans* can be analyzed. The two mating strains are capable of genetic crossing, and due to the segregation of alleles through meiosis, further genetic analysis within *C. neoformans* can occur (94). If a diploid strain contains a heterozygous mutation (e.g., *XFP1*/*xfp1*), the isolation and analysis of haploid spores can establish the essentiality of the gene. If the mutation (*xfp1*) is lethal, the surviving haploid spores will all have the *XFP1* allele, indicating that *XFP1* is essential (94).

Development of molecular techniques such as gene disruption was imperative to study *C. neoformans* pathogenesis. The development of two systems for transformation, electroporation and biolistics, occurred in the early 1990s (97, 98). Introduction of foreign DNA into *Cryptococcus* through electroporation transpired due to its success in *S. cerevisiae* (97). However, this method is only efficient when the DNA that needs to be introduced is maintained episomally (97). The electroporation of a plasmid-borne *URA5* selectable marker into *C. neoformans ura5* mutants resulted in only 0.001 to 0.1% stable transformants (97). Using electroporation to reconstitute capsule production in an acapsular mutant produced a transformation efficiency rate of just 0.25% (99).

Although electroporation can result in stable episomes, it is inefficient in introducing linear DNA that needs to integrate into the genome through homologous recombination. Depending on the gene that will be altered, biolistic transformation results in a stable transformation efficiency of 2-50% (98, 100, 101). Biolistic transformation is the best choice for introduction of linear DNAs into the *C. neoformans* genome via homologous recombination.

These transformation techniques provide other methods where the pathogenesis of *C. neoformans* can be unraveled further by analyzing gene function and evolution through targeted gene disruption, insertional mutagenesis, and genetic manipulation through the use of an episomal plasmid (94).

***Cryptococcus neoformans* Acetate Evolution**

Acetate is one of the principal metabolites produced by *C. neoformans* during *in vitro* growth in glucose-fed cultures (102) and during infection (1, 103). NMR studies conducted on cryptococcomas, large mass lesions resulting from cryptococcal infection, indicated high levels of acetate that may play a role in pathogenesis during pulmonary infection (1). In addition, the acidic environment of brain lesions, produced by *C. neoformans*, is consistent with the production of acetate during infection (103).

The Smith lab has identified three possible pathways that could be the source of acetate: Xfp1-Ack, Xfp2-Ack, and Pdc-Ald. The Xfp-Ack pathways are the focus of this dissertation. A microarray study of *C. neoformans* gene expression by Fan et al. (104) indicated *ACK* is expressed during murine macrophage infection; however, information about the expression of *XFP1* and *XFP2* was absent as neither were present on the microarray. Serial analysis of gene expression on cells recovered from the lungs of infected mice uncovered elevated transcripts of *XFP2*, as well as *PDC* and *ALD* (105). In addition, Chun et al. (106) executed a genome wide microarray study that revealed both *ACK* and *XFP2* are induced under hypoxic conditions. A global transcriptome profile of *C. neoformans* treated with hydrogen peroxide revealed induction of *XFP1* in response to oxidative stress (107). These studies suggest that the Ack-Xfp pathway would be functioning during infection and may be responsible for acetate production.

Although an investigation of the role of the Ack-Xfp1/Xfp2 pathway in *C. neoformans* has not been reported, Glenn et al. (108) provided the first characterization of a eukaryotic Xfp enzyme. *C. neoformans* Xfp2 is allosterically regulated by both positive and negative effector molecules; ATP, PEP and OAA inhibit Xfp2, whereas AMP activates the enzyme. This was the first biochemical investigation into this pathway in *C. neoformans*, which provided unique insight into the enzymology of Xfp (108).

VI. References

1. Himmelreich U, Allen C, Dowd S, Malik R, Shehan BP, Mountford C, Sorrell TC. 2003. Identification of metabolites of importance in the pathogenesis of pulmonary cryptococcoma using nuclear magnetic resonance spectroscopy. *Microb Infect / Institut Pasteur* **5**:285-290.
2. Reeves RE, Warren LG, Susskind B, Lo HS. 1977. An energy-conserving pyruvate-to-acetate pathway in *Entamoeba histolytica*. Pyruvate synthase and a new acetate thiokinase. *J Biol Chem* **252**:726-731.
3. Mazet M, Morand P, Biran M, Bouyssou G, Courtois P, Daulouede S, Millerioux Y, Franconi JM, Vincendeau P, Moreau P, Bringaud F. 2013. Revisiting the central metabolism of the bloodstream forms of *Trypanosoma brucei*: production of acetate in the mitochondrion is essential for parasite viability. *PLoS Negl Trop Dis* **7**:e2587.
4. Wolfe AJ. 2005. The acetate switch. *MMBR* **69**:12-50.
5. Ingram-Smith C, Martin SR, Smith KS. 2006. Acetate kinase: not just a bacterial enzyme. *Trends Microbiol* **14**:249-253.
6. Jeffries TW. 1983. Utilization of xylose by bacteria, yeasts, and fungi. *Adv Biochem Eng Biotechnol* **27**:1-32.
7. Wolfe AJ. 2010. Physiologically relevant small phosphodonors link metabolism to signal transduction. *Curr Opin Microbiol* **13**:204-209.
8. El-Mansi M, Cozzone AJ, Shiloach J, Eikmanns BJ. 2006. Control of carbon flux through enzymes of central and intermediary metabolism during growth of *Escherichia coli* on acetate. *Curr Opin Microbiol* **9**:173-179.
9. Brown TD, Jones-Mortimer MC, Kornberg HL. 1977. The enzymic interconversion of acetate and acetyl-coenzyme A in *Escherichia coli*. *J Gen Microbiol* **102**:327-336.

10. Rose IA, Grunberg-Manago M, Korey SF, Ochoa S. 1954. Enzymatic phosphorylation of acetate. *J Biol Chem* **211**:737-756.
11. Dittrich CR, Bennett GN, San KY. 2005. Characterization of the acetate-producing pathways in *Escherichia coli*. *Biotechnol Prog* **21**:1062-1067.
12. Hahm DH, Pan J, Rhee JS. 1994. Characterization and evaluation of a pta (phosphotransacetylase) negative mutant of *Escherichia coli* HB101 as production host of foreign lipase. *Appl Microbiol Biotechnol* **42**:100-107.
13. Yang YT, Aristidou AA, San KY, Bennett GN. 1999. Metabolic flux analysis of *Escherichia coli* deficient in the acetate production pathway and expressing the *Bacillus subtilis* acetolactate synthase. *Metab Eng* **1**:26-34.
14. Kumari S, Tishel R, Eisenbach M, Wolfe AJ. 1995. Cloning, characterization, and functional expression of *acs*, the gene which encodes acetyl coenzyme A synthetase in *Escherichia coli*. *J Bacteriol* **177**:2878-2886.
15. Meile L, Rohr LM, Geissmann TA, Herensperger M, Teuber M. 2001. Characterization of the D-xylulose 5-phosphate/D-fructose 6-phosphate phosphoketolase gene (*xfp*) from *Bifidobacterium lactis*. *J Bacteriol* **183**:2929-2936.
16. Yevenes A, Frey PA. 2008. Cloning, expression, purification, cofactor requirements, and steady state kinetics of phosphoketolase-2 from *Lactobacillus plantarum*. *Bioorg Chem* **36**:121-127.
17. Stadtman TC, Davis JN. 1991. Glycine reductase protein C. Properties and characterization of its role in the reductive cleavage of Se-carboxymethyl-selenoprotein A. *J Biol Chem* **266**:22147-22153.
18. Schrader T, Andreesen JR. 1992. Purification and characterization of protein PC, a component of glycine reductase from *Eubacterium acidaminophilum*. *Eur J Biochem* **206**:79-85.

19. Spellerberg B, Cundell DR, Sandros J, Pearce BJ, Idanpaan-Heikkila I, Rosenow C, Masure HR. 1996. Pyruvate oxidase, as a determinant of virulence in *Streptococcus pneumoniae*. *Mol Microbiol* **19**:803-813.
20. Ruff J, Denger K, Cook AM. 2003. Sulphoacetaldehyde acetyltransferase yields acetyl phosphate: purification from *Alcaligenes defragrans* and gene clusters in taurine degradation. *Biochem J* **369**:275-285.
21. McCleary WR, Stock JB, Ninfa AJ. 1993. Is acetyl phosphate a global signal in *Escherichia coli*? *J Bacteriol* **175**:2793-2798.
22. Kim YR, Brinsmade SR, Yang Z, Escalante-Semerena J, Fierer J. 2006. Mutation of phosphotransacetylase but not isocitrate lyase reduces the virulence of *Salmonella enterica* serovar *Typhimurium* in mice. *Infect Immun* **74**:2498-2502.
23. Chiang SL, Mekalanos JJ. 1998. Use of signature-tagged transposon mutagenesis to identify *Vibrio cholerae* genes critical for colonization. *Mol Microbiol* **27**:797-805.
24. Gueriri I, Bay S, Dubrac S, Cyncynatus C, Msadek T. 2008. The Pta-AckA pathway controlling acetyl phosphate levels and the phosphorylation state of the DegU orphan response regulator both play a role in regulating *Listeria monocytogenes* motility and chemotaxis. *Mol Microbiol* **70**:1342-1357.
25. Kaplan NO, Lipmann F. 1948. Reactions between acetate, acetyl phosphate and the adenylic acid system in tissue and bacterial extracts. *Fed Proc* **7**:163.
26. Stadtman ER. 1952. The purification and properties of phosphotransacetylase. *J Biol Chem* **196**:527-534.
27. Miles RD, Gorrell A, Ferry JG. 2002. Evidence for a transition state analog, MgADP-aluminum fluoride-acetate, in acetate kinase from *Methanosarcina thermophila*. *J Biol Chem* **277**:22547-22552.
28. Starai VJ, Garrity J, Escalante-Semerena JC. 2005. Acetate excretion during growth of *Salmonella enterica* on ethanolamine requires phosphotransacetylase

- (EutD) activity, and acetate recapture requires acetyl-CoA synthetase (Acs) and phosphotransacetylase (Pta) activities. *Microbiology* **151**:3793-3801.
29. Brinsmade SR, Escalante-Semerena JC. 2007. In vivo and in vitro analyses of single-amino acid variants of the *Salmonella enterica* phosphotransacetylase enzyme provide insights into the function of its N-terminal domain. *J Biol Chem* **282**:12629-12640.
 30. Campos-Bermudez VA, Bologna FP, Andreo CS, Drincovich MF. 2010. Functional dissection of *Escherichia coli* phosphotransacetylase structural domains and analysis of key compounds involved in activity regulation. *The FEBS J* **277**:1957-1966.
 31. Lawrence SH, Ferry JG. 2006. Steady-state kinetic analysis of phosphotransacetylase from *Methanosarcina thermophila*. *J Bacteriol* **188**:1155-1158.
 32. Lawrence SH, Luther KB, Schindelin H, Ferry JG. 2006. Structural and functional studies suggest a catalytic mechanism for the phosphotransacetylase from *Methanosarcina thermophila*. *J Bacteriol* **188**:1143-1154.
 33. Lundie LL, Jr., Ferry JG. 1989. Activation of acetate by *Methanosarcina thermophila*. Purification and characterization of phosphotransacetylase. *The Journal of biological chemistry* **264**:18392-18396.
 34. Iyer PP, Ferry JG. 2001. Role of arginines in coenzyme A binding and catalysis by the phosphotransacetylase from *Methanosarcina thermophila*. *J Bacteriol* **183**:4244-4250.
 35. Iyer PP, Lawrence SH, Yennawar HP, Ferry JG. 2003. Expression, purification, crystallization and preliminary X-ray analysis of phosphotransacetylase from *Methanosarcina thermophila*. *Acta Crystallogr D Biol Crystallogr* **59**:1517-1520.
 36. Iyer PP, Lawrence SH, Luther KB, Rajashankar KR, Yennawar HP, Ferry JG, Schindelin H. 2004. Crystal structure of phosphotransacetylase from the methanogenic archaeon *Methanosarcina thermophila*. *Structure* **12**:559-567.

37. Leipe DD, Koonin EV, Aravind L. 2003. Evolution and classification of P-loop kinases and related proteins. *J Mol Bio* **333**:781-815.
38. Baykov AA, Tuominen HK, Lahti R. 2011. The CBS domain: a protein module with an emerging prominent role in regulation. *Chem Biol* **6**:1156-1163.
39. Aceti DJ, Ferry JG. 1988. Purification and characterization of acetate kinase from acetate-grown *Methanosarcina thermophila*. Evidence for regulation of synthesis. *J Biol Chem* **263**:15444-15448.
40. Latimer MT, Ferry JG. 1993. Cloning, sequence analysis, and hyperexpression of the genes encoding phosphotransacetylase and acetate kinase from *Methanosarcina thermophila*. *J Bacteriol* **175**:6822-6829.
41. Lessner DJ, Li L, Li Q, Rejtar T, Andreev VP, Reichlen M, Hill K, Moran JJ, Karger BL, Ferry JG. 2006. An unconventional pathway for reduction of CO₂ to methane in CO-grown *Methanosarcina acetivorans* revealed by proteomics. *Proc Natl Acad Sci U S A* **103**:17921-17926.
42. Rother M, Metcalf WW. 2004. Anaerobic growth of *Methanosarcina acetivorans* C2A on carbon monoxide: an unusual way of life for a methanogenic archaeon. *Proc Natl Acad Sci U S A* **101**:16929-16934.
43. Henkin J, Abeles RH. 1976. Evidence against an acyl-enzyme intermediate in the reaction catalyzed by clostridial phosphotransacetylase. *Biochem* **15**:3472-3479.
44. Kandler O. 1983. Carbohydrate metabolism in lactic acid bacteria. *Antonie Van Leeuwenhoek* **49**:209-224.
45. Krampitz LO. 1969. Catalytic functions of thiamin diphosphate. *Annu Rev Biochem* **38**:213-240.
46. Posthuma CC, Bader R, Engelmann R, Postma PW, Hengstenberg W, Pouwels PH. 2002. Expression of the xylulose 5-phosphate phosphoketolase gene, *xpkA*, from *Lactobacillus pentosus* MD363 is induced by sugars that are fermented via the phosphoketolase pathway and is repressed by glucose mediated by CcpA and

- the mannose phosphoenolpyruvate phosphotransferase system. *Appl Environ Microbiol* **68**:831-837.
47. Servinsky MD, Germane KL, Liu S, Kiel JT, Clark AM, Shankar J, Sund CJ. 2012. Arabinose is metabolized via a phosphoketolase pathway in *Clostridium acetobutylicum* ATCC 824. *J Ind Microbiol Biotechnol* **39**:1859-1867.
 48. Grill JP, Crociani J, Ballongue J. 1995. Characterization of fructose 6 phosphate phosphoketolases purified from *Bifidobacterium* species. *Curr Microbiol* **31**:49-54.
 49. Schramm M, Klybas V, Racker E. 1958. Phosphorolytic cleavage of fructose-6-phosphate by fructose-6-phosphate phosphoketolase from *Acetobacter xylinum*. *J Biol Chem* **233**:1283-1288.
 50. Petrareanu G, Balasu MC, Vacaru AM, Munteanu CV, Ionescu AE, Matei I, Szedlaczek SE. 2014. Phosphoketolases from *Lactococcus lactis*, *Leuconostoc mesenteroides* and *Pseudomonas aeruginosa*: dissimilar sequences, similar substrates but distinct enzymatic characteristics. *Appl Microbiol Biotechnol* **98**:7855-7867.
 51. Glenn K, Smith KS. 2015. Allosteric Regulation of *Lactobacillus plantarum* Xylulose 5-phosphate/Fructose 6-phosphate Phosphoketolase (Xfp). *J Bacteriol* doi:10.1128/JB.02380-14.
 52. Moriyama T, Tajima N, Sekine K, Sato N. 2014. Characterization of three putative xylulose 5-phosphate/fructose 6-phosphate phosphoketolases in the cyanobacterium *Anabaena* sp. PCC 7120. *Biosci Biotechnol Biochem* doi:10.1080/09168451.2014.993357:1-8.
 53. Suzuki R, Katayama T, Kim BJ, Wakagi T, Shoun H, Ashida H, Yamamoto K, Fushinobu S. 2010. Crystal structures of phosphoketolase: thiamine diphosphate-dependent dehydration mechanism. *J Biol Chem* **285**:34279-34287.
 54. Takahashi K, Tagami U, Shimba N, Kashiwagi T, Ishikawa K, Suzuki E. 2010. Crystal structure of *Bifidobacterium Longum* phosphoketolase; key enzyme for glucose metabolism in *Bifidobacterium*. *FEBS Lett* **584**:3855-3861.

55. Tielens AG, van Grinsven KW, Henze K, van Hellemond JJ, Martin W. 2010. Acetate formation in the energy metabolism of parasitic helminths and protists. *Int J Parasitol* **40**:387-397.
56. Reeves RE, Guthrie JD. 1975. Acetate kinase (pyrophosphate). A fourth pyrophosphate-dependent kinase from *Entamoeba histolytica*. *Biochem Biophys Res Commun* **66**:1389-1395.
57. Montalvo FE, Reeves RE, Warren LG. 1971. Aerobic and anaerobic metabolism in *Entamoeba histolytica*. *Exp Parasitol* **30**:249-256.
58. Lee FJ, Lin LW, Smith JA. 1990. A glucose-repressible gene encodes acetyl-CoA hydrolase from *Saccharomyces cerevisiae*. *J Biol Chem* **265**:7413-7418.
59. Muller M, Mentel M, van Hellemond JJ, Henze K, Woehle C, Gould SB, Yu RY, van der Giezen M, Tielens AG, Martin WF. 2012. Biochemistry and evolution of anaerobic energy metabolism in eukaryotes. *Microbiol Mol Biol Rev* **76**:444-495.
60. Tielens AGM. 2000. The carbohydrate metabolism of *Fasciola hepatica*, an example of biochemical adaptations in parasitic helminths. *Acta Parasitologica* **45**:59-66.
61. Lindmark DG. 1980. Energy metabolism of the anaerobic protozoon *Giardia lamblia*. *Mol Biochem Parasitol* **1**:1-12.
62. Jones CP, Ingram-Smith C. 2014. Biochemical and kinetic characterization of the recombinant ADP-forming acetyl coenzyme A synthetase from the amitochondriate protozoan *Entamoeba histolytica*. *Eukaryot Cell* **13**:1530-1537.
63. Fowler ML, Ingram-Smith C, Smith KS. 2012. Novel pyrophosphate-forming acetate kinase from the protist *Entamoeba histolytica*. *Eukaryot Cell* **11**:1249-1256.
64. Riviere L, Moreau P, Allmann S, Hahn M, Biran M, Plazolles N, Franconi JM, Boshart M, Bringaud F. 2009. Acetate produced in the mitochondrion is the essential precursor for lipid biosynthesis in procyclic trypanosomes. *Proc Natl Acad Sci U S A* **106**:12694-12699.

65. Riviere L, van Weelden SW, Glass P, Vegh P, Coustou V, Biran M, van Hellemond JJ, Bringaud F, Tielens AG, Boshart M. 2004. Acetyl:succinate CoA-transferase in procyclic *Trypanosoma brucei*. Gene identification and role in carbohydrate metabolism. *J Biol Chem* **279**:45337-45346.
66. Mus F, Dubini A, Seibert M, Posewitz MC, Grossman AR. 2007. Anaerobic acclimation in *Chlamydomonas reinhardtii*: anoxic gene expression, hydrogenase induction, and metabolic pathways. *J Biol Chem* **282**:25475-25486.
67. Atteia A, van Lis R, Gelius-Dietrich G, Adrait A, Garin J, Joyard J, Rolland N, Martin W. 2006. Pyruvate formate-lyase and a novel route of eukaryotic ATP synthesis in *Chlamydomonas* mitochondria. *J Biol Chem* **281**:9909-9918.
68. Terashima M, Specht M, Hippler M. 2011. The chloroplast proteome: a survey from the *Chlamydomonas reinhardtii* perspective with a focus on distinctive features. *Curr Genet* **57**:151-168.
69. Atteia A, van Lis R, Tielens AG, Martin WF. 2013. Anaerobic energy metabolism in unicellular photosynthetic eukaryotes. *Biochim Biophys Acta* **1827**:210-223.
70. Yang W, Catalanotti C, D'Adamo S, Wittkopp TM, Ingram-Smith CJ, Mackinder L, Miller TE, Heuberger AL, Peers G, Smith KS, Jonikas MC, Grossman AR, Posewitz MC. 2014. Alternative Acetate Production Pathways in *Chlamydomonas reinhardtii* during Dark Anoxia and the Dominant Role of Chloroplasts in Fermentative Acetate Production. *Plant Cell* **26**:4499-4518.
71. Borja Sanchez MZ, Fernando Gonzalez-Candelas, Clara G. de los Reyes-Gavilan, and Abelard Margolles. 2010. Bacterial and Eukaryotic Phosphoketolases: Phylogeny, Distribution and Evolution. *J Mol Microbiol Biotech* **18**:37-51.
72. Panagiotou G, I. K, Jonsdottir SO, Olsson L. 2007. Monitoring novel metabolic pathways using metabolomics and machine learning: induction of the phosphoketolase pathway in *Aspergillus nidulans* cultivations. *Metabolomics* **3**:503-516.
73. Panagiotou G, Andersen MR, Grotkjaer T, Regueira TB, Hofmann G, Nielsen J, Olsson L. 2008. Systems analysis unfolds the relationship between the phosphoketolase pathway and growth in *Aspergillus nidulans*. *PloS one* **3**:e3847.

74. Duan Z, Shang Y, Gao Q, Zheng P, Wang C. 2009. A phosphoketolase Mpk1 of bacterial origin is adaptively required for full virulence in the insect-pathogenic fungus *Metarhizium anisopliae*. *Environ Microbiol* **11**:2351-2360.
75. Govers F, Gijzen M. 2006. *Phytophthora* genomics: the plant destroyers' genome decoded. *Mol Plant Microbe Interact* **19**:1295-1301.
76. Savidor A, Donahoo RS, Hurtado-Gonzales O, Land ML, Shah MB, Lamour KH, McDonald WH. 2008. Cross-species global proteomics reveals conserved and unique processes in *Phytophthora sojae* and *Phytophthora ramorum*. *Mol Cell Proteomics* **7**:1501-1516.
77. Grunwald NJ, Garbelotto M, Goss EM, Heungens K, Prospero S. 2012. Emergence of the sudden oak death pathogen *Phytophthora ramorum*. *Trends Microbiol* **20**:131-138.
78. Gregory TR, Nicol JA, Tamm H, Kullman B, Kullman K, Leitch IJ, Murray BG, Kapraun DF, Greilhuber J, Bennett MD. 2007. Eukaryotic genome size databases. *Nucleic Acids Res* **35**:D332-338.
79. Grunwald NJ, Goss EM, Press CM. 2008. *Phytophthora ramorum*: a pathogen with a remarkably wide host range causing sudden oak death on oaks and ramorum blight on woody ornamentals. *Mol Plant Pathol* **9**:729-740.
80. Lin X, Heitman J. 2006. The biology of the *Cryptococcus neoformans* species complex. *Annu Rev Microbiol* **60**:69-105.
81. Powderly WG. 1993. *Cryptococcal* meningitis and AIDS. *Clinical infectious diseases : an official publication of the Infectious Diseases Society of America* **17**:837-842.
82. Price MS, Betancourt-Quiroz M, Price JL, Toffaletti DL, Vora H, Hu G, Kronstad JW, Perfect JR. 2011. *Cryptococcus neoformans* requires a functional glycolytic pathway for disease but not persistence in the host. *mBio* **2**:e00103-00111.

83. Park BJ, Wannemuehler KA, Marston BJ, Govender N, Pappas PG, Chiller TM. 2009. Estimation of the current global burden of cryptococcal meningitis among persons living with HIV/AIDS. *AIDS* **23**:525-530.
84. Steenbergen JN, Casadevall A. 2003. The origin and maintenance of virulence for the human pathogenic fungus *Cryptococcus neoformans*. *Microbes Infect* **5**:667-675.
85. Hull CM, Heitman J. 2002. Genetics of *Cryptococcus neoformans*. *Annu Rev Gen* **36**:557-615.
86. Kronstad JW, Attarian R, Cadieux B, Choi J, D'Souza CA, Griffiths EJ, Geddes JM, Hu G, Jung WH, Kretschmer M, Saikia S, Wang J. 2011. Expanding fungal pathogenesis: *Cryptococcus* breaks out of the opportunistic box. *Nat Rev Microbiol* **9**:193-203.
87. Vecchiarelli A. 2000. Immunoregulation by capsular components of *Cryptococcus neoformans*. *Med Mycol* **38**:407-417.
88. van Duin D, Casadevall A, Nosanchuk JD. 2002. Melanization of *Cryptococcus neoformans* and *Histoplasma capsulatum* reduces their susceptibilities to amphotericin B and caspofungin. *Antimicrob Agents Chemother* **46**:3394-3400.
89. Jung WH, Kronstad JW. 2008. Iron and fungal pathogenesis: a case study with *Cryptococcus neoformans*. *Cell Microbiol* **10**:277-284.
90. Levitz SM, Nong SH, Seetoo KF, Harrison TS, Speizer RA, Simons ER. 1999. *Cryptococcus neoformans* resides in an acidic phagolysosome of human macrophages. *Infect Immun* **67**:885-890.
91. McQuiston TJ, Williamson PR. 2012. Paradoxical roles of alveolar macrophages in the host response to *Cryptococcus neoformans*. *J Infect Chemother* **18**:1-9.
92. Tucker SC, Casadevall A. 2002. Replication of *Cryptococcus neoformans* in macrophages is accompanied by phagosomal permeabilization and accumulation of vesicles containing polysaccharide in the cytoplasm. *Proc Natl Acad Sci U S A* **99**:3165-3170.

93. Charlier C, Nielsen K, Daou S, Brigitte M, Chretien F, Dromer F. 2009. Evidence of a role for monocytes in dissemination and brain invasion by *Cryptococcus neoformans*. *Infect Immun* **77**:120-127.
94. Idnurm A, Bahn YS, Nielsen K, Lin X, Fraser JA, Heitman J. 2005. Deciphering the model pathogenic fungus *Cryptococcus neoformans*. *Nat Rev Microbiol* **3**:753-764.
95. Kwon-Chung KJ, Bennett JE. 1978. Distribution of alpha and alpha mating types of *Cryptococcus neoformans* among natural and clinical isolates. *Am J Epidemiol* **108**:337-340.
96. Kwon-Chung KJ, Edman JC, Wickes BL. 1992. Genetic association of mating types and virulence in *Cryptococcus neoformans*. *Infect Immun* **60**:602-605.
97. Edman JC, Kwon-Chung KJ. 1990. Isolation of the URA5 gene from *Cryptococcus neoformans* var. *neoformans* and its use as a selective marker for transformation. *Mol Cell Biol* **10**:4538-4544.
98. Toffaletti DL, Rude TH, Johnston SA, Durack DT, Perfect JR. 1993. Gene transfer in *Cryptococcus neoformans* by use of biolistic delivery of DNA. *J Bacteriol* **175**:1405-1411.
99. Chang YC, Kwon-Chung KJ. 1994. Complementation of a capsule-deficient mutation of *Cryptococcus neoformans* restores its virulence. *Mol Cell Biol* **14**:4912-4919.
100. Davidson RC, Cruz MC, Sia RA, Allen B, Alspaugh JA, Heitman J. 2000. Gene disruption by biolistic transformation in serotype D strains of *Cryptococcus neoformans*. *Fungal Genet Biol* **29**:38-48.
101. del Poeta M, Toffaletti DL, Rude TH, Sparks SD, Heitman J, Perfect JR. 1999. *Cryptococcus neoformans* differential gene expression detected in vitro and in vivo with green fluorescent protein. *Infect Immun* **67**:1812-1820.
102. Bubb WA, Wright LC, Cagney M, Santangelo RT, Sorrell TC, Kuchel PW. 1999. Heteronuclear NMR studies of metabolites produced by *Cryptococcus*

- neoformans* in culture media: identification of possible virulence factors. Magn Reson Med **42**:442-453.
103. Wright L, Bubb W, Davidson J, Santangelo R, Krockenberger M, Himmelreich U, Sorrell T. 2002. Metabolites released by *Cryptococcus neoformans* var. *neoformans* and var. *gattii* differentially affect human neutrophil function. Microb Infect **4**:1427-1438.
 104. Fan W, Kraus PR, Boily MJ, Heitman J. 2005. *Cryptococcus neoformans* gene expression during murine macrophage infection. Eukaryot Cell **4**:1420-1433.
 105. Hu G, Cheng PY, Sham A, Perfect JR, Kronstad JW. 2008. Metabolic adaptation in *Cryptococcus neoformans* during early murine pulmonary infection. Mol Microbiol **69**:1456-1475.
 106. Chun CD, Liu OW, Madhani HD. 2007. A link between virulence and homeostatic responses to hypoxia during infection by the human fungal pathogen *Cryptococcus neoformans*. PLoS Pathog **3**:e22.
 107. Upadhy R, Campbell LT, Donlin MJ, Aurora R, Lodge JK. 2013. Global transcriptome profile of *Cryptococcus neoformans* during exposure to hydrogen peroxide induced oxidative stress. PLoS One **8**:e55110.
 108. Glenn K, Ingram-Smith C, Smith KS. 2014. Biochemical and kinetic characterization of xylulose 5-phosphate/fructose 6-phosphate phosphoketolase 2 (Xfp2) from *Cryptococcus neoformans*. Eukaryot Cell **13**:657-663.

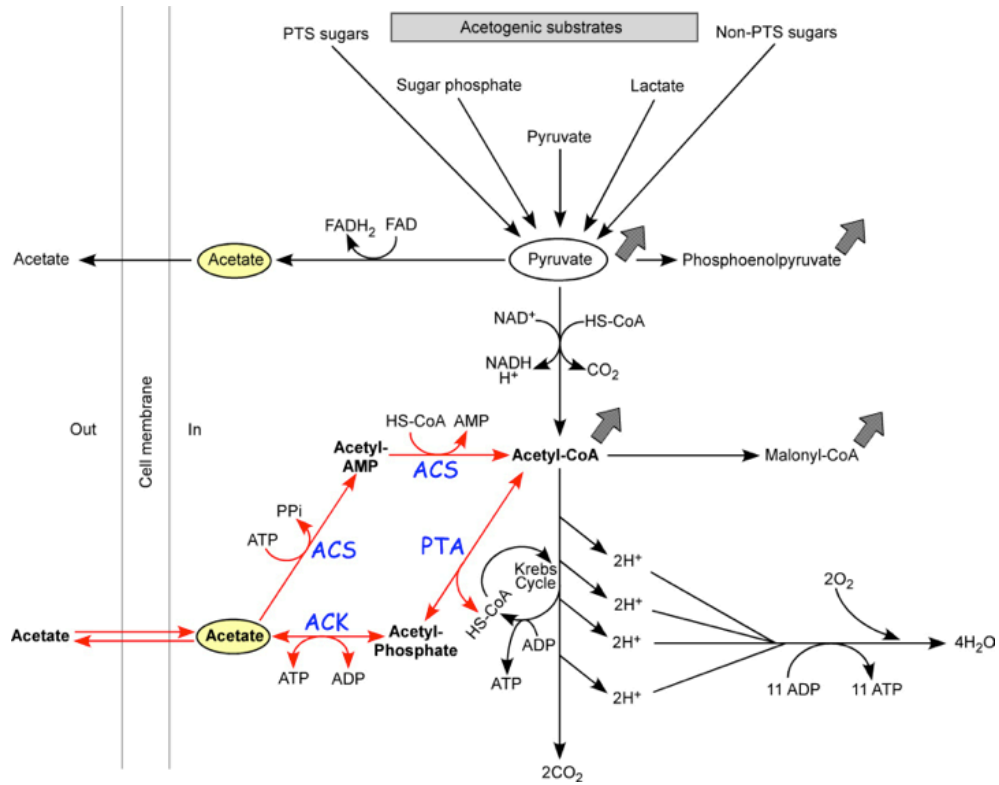


Figure 1.1. Main Acetate Metabolism Pathways in Bacteria. Acetate assimilation and dissimilation pathways make up the “acetate switch.” ACS, AMP-forming acetyl-CoA synthetase; ACK, acetate kinase; PTA, phosphotransacetylase. Modified from (8).

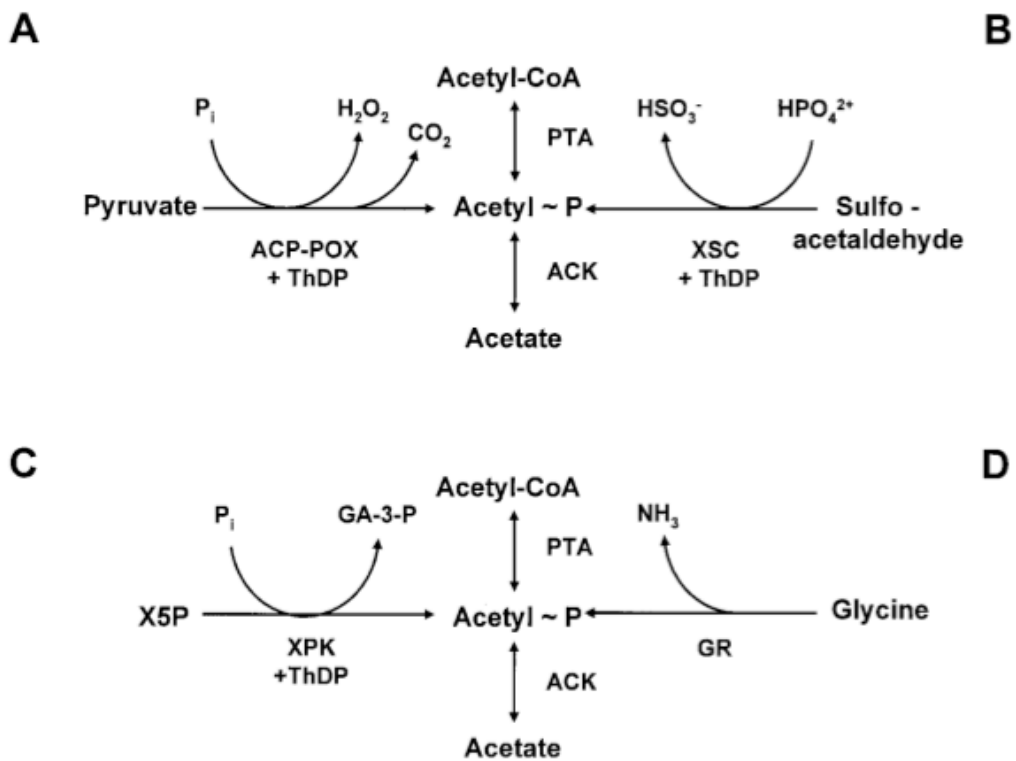


Figure 1.2. Acetyl Phosphate Producing Enzymes in Bacteria. In addition to Ack and Pta, other enzymes in bacteria catalyze reactions that produce acetyl phosphate as an intermediate metabolite. ACP-POX, acetyl phosphate forming pyruvate oxidase; XSC, sulfoacetaldehyde acetyltransferase; XPK, xylulose 5-phosphate phosphoketolase; GR, glycine reductase. Image is from (4), and permission was granted for reuse of this figure.

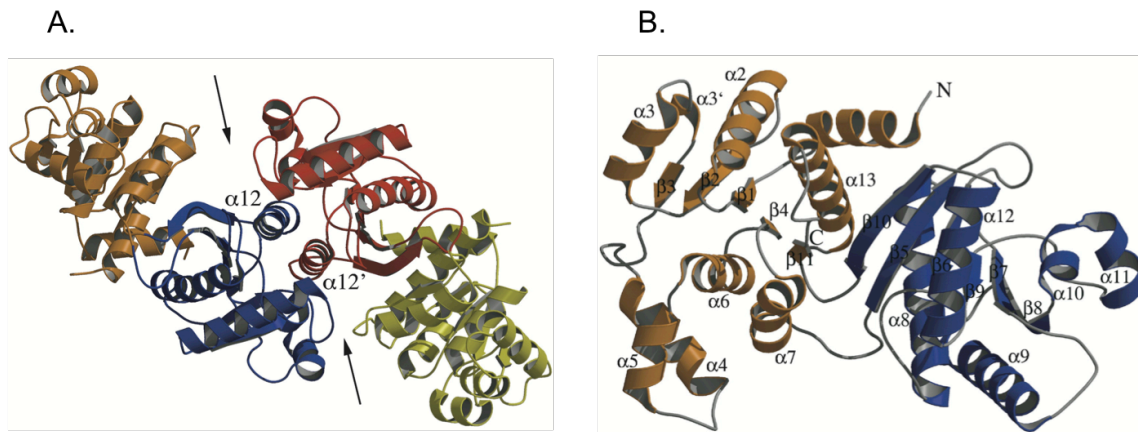


Figure 1.3. Structure of *M. thermophila* Pta. A) Phosphotransacetylase forms a dimer with domains I in orange and yellow and domains II in blue and red. B) The individual subunit of Pta is shown with domain I in orange and domain II in blue, with both the N-terminus and C-terminus located in domain I. Image is from (36), and permission was granted for reuse of this figure.

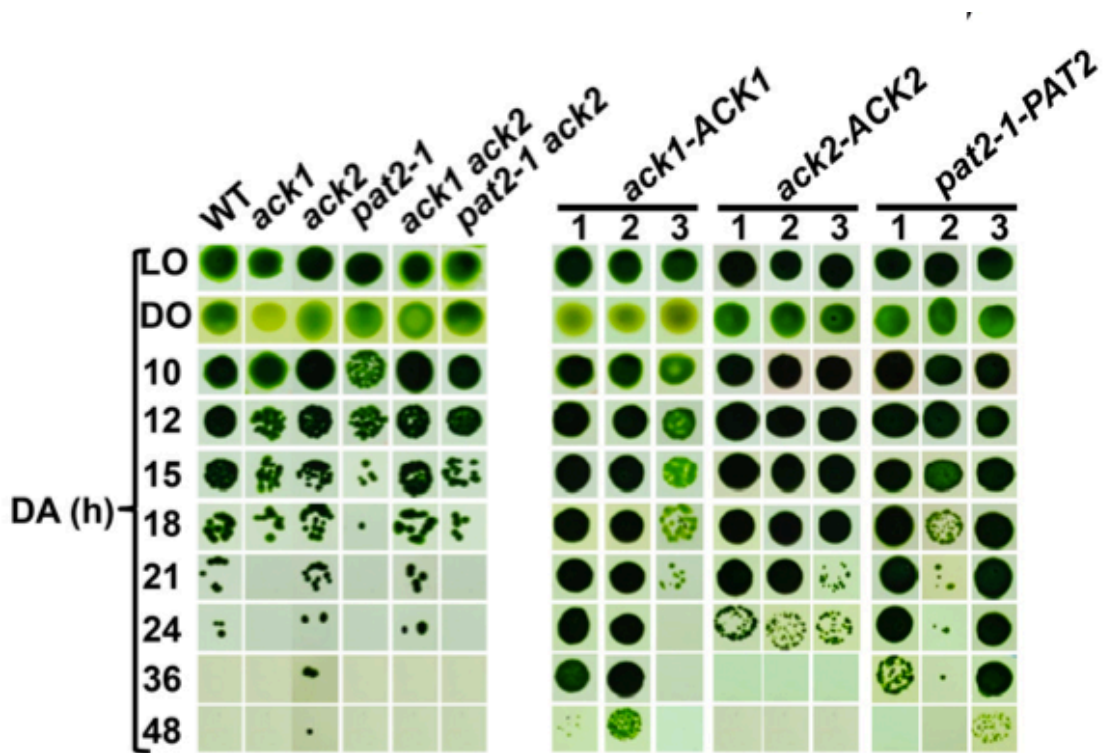


Figure 1.4. Dark, Anoxic Conditions Indicate Ack1 and Pat2 are Important in the Chloroplast. The first panel includes the wild type and knockout cells grown in low oxie (LO), dark oxie (DO) and dark anoxic (DA) conditions and spotted on solid tris acetate phosphate medium. The second panel includes complementation strains for each of the knockouts in triplicate. Image is from (70), and permission was granted for reuse of this figure.

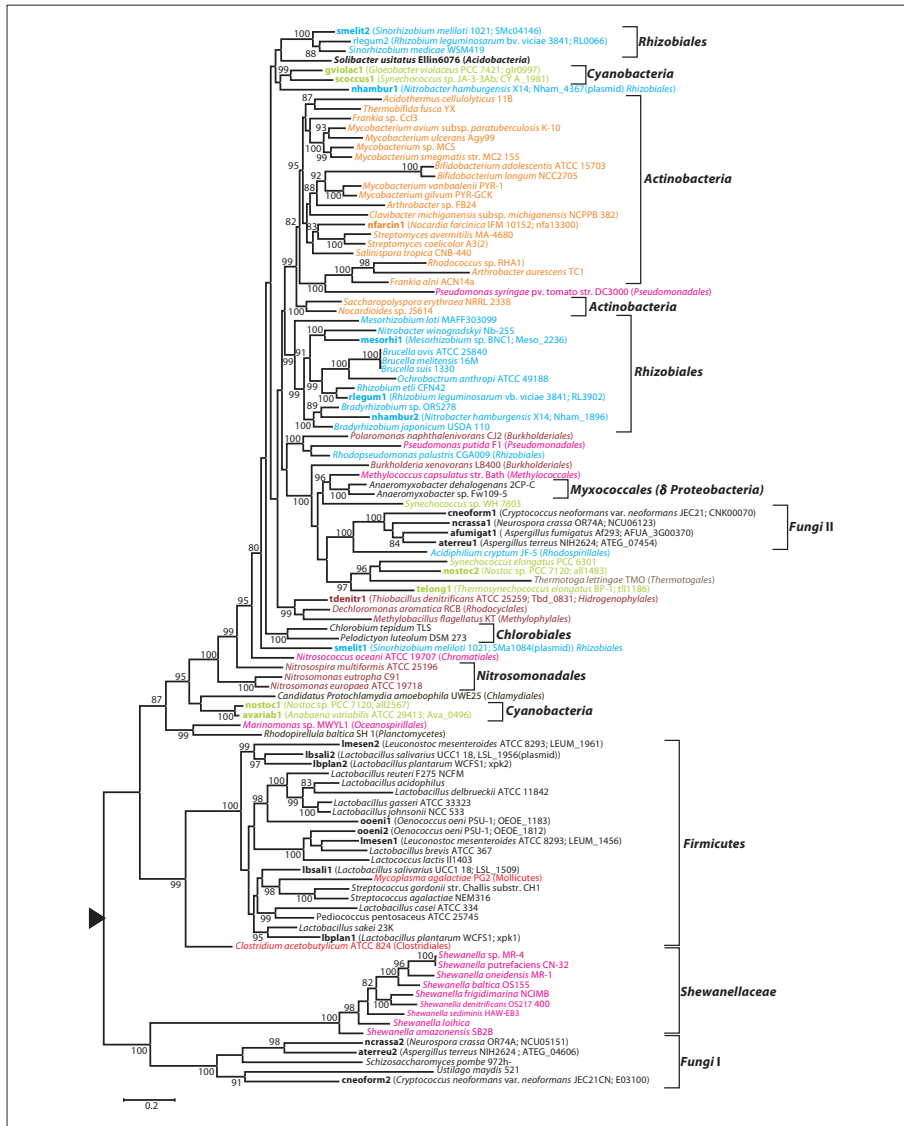


Figure 1.5. Phylogenetic Analysis of Bacterial and Eukaryotic Phosphoketolases. The fungal sequences separate into two specific clusters, Fungal 1 with *Shewanella* sequences and Fungal 2 together with the sequence from *Acidiphilium cryptum*. *B. longum* Xfp sequence was the query search. The Mega 4 program analyzed the aligned sequences using the maximum-likelihood algorithm, and only bootstrap values of 90% or higher are shown. Image is from (71), and permission was granted for reuse of this figure.

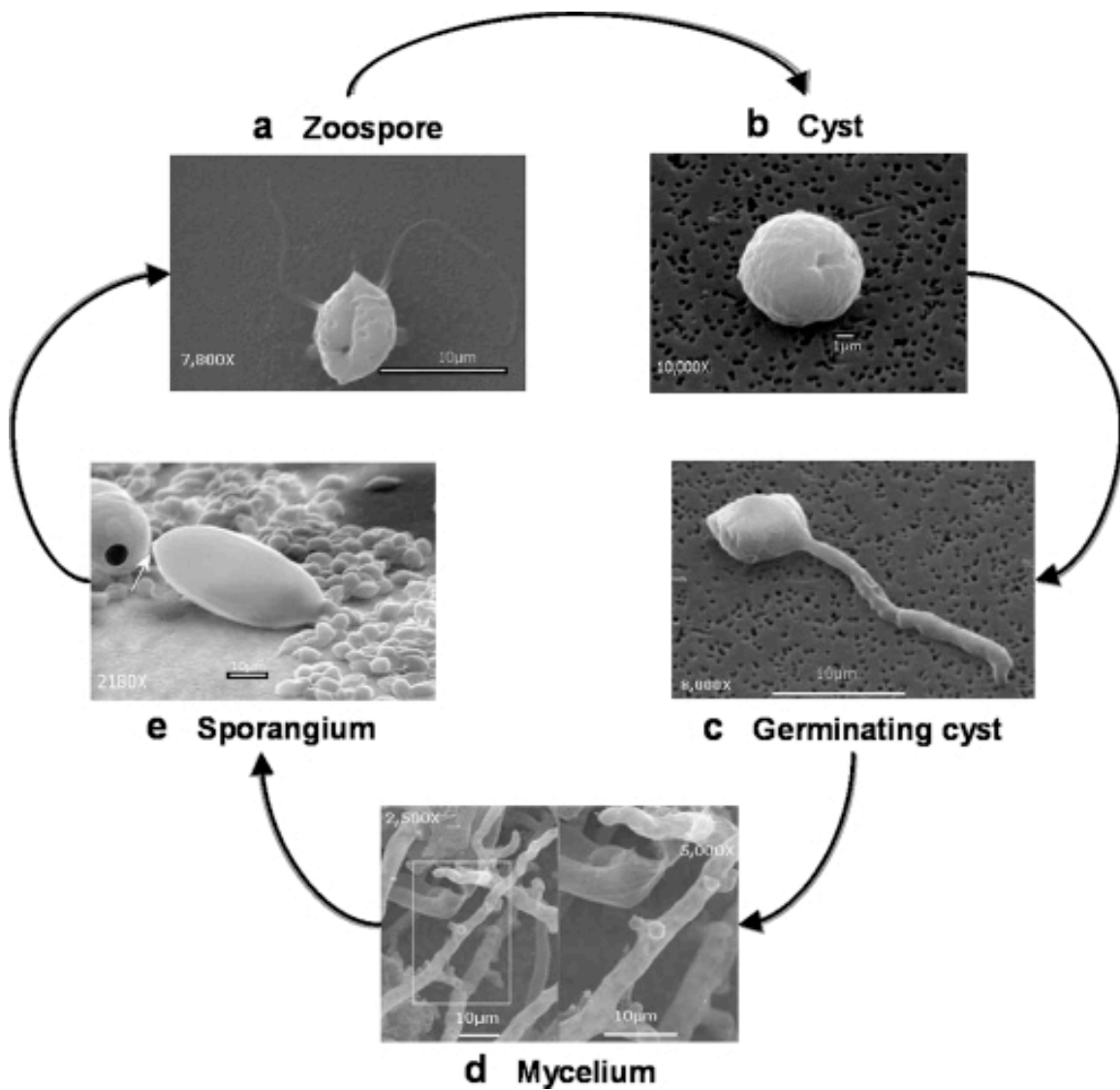


Figure 1.6. *Phytophthora ramorum* Asexual Life Cycle. Image is from (76) and permission was granted for the reuse of this figure. (A) The zoospore initiates infection by making contact with the plant host, and once the connection has been made, (B) the zoospore encysts after shedding the flagella. (C) Once germination occurs, a germ tube sprouts from the cyst that can be used to infiltrate the plant cells. (D) Growth then begins throughout the plant tissue by the mycelium. (E) The mycelium end differentiates into the sporangium, which produces the zoospores that re-initiate the cycle.

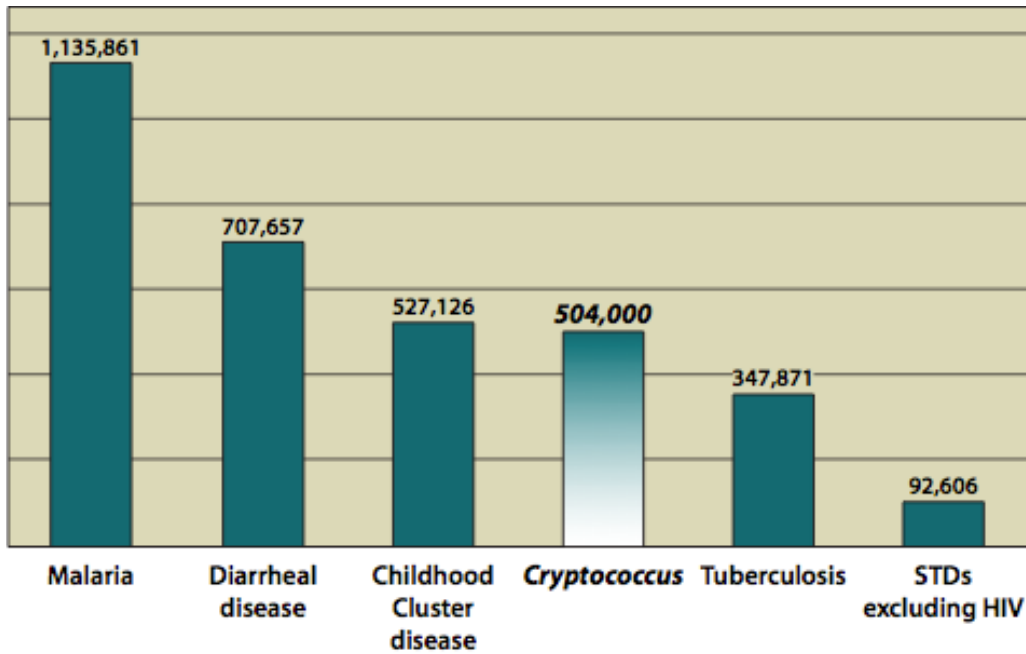


Figure 1.7. AIDS-related *Cryptococcosis* Kills Approximately 504,000 Individuals in Sub-Saharan Africa. In 2009, a study indicated that among common infectious diseases in Sub-Saharan Africa, excluding HIV, *Cryptococcus* infections are the 4th leading cause of death.

Image is from (83) and was adapted by CDC.gov. Permission was granted for reuse of this figure.

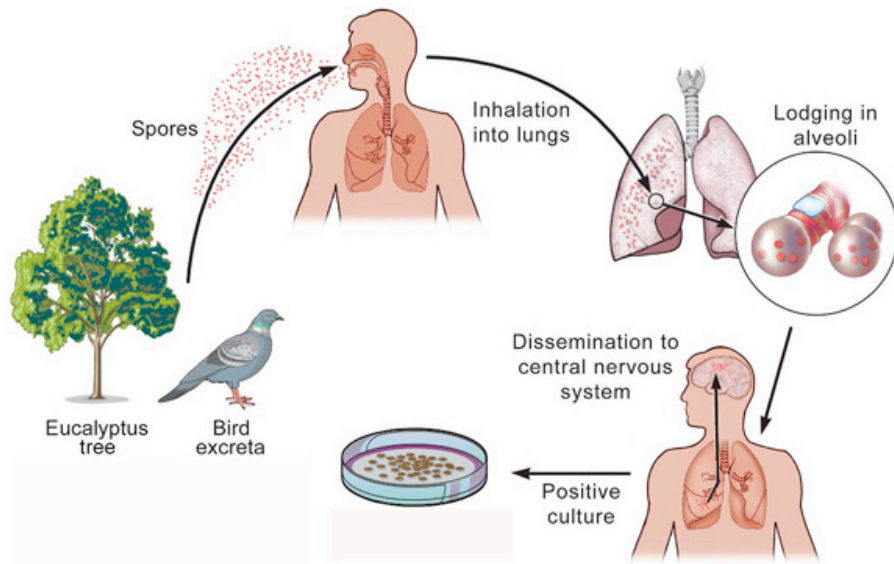


Figure 1.8. The Infection Cycle of *Cryptococcus neoformans*. *C. neoformans* is found within the environment, such as in the soil that is fertilized by pigeon excreta and eucalyptus trees. The spores of the fungus are inhaled into the lungs, and as consequence, a pulmonary infection is established. If an individual becomes immunocompromised, *C. neoformans* will disseminate throughout the body and enter the central nervous system (CNS). Cryptococcal meningitis can be detected through a positive cerebrospinal fluid culture. Image is from (85), and permission was granted for reuse of this figure.

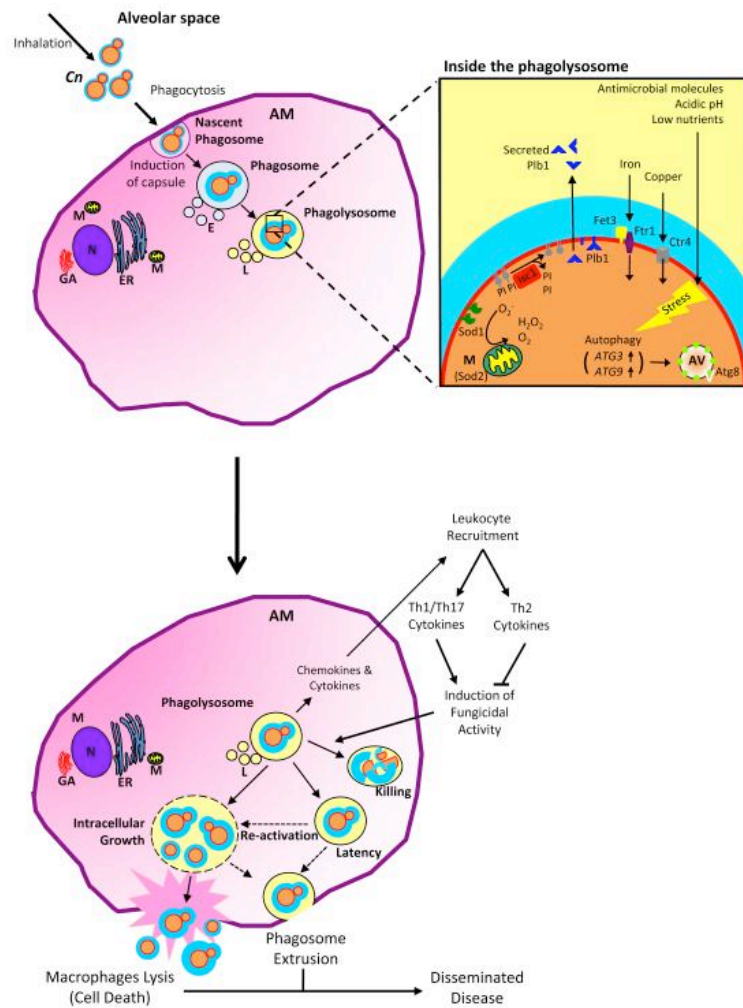


Figure 1.9. Survival and Replication of *C. neoformans* Within the Macrophage. The macrophage is used to hold and kill invading organisms within the host. However, *C. neoformans* has adapted to survive within the low pH of the macrophage, which provides protection from other immune cells activated due to the infection. The protection and mobility the macrophage provides, facilitates further *C. neoformans* infection. Image is from (90) and permission was granted for the reuse of this figure.

CHAPTER TWO

Biochemical and Kinetic Characterization of the Eukaryotic Phosphotransacetylase Type IIa Enzyme from *Phytophthora ramorum*¹

Tonya Taylor, Cheryl Ingram-Smith, and Kerry Smith

Abstract

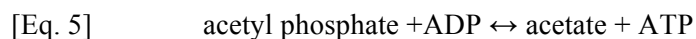
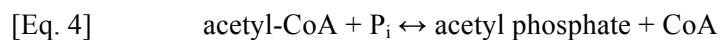
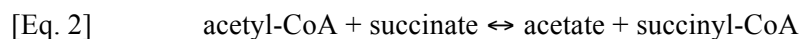
Phosphotransacetylase (Pta), a key enzyme in bacterial metabolism, catalyzes the reversible transfer of an acetyl group from acetyl phosphate to CoA to produce acetyl-CoA and P_i. Two classes of Pta have been identified based on the absence (Pta^I) or presence (Pta^{II}) of an N-terminal regulatory domain. Pta^I has been fairly well studied in bacteria and one genus of archaea; however, only the *Escherichia coli* and *Salmonella enterica* Pta^{II} enzymes have been biochemically characterized, and both are allosterically regulated. Here we describe the first biochemical and kinetic characterization of a eukaryotic Pta from the oomycete *Phytophthora ramorum*. The two Ptas from *P. ramorum*, designated as PrPta^{II}1 and PrPta^{II}2, both belong to class II. PrPta^{II}1 displayed positive cooperativity for both acetyl phosphate and CoA and is allosterically regulated. We compared the effect of different metabolites on PrPta^{II}1 and the *S. enterica* Pta^{II} and found that although the N-terminal regulatory domains share only 19% identity, both enzymes are inhibited by ATP, NADP, NADH, PEP, and pyruvate in the acetyl-CoA/P_i-forming direction but are differentially regulated by AMP. Phylogenetic analysis of bacterial, archaeal, and eukaryotic sequences identified four subtypes of Pta^{II} based on the presence or absence of the P-loop and DRTGG subdomains within the N-terminal regulatory domain. Although the *E. coli*, *S. enterica*, and *P. ramorum* enzymes all belong to the IIa subclass, our

¹ *Eukaryotic Cell*

kinetic analysis has indicated that enzymes within a subclass can still display differences in their allosteric regulation.

Introduction

Acetate production has been studied for many years in bacteria, but has received less attention in eukaryotic microbes even though acetate is produced as an important end product of energy metabolism in fungi (1-3) and protists (4-6). Four different pathways for production of acetate from acetyl-CoA have been identified in eukaryotic microbes (7). ADP-forming acetyl-CoA synthetase (Eq. 1; EC 6.2.1.13) has been implicated in acetate production in amitochondriate protists and some species of archaea. Acetate:succinate CoA-transferase (Eq. 2; EC 2.8.3.8) is present in kinetoplastids and *Trichomonas*. Acetyl-CoA hydrolase (Eq. 3; EC 3.1.2.1) is involved in peroxisomal acetate formation in yeast and kinetoplastids, such as *Trypanosoma brucei* (7, 8). Phosphotransacetylase (Pta; Eq. 4; EC 2.3.1.8) and acetate kinase (Ack; Eq. 5; EC 2.7.2.1) form a pathway for the interconversion of acetate and acetyl-CoA that was previously thought to be limited to bacteria and one genus of archaea but has now been shown to be present in eukaryotes such as green algae and *Phytophthora* (9, 10).



The Pta-Ack pathway is best understood in its roles in both acetate production and assimilation in *Escherichia coli* and other bacteria. This pathway is responsible for the production of acetate during mixed acid fermentation under hypoxic conditions, and in a metabolic overflow mechanism in which acetyl-CoA is diverted from the TCA cycle when there is an imbalance between the rapid uptake of glucose and its conversion into products (11). Under high acetate

concentrations, this low affinity pathway can also be used for assimilation of acetate by its conversion to acetyl-CoA (12).

In eukaryotes, the Pta-Ack pathway has only been investigated in the green algae *Chlamydomonas*, in which two parallel Pta-Ack pathways have been identified (9). Proteomic studies have suggested that the Pat1-Ack2 pathway is localized to mitochondria (note that phosphotransacetylase is designated as Pat in *Chlamydomonas*), and the Pat2-Ack1 pathway is localized to chloroplasts (9, 13). Acetate is found to be one of the major fermentative products excreted by *Chlamydomonas* during growth in dark, anoxic conditions, and *ACK1*, *ACK2*, *PAT1*, and *PAT2* transcript levels are increased, in agreement with a role for the Pat-Ack pathway in acetate production (14). The *ack1* and *pat2* mutants were the most vulnerable to anoxia and strains could not be recovered after a 24 hour exposure to anoxia (15). Far less acetate was produced in each of the mutants after imposition of anoxia, yet small amounts of acetate (<20%) were still produced in the *ack1-ack2* double mutant suggesting Pat-Ack is not the only pathway for acetate production in *Chlamydomonas* (15).

Analysis of bacterial and archaeal Pta sequences revealed two classes (16). Pta^I enzymes consist of a single catalytic domain, whereas the Pta^{II} enzymes have an additional N-terminal regulatory domain (16, 17). The Pta from the archaeon *Methanosarcina thermophila* is the best studied class I enzyme (18-21), and several structures have been solved (22, 23). A ternary complex mechanism based on kinetic and structural studies has been proposed for this enzyme (20). Two Pta^{II} enzymes have been characterized, one from *Salmonella enterica* (SePta^{II}) and one from *E. coli* (EcPta^{II}) (16, 17); however, a structure for a Pta^{II} has not been reported. The N-terminal regulatory domain of EcPta^{II} and SePta^{II} contains two recognizable subdomains designated as the P-loop and the DRTGG subdomains (17). Truncations of the N-terminal domain of EcPta^{II} revealed that the P-loop subdomain is required for regulation of the enzyme by NADH,

ATP, PEP and pyruvate, and that the DRTGG subdomain is vital for the sigmoidal response that is observed in allosteric enzymes (16, 17).

Here we report the first biochemical and kinetic investigation of a eukaryotic Pta, the Pta^{II} enzyme from *Phytophthora ramorum*, a pathogenic oomycete that causes Sudden Oak Death (24). *P. ramorum* has a single ORF that encodes Ack and two ORFs that encode class II Ptas (designated here as PrPta^{II}1 and PrPta^{II}2). Our characterization of PrPta^{II}1 demonstrates that this enzyme strongly prefers the acetyl-CoA/P_i-forming direction, unlike the *S. enterica* and *E. coli* enzymes. PrPta^{II}1 displays substrate cooperativity for acetyl phosphate and CoA, and is allosterically regulated through inhibition by ATP, AMP, NADP, NADH, PEP, and pyruvate. Our phylogenetic analysis of the Pta family, the first reported that includes eukaryotic sequences, indicates there are four different subclasses of Pta^{II} based on differences in the N-terminal regulatory domain. A comparison of the bacterial and eukaryotic enzymes and the phylogenetic diversity suggests that the N-terminal domain and its regulatory role have evolved throughout the Bacteria and Eukarya domains.

Materials and Methods

Materials

Chemicals were purchased from Sigma-Aldrich, VWR, Fisher Scientific, and Gold Biotechnology. Oligonucleotide primers were purchased from Integrated DNA Technologies. A codon-optimized gene encoding *P. ramorum* PrPta^{II}1 (JGI 78441; http://genome.jgi-psf.org/Phyra1_1/Phyra1_1.home.html) was synthesized by GenScript and supplied in the *E. coli* expression vector pET21b, which provides for addition of a C-terminal His tag for use in nickel affinity column purification. Plasmid pPTA69 (kindly provided by Dr. Jorge Escalante-Semerena, University of Georgia) encodes *S. enterica* Pta^I with a His₆ tag fused to the N-terminus of the protein (16).

Phylogenetic Analysis of Pta

BLASTP and TBLASTN (25, 26) were used to search the sequence databases at the National Center for Biotechnology Information (NCBI) (www.ncbi.nlm.nih.gov), the Broad Institute (<http://www.broadinstitute.org/>), and the U.S. Department of Energy Joint Genome Institute (<http://genome.jgi-psf.org/>) for putative Pta amino acid sequences, using the *M. thermophila* Pta^I as the query sequence. Sequences were aligned using ClustalW with the Gonnet protein weight matrix, a gap-opening penalty of 10.0, and a gap extension penalty of 0.2 (27). Phylogenetic analysis of the aligned sequences was performed with the MEGA 5.1 program (28) using the neighbor-joining algorithm with partial deletion estimates. Five hundred bootstrap replicates were executed, and bootstrap values of 75% or greater are shown. The EMBOSS Needle Pairwise Sequence Alignment program (<http://www.ebi.ac.uk>) was used to determine sequence identity and similarity (29). The presence or absence of the P-loop and DRTGG

subdomains in each Pta^{II} sequence was analyzed using the Pfam Protein Families Database (<http://pfam.xfam.org/search>) with an e-value cutoff of E^{-10} (30).

Heterologous Production and Purification of Pta

Recombinant plasmids were transformed into *E. coli* RosettaTM 2 (DE3) pLysS, and cells were grown in Luria-Bertani broth with 50 $\mu\text{g}/\text{mL}$ ampicillin and 34 $\mu\text{g}/\text{mL}$ chloramphenicol at 37°C shaking at 200 rpm until an OD₆₀₀ of 0.6 – 0.8 was reached. Production of recombinant Pta was induced by addition of isopropyl- β -D-thiogalactopyranoside to a final concentration of 1 mM.

Following overnight incubation at ambient temperature, cells were harvested by centrifugation. Cells were resuspended in Buffer A (25 mM Tris, 150 mM NaCl, 25 mM imidazole, 10% glycerol; pH 7.5), disrupted by three passages through a chilled French pressure cell at 138 mPa, and centrifuged at 100,000 x g for 90 minutes at 4°C. The supernatant was applied to a HisTrapTM HP Ni²⁺ affinity column (GE Healthcare, Inc.) equilibrated with Buffer A. The protein was eluted using a linear gradient from 25 mM to 500 mM imidazole in 25 mM Tris-HCl, 150 mM NaCl, and 10% glycerol (pH 7.5). Fractions with Pta activity were pooled and dialyzed against buffer containing 25 mM Tris-HCl and 10% glycerol (pH 7.5). The recombinant enzyme was determined to be electrophoretically pure by SDS-PAGE. The protein concentration for purified PrPta^{II}1 was calculated from the absorbance at 280 nm using an extinction coefficient of 36,330 $\text{M}^{-1}\text{cm}^{-1}$.

Activity Assays

PrPta^{II}1 activity in the acetyl-CoA forming direction was measured by monitoring the increase in absorbance at 233 nm due to thioester bond formation ($\epsilon_{233 \text{ nm}} = 5.55 \text{ mM}^{-1} \text{ cm}^{-1}$) (16,

17). The reaction mixture contained 50 mM Tris (pH 7.5), 20 mM KCl, 20 mM NH₄Cl, 1 mM DTT, and the concentrations of acetyl phosphate and CoA were varied. Activity in the acetyl phosphate forming direction was measured with two different assays. The thioester assay monitors the decrease in absorbance at 233 nm due to the release of CoA ($\epsilon_{233 \text{ nm}} = 4.44 \text{ mM}^{-1} \text{ cm}^{-1}$) (18), and the Ellman's thiol reagent assay monitors the increase in absorbance at 412 nm due to the formation of the thiophenolate anion with DTNB [5',5-dithiobis(2-nitrobenzoic acid); $\epsilon_{233 \text{ nm}} = 14,150 \text{ M}^{-1} \text{ cm}^{-1}$] (16, 17). The reaction mixtures for both assays contained 50 mM Tris (pH 7.5), 20 mM KCl, 20 mM NH₄Cl, 1 mM DTT, and the concentrations of acetyl-CoA and P_i were varied. The Ellman's thiol reagent assay also included 1 mM DTNB. Reaction mixtures for all assays were pre-incubated for 3 minutes at 37°C. Reactions were initiated by the addition of enzyme and were performed in triplicate.

SePta^{II} activity in the acetyl-CoA forming direction was measured by monitoring the increase in absorbance at 233 nm. The reaction mixture contained 50 mM Tris (pH 7.5), 40 mM NH₄Cl, 1 mM CoA, and 3 mM acetyl phosphate. Reaction mixtures containing acetyl phosphate and enzyme were pre-incubated for 1 min at 37°C, and reactions were initiated by the addition of CoA. All reactions were performed in triplicate.

Assays were performed in 96-well plates and the absorbance was monitored using the Synergy HT Multi-mode Microplate Reader (BioTek Instruments, Inc.). Data are expressed as mean \pm S.D.

Kinetic Analysis

To determine apparent kinetic parameters for PrPta^{II}1 in the acetyl-CoA forming direction, the concentration of one substrate was varied while the second substrate was held constant at saturating concentration (determined to be 4 mM for CoA and 5 mM for acetyl

phosphate). KaleidaGraph (Synergy Software) was used to fit the data to the Michaelis-Menten equation [Equation 6], where V_0 is initial velocity, $[S]$ is substrate concentration, V is maximum velocity, and K_m is the Michaelis constant.

$$\text{[Eq. 6]} \quad V_0 = V \times [S] / (K_m + [S])$$

When acetyl phosphate was varied, the data displayed positive cooperativity when fit to the Hill equation [Equation 7] (31, 32), where $K_{0.5}$ is the substrate concentration at half maximal velocity and h is the Hill constant.

$$\text{[Eq. 7]} \quad V_0 = V \times [S]^h / (K_{0.5}^h + [S]^h)$$

Determining IC₅₀ Concentration

Metabolic intermediates, coenzymes, and nucleotide triphosphates were tested as allosteric effectors of PrPta^{II}1 and SePta^{II}. Substrate concentrations were held at saturating conditions, and effector molecule concentrations were varied from 3 μ M to 3 mM. Half maximal inhibitory concentrations (IC₅₀) were determined for all PrPta^{II}1 and SePta^{II} allosteric inhibitors by measuring the decrease in activity as a function of increasing inhibitor concentration. IC₅₀ values were determined using GraphPad Prism 5 (GraphPad Software, Inc.) by fitting the data with a log [inhibitor] vs. response curve.

Site-directed Mutagenesis

The QuikChange[®] Lightning Site-Directed Mutagenesis kit (Stratagene, Inc.) was used for mutagenesis according to the manufacturer's instructions. Primers used in the alteration of the Gly-300 codon are as follows: 5'PrPTAG300D, CACCTGAAAAATATAAAGACGACGCGATGATTATCACCAGTGGT; 3'PrPTAG300D, ACCACTGGTGATAATCATCGCGTCGTCTTTATATTTTTTCAGGTG; 5'PrPTAG300A

CACCTGAAAAAATATAAAGACGCGGCGATGATTATCACCAGTGGT; 3'PrPTAG300A
ACCACTGGTGATAATCATCGCCGCGTCTTTATATTTTTTCAGGTG. Alterations were
confirmed by sequencing at the Clemson University Genomic Institute (CUGI).

Gel Filtration Chromatography

The native molecular mass of recombinant PrPta^{II}1 was examined by gel filtration chromatography using an ÄKTA Fast Protein Liquid Chromatography (FPLC) system with a Superose 12 column (GE Healthcare). The gel filtration column was calibrated with cytochrome C (12.4 kDa), carbonic anhydrase (29 kDa), albumin (66 kDa), amylase (200 kDa), apoferritin (443 kDa), and thyroglobulin (669 kDa) (Sigma Aldrich Co.). The column was equilibrated with buffer containing 50 mM Tris and 150 mM KCl (pH 7.5) and developed at a rate of 0.5 mL/min.

Results

Discovery of the Different Subclasses of Pta^{II}

The Pta enzyme family has previously been divided into two classes (16). Pta^I enzymes are approximately 350 amino acids long and consist of only a catalytic domain. Pta^{II} enzymes are approximately twice the size, with a C-terminal catalytic domain and an N-terminal regulatory domain (16, 17). Although Pta was commonly considered to be a bacterial enzyme, sequences have now been identified in the Eukarya (10). To determine the extent of the Pta enzyme family in this domain, searches of the sequence databases were performed using the *Methanosarcina thermophila* Pta^I sequence as the query. Pta sequences were identified in a number of eukaryotes such as green algae, lycophytes, moss, and oomycetes, but were absent in fungi, higher plants, and metazoans. Every completed eukaryotic genome that has a Pta sequence also has an ORF with identity to Ack, consistent with these enzymes acting as a pathway as in bacteria. In a phylogeny of Pta sequences constructed based on the catalytic domain, the Pta^{II} sequences form a separate clade (**Figure 1**). All of the eukaryotic sequences belong to the Pta^{II} class except for those from *Perkinsus marinus* and *Thecamonas trahens*. The *Emiliana huxleyi* Pta (shown in red in **Figure 1**) is a fusion to Ack, and thus is also considered to be a Pta^I rather than Pta^{II}.

The N-terminal regulatory domains of EcPta^{II} and SePta^{II} contain two recognizable subdomains designated as the P-loop and the DRTGG subdomains (17). The P-loop NTPase subdomain contains a conserved nucleotide triphosphate-binding motif similar to that found in enzymes involved in translation, transcription, intracellular trafficking, membrane transport, and DNA replication and repair (33). The DRTGG subdomain has an unknown function, but is named after some of its most conserved residues. This domain is related to the cystathione-beta-synthase

domain (CBS) that exists in both membrane-bound and cytosolic proteins, and is known to function in eukaryotes, prokaryotes, and archaea (34).

Although the Pta^{II} N-terminal domains are similar in size, analysis of their sequences has revealed four subclasses based on the presence or absence of the P-loop and DRTGG subdomains (**Figure 2**). The Pta^{IIa} N-terminal domain includes both subdomains, whereas the Pta^{IIb}, Pta^{IIc}, and Pta^{II} subclasses lack one or both subdomains. The majority of Pta^{II} sequences belong to the Pta^{IIa} subclass, with Pta^{IIb}, Pta^{IIc}, and Pta^{II d} sequences distributed infrequently throughout the phylogeny. Surprisingly, the two *C. reinhardtii* Pta^{II} enzymes belong to two different subclasses, Pta^{II d} and Pta^{IIc}.

Purification and Molecular Properties of PrPta^{II}1

The genome of *P. ramorum* (http://genome.jgi-psf.org/Phyra1_1/Phyra1_1.home.html) has two Pta^{IIa} ORFs, designated as Pta^{II}1 (Protein ID 78441) and Pta^{II}2 (Protein ID 78440). An *E. coli* codon-optimized gene encoding PrPta^{II}1 (GenScript Inc.) was cloned into pET21b (C-terminal His tag), and the recombinant enzyme was produced in *E. coli* and purified by nickel affinity chromatography to electrophoretic homogeneity. In determining optimal reaction conditions for PrPta^{II}1, we tested the requirement for KCl and NH₄Cl, as other Pta^{II} enzymes have been shown to have increased activity in the presence of one or both salts (16, 17). Maximum activity was observed in the presence of 20 mM NH₄Cl and 20 mM KCl, and both salts are required. Increasing the concentration of either or both salts does not further increase enzyme activity. Optimal activity also requires the presence of 1 mM DTT final concentration. PrPta^{II}1 has highest activity at 37°C; therefore, all experiments were conducted at 37°C. Due to aggregation issues, the molecular mass of the enzyme could not be determined by gel filtration. Brinsmade and Escalante-Semerena (16) encountered similar discrepancies with the *S. enterica*

Pta.

Kinetic Analysis of PrPta^{II}1

In determining kinetic parameters for PrPta^{II}1 in the acetyl-CoA/P_i – forming direction, plots of substrate concentration versus velocity were sigmoidal. Apparent kinetic parameters were determined by fitting the experimental data to the Hill equation (**Eq. 7**) in which a Hill constant (*h*) greater than 1.0 represents positive cooperativity and a Hill constant less than 1.0 represents negative cooperativity (35, 36). PrPta^{II}1 exhibited positive cooperativity ($h = 1.75 \pm 0.18$) with acetyl phosphate and slight positive cooperativity ($h = 1.04 \pm 0.05$) with CoA (**Table 1**). The maximum activity observed in the acetyl phosphate/CoA-forming direction is approximately three-fold lower than that in the acetyl-CoA/P_i-forming direction ($8.9 \pm 0.5 \mu\text{mol min}^{-1} \text{mg}^{-1}$ versus $23.8 \pm 0.7 \mu\text{mol min}^{-1} \text{mg}^{-1}$, respectively), but kinetics parameters could not be determined in this direction due to an inability to reach saturation with inorganic phosphate.

Allosteric Regulation of the Pta^{IIa} Enzyme Family

Although the catalytic domains of all Pta enzymes share strong identity (e.g., the catalytic domains of PrPta^{II}1 and SePta^{II} share 52.0% identity), the N-terminal domains within a subclass can differ substantially. The PrPta^{II}1 N-terminal domain shares only 19% identity with the N-terminal domains of the *E. coli* and *S. enterica* Pta^{IIa} enzymes, raising the question of whether this eukaryotic Pta is subject to similar allosteric regulation as the bacterial Pta^{II} enzymes. We tested metabolic intermediates from both the glycolytic pathway and citric acid cycle as effector molecules of PrPta^{II}1. NAD⁺, NADH, NADP, and NADPH were potent inhibitors, with NADP having the strongest effect (**Figure 3A**). ATP, ADP, AMP, PEP, and pyruvate were also found to inhibit activity (**Figure 3B**), but to a lesser extent than the nicotinamide derivatives. Fructose-1,6-

bisphosphate (1 mM), oxaloacetate (1 mM), a-ketoglutarate (1.5 mM), and citrate (1.5 mM) had no effect on PrPta^{II}1 activity.

Although SePta^{II} and EcPta^{II} were shown to be allosterically regulated (16, 17), only ATP, NADH, PEP and pyruvate were examined for EcPta^{II}, and only pyruvate and NADH were tested in the acetyl phosphate-forming direction for SePta^{II}. IC₅₀ values were not reported for EcPta^{II} and the IC₅₀ values for SePta^{II} were reported only in the acetyl phosphate/CoA – forming direction. To allow direct comparison between the eukaryotic and bacterial enzymes, the effects of ATP, AMP, NADP, NADH, PEP and pyruvate on SePta^{II} enzymatic activity were determined in the acetyl-CoA/P_i – forming direction and IC₅₀ values were determined (**Table 2**). Our results show that both SePta^{II} and PrPta^{II}1 are regulated by the same allosteric effectors although the potency differed.

Because NADP was the most potent inhibitor for PrPta^{II}1, we evaluated its effect on substrate affinity. The K_m values for CoA were relatively unchanged by the presence of increasing concentrations of NADP but the V_{max} decreased (**Figure 4A**), suggesting mixed inhibition by NADP towards CoA. The $K_{0.5}$ values for acetyl phosphate increase and the cooperativity decreases as the NADP concentration is increased (**Figure 4B**), indicating that NADP has a direct effect on the affinity of PrPta^{II}1 for acetyl phosphate.

For PrPta^{II}1, activity steadily decreases as AMP concentration is increased, similar to the behavior observed with other PrPta^{II}1 effectors. Surprisingly, AMP has a much different effect on SePta^{II}, resulting in activation of the enzyme when present at low concentrations and inhibition at higher concentrations. SePta^{II} has 28% higher activity in the presence versus absence of 30 μ M AMP (**Figure 5**); however, as the concentration of AMP was increased to 100 μ M, the activity returned to the level observed in the absence of effector. Activity is inhibited further as the AMP

concentration is increased, with approximately 50% inhibition in the presence of 1 mM and complete loss of activity at 3 mM AMP.

Analysis of PrPta^IG^{300D} and PrPta^IG^{300A}

Brinsmade and Escalante-Semerena (16) previously identified three single amino acid changes in the N-terminal domain of PrPta^I1 that resulted in altered responses to allosteric effectors. A G²⁷³D variant had approximately two-fold increased V_{\max} in the acetyl-CoA/P_i – forming direction and three-fold increased V_{\max} in the acetyl phosphate/CoA – forming direction. This variant also showed approximately three-fold stimulation by pyruvate versus 0.2-fold stimulation for the wild type enzyme, but remained subject to strong inhibition by NADH (16). This Gly residue is conserved in both PrPta^I1 and PrPta^I2, unlike the other two residues identified that altered the wild type SePta^I response to allosteric regulators.

To investigate the role of the conserved Gly residue in allosteric regulation of PrPta^I1, we targeted the corresponding residue Gly³⁰⁰ for alteration. The G³⁰⁰A variant was soluble but was not active in either direction of the reaction. Kinetic analysis of the PrPta^I1 G³⁰⁰D variant revealed a nearly 450-fold reduction in the catalytic rate in the acetyl-CoA forming direction (**Table 1**) and activity was completely abolished in the acetyl phosphate forming direction, indicating the importance of this residue in catalysis. A slight decrease in the $K_{0.5}$ for acetyl phosphate and a four-fold decrease in the $K_{0.5}$ for CoA were observed for the G³⁰⁰D variant versus the wild type enzyme. The $k_{\text{cat}}/K_{0.5}$ value for each substrate decreased significantly, with a 420-fold decrease for acetyl phosphate and a 110-fold decrease observed for CoA (**Table 1**). This alteration resulted in increased substrate cooperativity for both CoA and acetyl phosphate. The Hill constant for CoA increased by half, and that for acetyl phosphate increased 3.7-fold versus the wild type (**Table 1**).

We analyzed the effect of several allosteric inhibitors on the PrPta^{II}1 G³⁰⁰D variant and found that the IC₅₀ values for ATP, AMP, and NADH decreased approximately five-fold versus the wild type, whereas only a 1.6-fold decrease was observed for NADP (**Table 2**). A nearly 14-fold decrease was observed in the IC₅₀ for PEP (**Table 2**). Interestingly, nearly 50% inhibition was observed with 50 μM pyruvate, but activity increased as the pyruvate concentration was increased. At 1 mM pyruvate, enzyme activity had reached the uninhibited level and by 3 mM pyruvate concentration activity was 124% that of the control (**Figure 6**). The EC₅₀ for pyruvate was determined to be 503 ± 24 μM.

Discussion

Phylogenetic analysis of Pta sequences shows that Pta^I and Pta^{II} sequences form separate clades (**Figure 1**). Notably, nearly all of the eukaryotic enzymes belong to the Pta^{II} class, whereas both Pta^I and Pta^{II} enzymes are well represented in the bacteria. In fact, *E. coli* and *S. enterica* possess both Pta^I and Pta^{II} enzymes. Based on these distributions and what is currently known about the roles of Pta in various bacteria and *Chlamydomonas*, it is difficult to determine what dictates whether an organism is more likely to have a Pta^I or a Pta^{II}.

Our sequence analysis of the regulatory domain of Pta^{II} enzymes has revealed four subclasses based on the presence or absence of the P-loop and DRTGG subdomains. Our phylogeny indicates that the eukaryotic enzymes group together within the Pta^{II} clade, and that the eukaryotic Pta^{IIa} sequences are clustered together. Both of the *P. ramorum* Pta^{II} sequences belong to this subclass and fall within this cluster.

Like *P. ramorum*, *Chlamydomonas reinhardtii* and *Volvox carteri* also have two Pta^{II} enzymes. However, Pat2 from *C. reinhardtii* lacks the DRTGG subdomain and thus belongs to the Pta^{IIc} subclass, whereas Pat1 lacks identity to either subdomain within the N-terminus and is classified as a Pta^{II d}. The *V. carteri* Pta^{II} sequences both belong to Pta^{IIc} and are most closely related to the *P. ramorum* enzymes. The Pta^{IIa} subclass is the most prevalent, followed by Pta^{II d}. The infrequent number of Pta^{IIb} and Pta^{IIc} sequences and their distribution throughout the phylogeny suggests these subclasses arose recently and sporadically through the loss of domains.

Eukaryotic Pta^{II} versus Bacterial Pta^{II}

Our characterization of PrPta^{II1} allowed us to investigate the similarities and differences between bacterial and eukaryotic Pta^{II} enzymes and provides us with a better overall picture of the regulation of this subclass. PrPta^{II1}, SePta^{II}, and EcPta^{II} all display positive cooperativity but for

different substrates. SePta^{II} and PrPta^{II}1 display positive cooperativity for acetyl phosphate but little or no cooperativity for CoA, whereas EcPta^{II} displays positive cooperativity for CoA but not for acetyl phosphate.

As EcPta^{II} and SePta^{II} are both allosterically regulated (16, 17), we examined whether PrPta^{II}1 is also subject to allosteric regulation and if the same metabolites are effectors for all three enzymes. ATP, NADH, PEP and pyruvate were previously shown to be inhibitors of EcPta^{II} (17), and we have now shown that they are also inhibitors of SePta^{II} and PrPta^{II}1, although the order of potency of these inhibitors differs. We have also found that AMP influences both SePta^{II} and PrPta^{II}1 activity but in different ways. AMP inhibits PrPta^{II}1 but activates SePta^{II} at lower concentration and then inhibits activity at higher concentrations. AMP has a similar effect on glycogen phosphorylase (37). At low concentrations, AMP acts as a strong activator by binding to a site close to the subunit interface and increasing release of glucose 1-phosphate from glycogen (38, 39). At higher concentrations, AMP binds to the ATP inhibitor site (40, 41) located at the entrance to the channel to the catalytic site (41), resulting in inhibition. By analogy, this may suggest that AMP and ATP bind at separate effector sites on SePta^{II}.

The Role of the P-loop and DRTGG Subdomains in Catalysis and Allosteric Regulation

Through analysis of EcPta^{II} truncations, Campos-Bermudez *et al.* (17) demonstrated that the N-terminal domain is required for maximal catalytic activity and that the P-loop subdomain is required for the regulation of the enzyme by metabolic effector molecules. Using a positive selection method to identify Pta variants that allow *S. enterica* growth on low acetate concentrations in an *acs* mutant, Brinsmade and Escalante-Semerena (16) identified three single amino acid variants altered in the N-terminal domain for which regulation by allosteric effectors differs. Of particular interest is the G²⁷³D SePta^{II} variant, which displayed much stronger

activation by pyruvate than the wild type enzyme but similar inhibition by NADH (16). This glycine is located in the DRTGG subdomain and is conserved among all Pta^{IIa} and Pta^{IIb} enzymes, including both enzymes from *P. ramorum*.

We altered Gly³⁰⁰, the equivalent residue in PrPta^{II1}, to Ala and Asp to investigate whether this enzyme is regulated similarly to SePta^{II}. The G³⁰⁰A variant lacked activity in either direction, and the G³⁰⁰D variant had greatly reduced activity in the acetyl-CoA/P_i – forming direction and no activity in the acetyl phosphate/CoA forming direction. With the exception of pyruvate, each allosteric effector had a similar effect on activity of the PrPta^{II1} G³⁰⁰D variant as for the wild type, although IC₅₀ values were reduced. Remarkably, pyruvate enhanced activity of the variant in the acetyl-CoA/P_i-forming direction. However, activity was still very low in the opposite direction. In the corresponding SePta^{II} variant, this alteration greatly stimulated activity in the acetyl phosphate/CoA forming direction. This result demonstrates that residue G³⁰⁰ in the DRTGG subdomain of the N-terminal regulatory domain is important across both bacteria and eukaryotes in how the enzyme reacts to the presence and absence of pyruvate.

Concluding Remarks

Our knowledge of Pta and its physiological role has largely been limited to bacterial enzymes. The Pta-Ack pathway has been shown to be essential for growth and invasion in several pathogenic bacteria, including *Vibrio cholera* (42), uropathogenic *E. coli* (43), *S. enterica* (44), and *Listeria monocytogenes* (45). A eukaryotic Pta has not previously been characterized, and the only reports on the physiological role of a non-bacterial Pta are from the green algae *Chlamydomonas* (15). PrPta^{II1} preferentially operates in the acetyl-CoA/P_i-forming direction, suggesting acetyl-CoA formation is its physiological role in *Phytophthora*. The presence of a second Pta raises the possibility that the two enzymes are specialized, with PrPta^{II2} operating in

the acetyl phosphate/CoA-forming direction. Alternatively, PrPta^{II}2 may catalyze both directions of the reaction and metabolic effectors may regulate these activities as well as the activity of PrPta^{II}1.

The Pta^{II} class is much more complex than previously thought, with four subclasses, and Pta^{IIa} enzymes are subject to allosteric regulation by a number of effectors (46, 47). Regulation of enzymes from the other three subclasses and further study of the N-terminal domain is needed. An understanding of the regulation exerted by this domain would be greatly facilitated by having a structure of a Pta^{II} enzyme. Characterization of PrPta^{II}2 might help answer some of elusive questions regarding the N-terminal domain.

Acknowledgments

This work was supported by awards from the National Science Foundation (Award# 0920274) and the South Carolina Experiment Station Project SC-1700340, and represents Technical Contribution #6242 of the Clemson University Experiment Station.

References

1. Bubb WA, Wright LC, Cagney M, Santangelo RT, Sorrell TC, Kuchel PW. 1999. Heteronuclear NMR studies of metabolites produced by *Cryptococcus neoformans* in culture media: identification of possible virulence factors. *Magn Reson Med* **42**:442-453.
2. Himmelreich U, Allen C, Dowd S, Malikic R, Shehan BP, Mountford C, Sorrell TC. 2003. Identification of metabolites of importance in the pathogenesis of pulmonary cryptococcoma using nuclear magnetic resonance spectroscopy. *Microbes and Infection* **5**:1427-1438.
3. Oura E. 1977. Reaction products of yeast fermentations. *Process Biochem* **12**:19-21.
4. Mazet M, Morand P, Biran M, Bouyssou G, Courtois P, Daulouede S, Millerieux Y, Franconi JM, Vincendeau P, Moreau P, Bringaud F. 2013. Revisiting the central metabolism of the bloodstream forms of *Trypanosoma brucei*: production of acetate in the mitochondrion is essential for parasite viability. *PLoS Negl Trop Dis* **7**:e2587.
5. Montalvo FE, Reeves RE, Warren LG. 1971. Aerobic and anaerobic metabolism in *Entamoeba histolytica*. *Exp Parasitol* **30**:249-256.
6. Reeves RE, Warren LG, Susskind B, Lo HS. 1977. An energy-conserving pyruvate-to-acetate pathway in *Entamoeba histolytica*. Pyruvate synthase and a new acetate thiokinase. *J Biol Chem* **252**:726-731.
7. Tielens AG, van Grinsven KW, Henze K, van Hellemond JJ, Martin W. 2010. Acetate formation in the energy metabolism of parasitic helminths and protists. *Int J Parasitol* **40**:387-397.
8. Lee FJ, Lin LW, Smith JA. 1990. A glucose-repressible gene encodes acetyl-CoA hydrolase from *Saccharomyces cerevisiae*. *J Biol Chem* **265**:7413-7418.
9. Atteia A, van Lis R, Gelius-Dietrich G, Adrait A, Garin J, Joyard J, Rolland N, Martin W. 2006. Pyruvate formate-lyase and a novel route of eukaryotic ATP synthesis in *Chlamydomonas* mitochondria. *J Biol Chem* **281**:9909-9918.

10. Ingram-Smith C, Martin SR, Smith KS. 2006. Acetate kinase: not just a bacterial enzyme. *Trends Microbiol* **14**:249-253.
11. Akesson M, Karlsson EN, Hagander P, Axelsson JP, Tocaj A. 1999. On-line detection of acetate formation in *Escherichia coli* cultures using dissolved oxygen responses to feed transients. *Biotechnol Bioeng* **64**:590-598.
12. Wolfe AJ. 2005. The acetate switch. *Microbiol Mol Biol Rev* **69**:12-50.
13. Terashima M, Specht M, Naumann B, Hippler M. 2010. Characterizing the anaerobic response of *Chlamydomonas reinhardtii* by quantitative proteomics. *Mol Cell Proteomics* **9**:1514-1532.
14. Mus F, Dubini A, Seibert M, Posewitz MC, Grossman AR. 2007. Anaerobic acclimation in *Chlamydomonas reinhardtii*: anoxic gene expression, hydrogenase induction, and metabolic pathways. *J Biol Chem* **282**:25475-25486.
15. Yang W, Catalanotti C, D'Adamo S, Wittkopp TM, Ingram-Smith CJ, Mackinder L, Miller TE, Heuberger AL, Peers G, Smith KS, Jonikas MC, Grossman AR, Posewitz MC. 2014. Alternative acetate production pathways in *Chlamydomonas reinhardtii* during dark anoxia and the dominant role of chloroplasts in fermentative acetate production. *Plant Cell* doi:10.1105/tpc.114.129965.
16. Brinsmade SR, Escalante-Semerena JC. 2007. In vivo and in vitro analyses of single-amino acid variants of the *Salmonella enterica* phosphotransacetylase enzyme provide insights into the function of its N-terminal domain. *J Biol Chem* **282**:12629-12640.
17. Campos-Bermudez VA, Bologna FP, Andreo CS, Drincovich MF. 2010. Functional dissection of *Escherichia coli* phosphotransacetylase structural domains and analysis of key compounds involved in activity regulation. *FEBS J* **277**:1957-1966.
18. Lawrence SH, Ferry JG. 2006. Steady-state kinetic analysis of phosphotransacetylase from *Methanosarcina thermophila*. *J Bacteriol* **188**:1155-1158.

19. Lundie LL, Jr., Ferry JG. 1989. Activation of acetate by *Methanosarcina thermophila*. Purification and characterization of phosphotransacetylase. J Biol Chem **264**:18392-18396.
20. Lawrence SH, Luther KB, Schindelin H, Ferry JG. 2006. Structural and functional studies suggest a catalytic mechanism for the phosphotransacetylase from *Methanosarcina thermophila*. J Bacteriol **188**:1143-1154.
21. Iyer PP, Ferry JG. 2001. Role of arginines in coenzyme A binding and catalysis by the phosphotransacetylase from *Methanosarcina thermophila*. J Bacteriol **183**:4244-4250.
22. Iyer PP, Lawrence SH, Luther KB, Rajashankar KR, Yennawar HP, Ferry JG, Schindelin H. 2004. Crystal structure of phosphotransacetylase from the methanogenic archaeon *Methanosarcina thermophila*. Structure **12**:559-567.
23. Iyer PP, Lawrence SH, Yennawar HP, Ferry JG. 2003. Expression, purification, crystallization and preliminary X-ray analysis of phosphotransacetylase from *Methanosarcina thermophila*. Acta Crystallogr D Biol Crystallogr **59**:1517-1520.
24. Grunwald NJ, Garbelotto M, Goss EM, Heungens K, Prospero S. 2012. Emergence of the sudden oak death pathogen *Phytophthora ramorum*. Trends Microbiol **20**:131-138.
25. Altschul SF, Gish W, Miller W, Myers EW, Lipman DJ. 1990. Basic local alignment search tool. J Mol Biol **215**:403-410.
26. Altschul SF, Madden TL, Schaffer AA, Zhang J, Zhang Z, Miller W, Lipman DJ. 1997. Gapped BLAST and PSI-BLAST: a new generation of protein database search programs. Nucleic Acids Res **25**:3389-3402.
27. Thompson JD, Gibson TJ, Plewniak F, Jeanmougin F, Higgins DJ. 1997. The Clustal X windows interface: flexible strategies for multiple sequence alignment aided by quality analysis tools. Nucl Acids Res **25**:4876-4882.

28. Tamura K, Peterson D, Peterson N, Stecher G, Nei M, Kumar S. 2011. MEGA5: molecular evolutionary genetics analysis using maximum likelihood, evolutionary distance, and maximum parsimony methods. *Mol Biol Evol* **28**:2731-2739.
29. Rice P, Longden I, Bleasby A. 2000. EMBOSS: the European Molecular Biology Open Software Suite. *Trends Genet* **16**:276-277.
30. Finn RD, Mistry J, Tate J, Coggill P, Heger A, Pollington JE, Gavin OL, Gunasekaran P, Ceric G, Forslund K, Holm L, Sonnhammer EL, Eddy SR, Bateman A. 2010. The Pfam protein families database. *Nucleic Acids Res* **38**:D211-222.
31. Hill AV. 1910. The possible effects of the aggregation of the molecules of haemoglobin on its dissociation curves. *J Physiol* **40**:iv-vii.
32. Motulsky H. 2004. *Fitting Models to Biological Data Using Linear and Nonlinear Regression: A Practical Guide to Curve Fitting: A Practical Guide to Curve Fitting*. Oxford University Press.
33. Leippe DD, Koonin EV, Aravind L. 2003. Evolution and classification of P-loop kinases and related proteins. *J Mol Biol* **333**:781-815.
34. Baykov AA, Tuominen HK, Lahti R. 2011. The CBS domain: a protein module with an emerging prominent role in regulation. *ACS Chem Biol* **6**:1156-1163.
35. Traut T. 2008. *Allosteric Regulatory Enzymes* doi:10.1007/978-0-387-72891-9. Springer US.
36. Copeland RA. 2000. *Enzymes: A Practical Introduction to Structure, Mechanism, and Data Analysis*, 2nd edition ed. Wiley-VCH.
37. Black WJ, Wang JH. 1968. Studies on the allosteric activation of glycogen phosphorylase b by Nucleotides. I. Activation of phosphorylase b by inosine monophosphate. *J Biol Chem* **243**:5892-5898.

38. Johnson LN, Stura EA, Wilson KS, Sansom MS, Weber IT. 1979. Nucleotide binding to glycogen phosphorylase b in the crystal. *J Mol Biol* **134**:639-653.
39. Stura EA, Zanotti G, Babu YS, Sansom MS, Stuart DI, Wilson KS, Johnson LN, Van de Werve G. 1983. Comparison of AMP and NADH binding to glycogen phosphorylase b. *J Mol Biol* **170**:529-565.
40. Kasvinsky PJ, Madsen NB, Sygusch J, Fletterick RJ. 1978. The regulation of glycogen phosphorylase alpha by nucleotide derivatives. Kinetic and x-ray crystallographic studies. *J Biol Chem* **253**:3343-3351.
41. Klinov SV, Kurganov BI. 2001. Combined kinetic mechanism describing activation and inhibition of muscle glycogen phosphorylase b by adenosine 5'-monophosphate. *Biophys Chem* **92**:89-102.
42. Chiang SL, Mekalanos JJ. 1998. Use of signature-tagged transposon mutagenesis to identify *Vibrio cholerae* genes critical for colonization. *Mol Microbiol* **27**:797-805.
43. Anfora AT, Halladin DK, Haugen BJ, Welch RA. 2008. Uropathogenic *Escherichia coli* CFT073 is adapted to acetatogenic growth but does not require acetate during murine urinary tract infection. *Infect Immun* **76**:5760-5767.
44. Kim YR, Brinsmade SR, Yang Z, Escalante-Semerena J, Fierer J. 2006. Mutation of phosphotransacetylase but not isocitrate lyase reduces the virulence of *Salmonella enterica* serovar *Typhimurium* in mice. *Infect Immun* **74**:2498-2502.
45. Gueriri I, Bay S, Dubrac S, Cyncynatus C, Msadek T. 2008. The Pta-AckA pathway controlling acetyl phosphate levels and the phosphorylation state of the DegU orphan response regulator both play a role in regulating *Listeria monocytogenes* motility and chemotaxis. *Mol Microbiol* **70**:1342-1357.
46. Kuhn ML, Zemaitaitis B, Hu LI, Sahu A, Sorensen D, Minasov G, Lima BP, Scholle M, Mrksich M, Anderson WF, Gibson BW, Schilling B, Wolfe AJ. 2014. Structural, kinetic and proteomic characterization of acetyl phosphate-dependent bacterial protein acetylation. *PLoS One* **9**:e94816.

47. Weinert BT, Iesmantavicius V, Wagner SA, Scholz C, Gummesson B, Beli P, Nystrom T, Choudhary C. 2013. Acetyl phosphate is a critical determinant of lysine acetylation in *E. coli*. *Mol Cell* **51**:265-272.

Table 2.1. Kinetic Parameters for PrPta^{II} Wild Type and the G³⁰⁰D Variant in the Acetyl-CoA-Forming Direction

<i>Enzyme</i>	$K_{0.5}$ CoA (mM)	$K_{0.5}$ AcP (mM)	$k_{cat}/K_{0.5}$ CoA (sec ⁻¹ mM ⁻¹)	$k_{cat}/K_{0.5}$ AcP (sec ⁻¹ mM ⁻¹)	Hill constant CoA (h)	Hill constant AcP (h)
Wild type	1.05 ± 0.31	1.85 ± 0.14	35.1 ± 6.0	18.04 ± 1.26	1.04 ± 0.05	1.75 ± 0.18
G ³⁰⁰ D	0.24 ± 0.05	1.75 ± 0.10	0.32 ± 0.06	0.043 ± 0.001	1.50 ± 0.05	6.50 ± 1.76

Table 2.2. IC₅₀ Values for Pta^{II} Enzymes in the Acetyl-CoA Direction

Effector Molecule	PrPta IC ₅₀ (μ M)	PrPtaG300D IC ₅₀ (μ M)	SePta IC ₅₀ (μ M)
ATP	736 \pm 6	133 \pm 8	364 \pm 19
AMP	287 \pm 4	53 \pm 2	ND
NADP	135 \pm 4	81 \pm 3	97 \pm 8
NADH	275 \pm 21	52 \pm 2	24 \pm 6
PEP	1018 \pm 128	74 \pm 4	67 \pm 3

ND: IC₅₀ could not be determined.

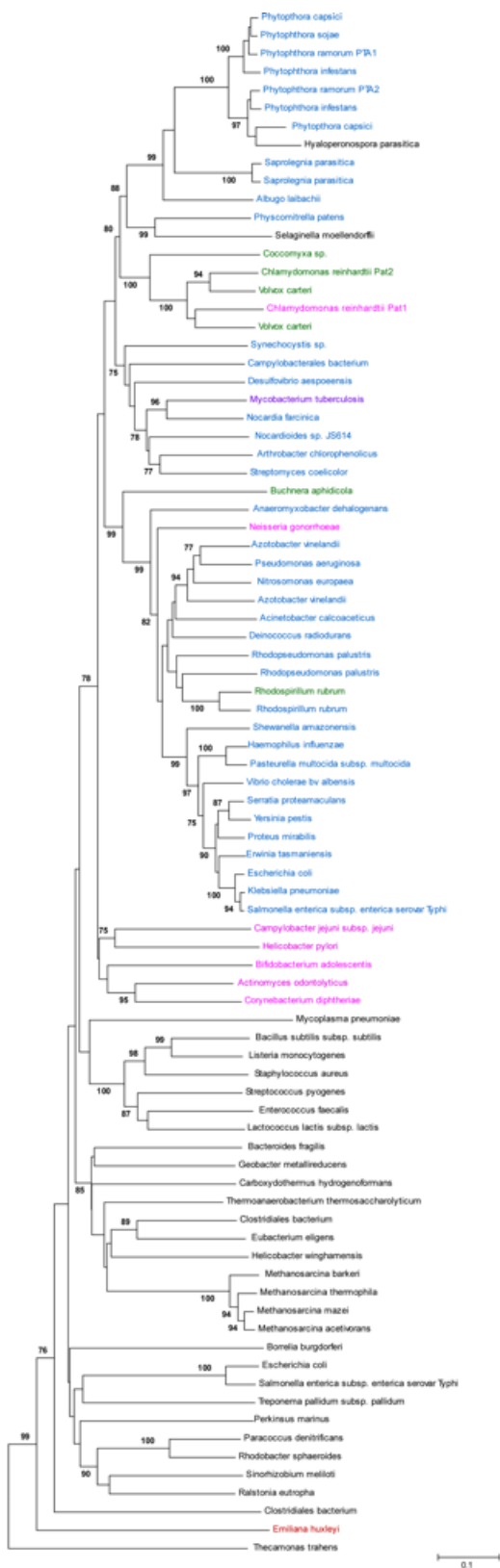


Figure 2.1. **Phylogeny of Pta^I and Pta^{II} family.** The phylogenetic tree was constructed based on the sequences of the Pta catalytic domains. Pta^I sequences are shown in black, Pta^{IIa} sequences are shown in blue, Pta^{IIb} sequences are shown in purple, Pta^{IIc} sequences are shown in green, and Pta^{IId} sequences are shown in pink. Only bootstrap value of 75% or higher are shown.

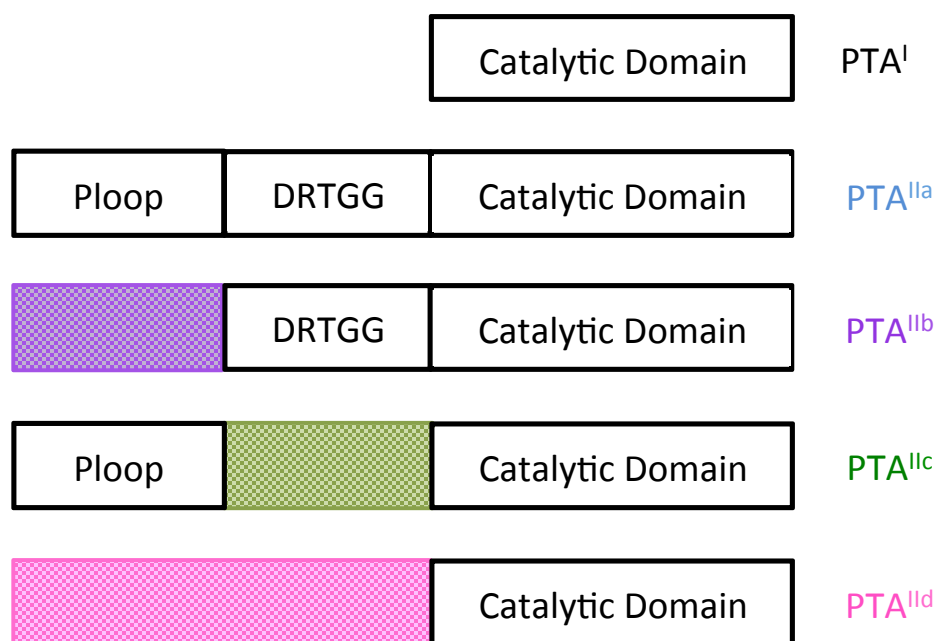


Figure 2.2. **Subdomain Structure of the Pta^I and Pta^{II} classes.** Pta^I enzymes have just a catalytic domain; Pta^{II} enzymes have a catalytic domain and an N-terminal domain. Four subclasses of Pta^{II} enzymes have been identified based on the presence or absence of the P-loop and DRTGG subdomains, as shown. Domains are not drawn to scale.

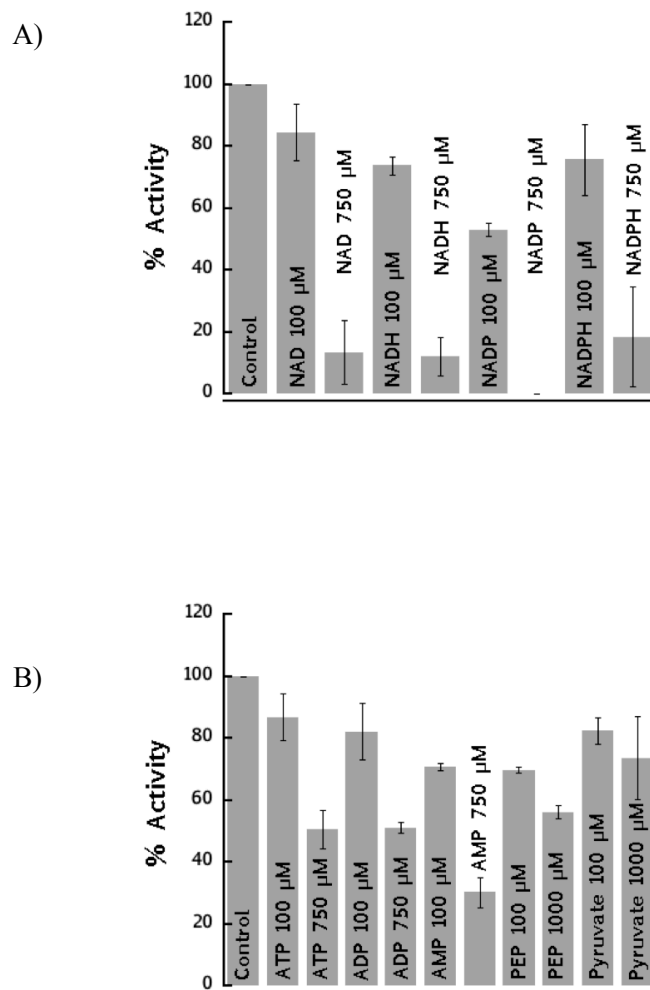


Figure 2.3. **Regulation of PrPta^{II}1 by Allosteric Effectors.** PrPta^{II}1 activity in the acetyl-CoA forming direction was monitored in the absence and presence of allosteric effector molecules. All data was normalized to the control, which represents the enzymatic activity observed in the absence of effector molecule. (a) Results are displayed as percent activity in the presence of 100 μM and 750 μM NAD⁺, NADH, NADP, and NADPH. (b) Results are displayed as percent activity in the presence of 100 μM and 750 μM ATP, ADP, and AMP, and 100 μM and 1000 μM PEP and pyruvate.

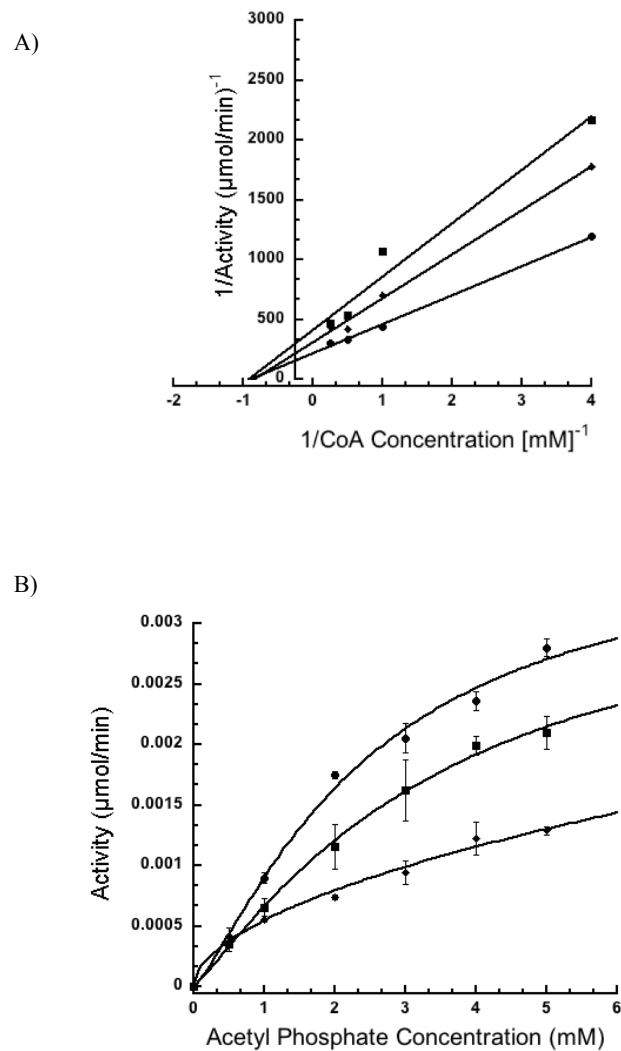


Figure 2.4. **Effect of NADP on CoA and Acetyl Phosphate Utilization** (a) Enzymatic activity was measured in the acetyl-CoA forming direction in the presence of 5 mM acetyl phosphate with varying concentrations of NADP using the thioester-forming assay. (●) 0 μM NADP, (■) 67.1 μM NADP, (◆) 134.2 μM NADP. (b) Enzymatic activity in the acetyl-CoA forming direction was measured in the presence of 4 mM CoA with varying concentrations of NADP using the thioester-forming assay. (●) 0 μM NADP, (■) 67.1 μM NADP, (◆) 134.2 μM NADP.

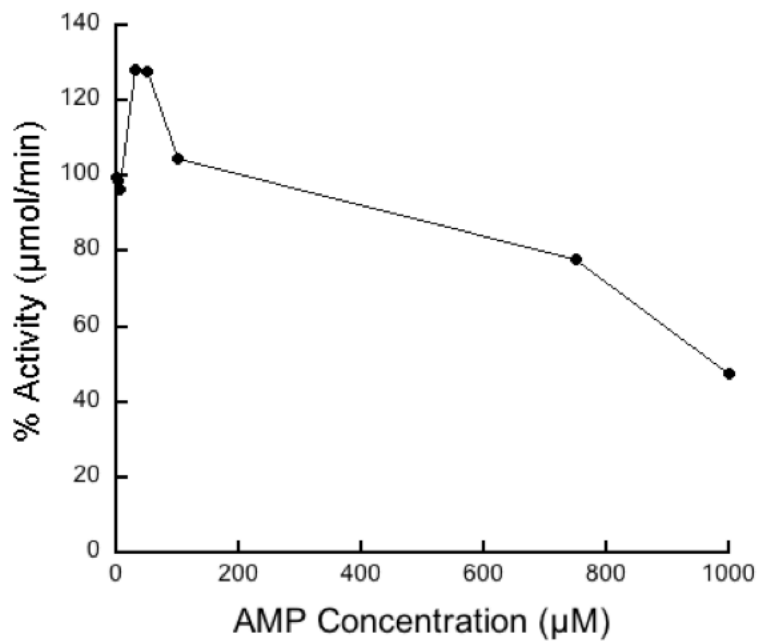


Figure 2.5. **AMP Inhibits and Activates SePta^{II}**. SePta^{II} activity in the acetyl-CoA forming direction was determined in the presence of increasing concentrations of AMP. All data was normalized to the control, which represents the enzymatic activity observed in the absence of effector molecule.

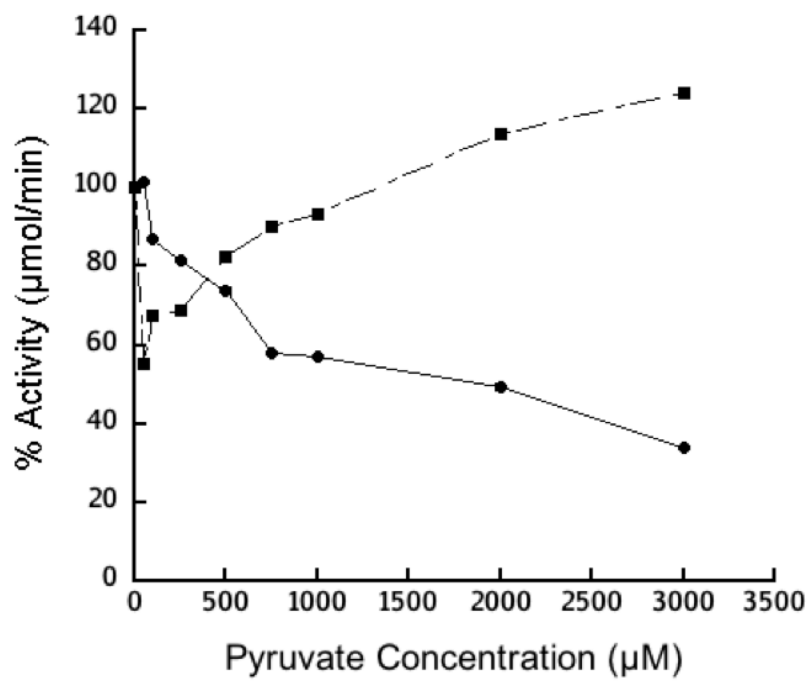


Figure 2.6. Alteration of the Gly³⁰⁰ Residue in PrPta^{II} Changes the Effect of Pyruvate.

Enzyme activity was determined in the presence of increasing amounts of pyruvate in the acetyl-CoA forming direction for PrPta1 (●) and PrPta1^{G300D} (■).

CHAPTER THREE

Biolistic Transformation of a Fluorescent Tagged Gene into the Opportunistic Fungal Pathogen *Cryptococcus neoformans*¹

Tonya Taylor, Indrani Bose, Taylor Luckie, and Kerry Smith

Abstract

The basidiomycete *Cryptococcus neoformans*, an invasive opportunistic pathogen of the central nervous system, is the most frequent cause of fungal meningitis worldwide resulting in more than 625,000 deaths per year worldwide. Although electroporation has been developed for the transformation of plasmids in *Cryptococcus*, only biolistic delivery provides an effective means to transform linear DNA that can be integrated into the genome by homologous recombination.

Acetate has been shown to be a major fermentation product during cryptococcal infection, but the significance of this is not yet known. A bacterial pathway composed of the enzymes xylulose-5-phosphate/fructose-6-phosphate phosphoketolase (Xfp) and acetate kinase (Ack) is one of three potential pathways for acetate production in *C. neoformans*. Here, we demonstrate the biolistic transformation of a construct, which has the gene encoding Ack fused to the fluorescent tag mCherry, into *C. neoformans*. We then confirm integration of the *ACK*-mCherry fusion into the *ACK* locus.

¹ **Taylor, T.**, Bose, I., Luckie, T., Smith, K. Biolistic Transformation of a Fluorescent Tagged Gene into the Opportunistic Fungal Pathogen *Cryptococcus neoformans*. *J. Vis. Exp.* (97), e52666, doi:10.3791/52666 (2015).

I. Introduction

Cryptococcus neoformans, an invasive opportunistic pathogen of the central nervous system, is the most frequent cause of fungal meningitis resulting in more than 625,000 deaths per year worldwide (1). Acetate has been shown to be a major fermentation product during cryptococcal infection (2-4), and genes encoding enzymes from three putative acetate-producing pathways have been shown to be upregulated during infection (5). This suggests that acetate production and transport may be a necessary and required part of the pathogenic process; however, the significance of this is not yet understood. One possible pathway for acetate production is the xylulose 5-phosphate/fructose 6-phosphate phosphoketolase (Xfp) - acetate kinase (Ack), a pathway previously thought to be present only in bacteria but recently identified in both eukaryotic as well as basidiomycete fungi, including *C. neoformans* (6).

To determine the localization of these enzymes of this pathway in the cell, a construct carrying a neomycin resistance gene downstream of an *ACK* gene fusion to the fluorescent tag mCherry (*ACK:mCherry:Neo*) will be introduced into *C. neoformans* using the well-established method of biolistic transformation (7, 8). Although electroporation is an efficient method for transformation of plasmids that will be maintained as episomes into *Cryptococcus* (9), it is not useful in creating stable homologous transformants (8). Only biolistic delivery using a gene gun provides an effective means to transform linear DNAs that will be integrated into the genome by homologous recombination. For example, Edman *et al.* showed that of the transformants resulting from electroporation of a plasmid-borne *URA5* selectable marker into *C. neoformans* *ura5* mutants, just 0.001 to 0.1% of transformants were stable (9). Chang *et al.* achieved just a 0.25% stable transformation efficiency using electroporation to reconstitute capsule production in an acapsular mutant (10). Unlike electroporation, biolistic transformation has been shown to

result in stable transformation efficiency of 2-50% depending on the gene that is being altered (7, 8, 11).

This visual experiment will provide a step-by-step demonstration of biolistic transformation of the linear ACK:mCherry:Neo DNA construct into *C. neoformans*, and will describe how to confirm its proper integration via homologous recombination into the *ack* locus. The protocol demonstrated here is a modification of the method developed in the Perfect laboratory (7, 8, 11).

II. Materials and Methods

The overall scheme of this protocol is outlined in **Figure 2.1**.

1) *C. neoformans* Preparation

1.1) For each transformation reaction, grow a 2-3 mL overnight culture of *C. neoformans* in YPD medium at 30 °C shaking at 250 RPM.

1.2) Centrifuge the overnight culture for 5 min at 900 x g at 10 °C and discard the supernatant.

1.3) Resuspend each cell pellet in 300 µL of Yeast Peptone Dextrose (YPD) medium.

1.4) Using glass beads, gently spread 300 µL of the washed cell suspension onto YPD agar containing 1M sorbitol.

1.5) Allow plates to dry at ambient temperature for 3-4 hours.

2) Gold Microcarrier Preparation

2.1) Resuspend 0.25 g of 0.6 µm gold beads in 1 mL of ddH₂O, centrifuge for 1 min at 900 x g to pellet the beads, and remove the supernatant.

2.2) Resuspend the gold beads in 1 mL of 100% ethanol.

2.3) Distribute the beads into 4 tubes, 250 µL each, and add 750 µL of 100% ethanol.

2.4) Store gold bead aliquots at 4°C.

3) DNA Preparation

3.1) Prepare orange macrocarrier biolistic discs by submerging them in 100% ethanol using forceps. Place discs into a large petri dish containing drierite to dry (make sure the drierite does not touch the discs).

3.2) Once dry, press the macrocarrier discs into the silver disc holders (previously wiped down with 100% ethanol).

3.3) Vortex gold beads (prepared as in step 2) and aliquot 12 μL into a 1.5 mL microcentrifuge tube, one tube per transformation.

3.4) Add to each tube in order: 2 μg of DNA (preferably 2 μL of 1 $\mu\text{g}/\mu\text{L}$ of DNA), 10 μL 2.5 M CaCl_2 , and 2 μL 1M spermidine free base.

3.5) Set up a negative control as in step 3.4 but with no DNA.

3.6) Vortex each tube and incubate at ambient temperature for 5 min. Gently flick each tube occasionally to resuspend the settled beads during this incubation.

3.7) Spin tubes at 225 x g for 30 sec to pellet the DNA-coated gold beads. Carefully remove the supernatant (by pipetting or aspiration) and discard.

3.8) Resuspend beads completely in 600 μL of 100% ethanol by slowly pipetting up and down.

3.9) Spin tubes at 225 x g for 30 sec to pellet the beads without packing. Carefully remove and discard the supernatant.

3.10) Resuspend the DNA-coated gold beads in 8 μL of 100% ethanol by slowly pipetting up and down.

3.11) Pipette the DNA-coated gold beads onto the center of the biolistic disc in a 1 cm diameter and allow to dry. Note: A dried gold circle visible on the center of the biolistic disc indicates that a sufficient concentration of gold beads is present.

Note: The macrocarrier discs loaded with DNA-coated gold beads are now ready for use with the gene gun.

4) Operating the Gene Gun

4.1) Turn on the vacuum pump.

4.2) Turn on the helium gas by turning the knob counterclockwise until a pressure of approximately 2200 psi is reached on the pressure gauge.

4.3) Turn on the gene gun by flipping the red switch on the left.

4.4) Be sure that the flow rates for the vacuum and the vent are adjusted so the vacuum will reach 28 inches Hg within 15 sec.

4.5) Be sure the distance between the rupture disc and macrocarrier is approximately 3/8 inch.

4.6) Clean the entire chamber by wiping down with ethanol.

4.7) Submerge the rupture discs in 100% ethanol. Allow to dry on a sterile surface (e.g., petri dish).

4.8) Use a torque wrench to loosen the rupture disc holder. Insert a clean rupture disc into the holder. Screw the rupture disc holder back into place and tighten with torque wrench by turning it once to the right. Note: Rupture discs will be replaced following each shoot.

4.9) Submerge the mesh screens in 100% ethanol. Allow to dry on a sterile surface (e.g., petri dish).

4.10) Once dry, place a washed mesh screen on the white plastic mounting plate. Place the macrocarrier disc holder DNA side down into the disc chamber. Screw on the silver cap, and place the mounting plate in the highest slot. Note: The mesh screen will be replaced after each shoot.

4.11) Place a YPD agar plate containing 1M sorbitol on the bottom plate.

4.12) Shut chamber door and lock into place.

4.13) Push and hold the middle red switch up to engage vacuum and allow the vacuum to reach 28 inches Hg. Once proper vacuum level is reached, move this switch to the down position. When ready, hold down the red switch on the right to fire. When the rupture disc pops, immediately release the fire button and push the middle red switch to the middle position to vent the chamber to 0 psi.

4.14) Clean out rupture disc debris and turn off the gene gun. Then turn off the helium gas by turning the knob clockwise, and finally, turn off the vacuum pump.

5) Plating Transformed Cells

5.1) Allow the transformation plates to sit at room temperature for four hours to allow the cells to recover.

5.2) Pipette 700 μ L of YPD onto the plate. Use a cell scraper to gently scrape the cells off of the agar and pipette liquid into a sterile 1.5 mL microfuge tube. Repeat this step to ensure all cells have been recovered from the plate.

5.3) Pellet cells at 225 x g for 30 sec. Remove and discard the supernatant.

5.4) Resuspend the pellet in 500 μ L of YPD.

5.5) Pipette 100 μ L of the cell suspension onto the center of the YPD + antibiotic plates and spread using glass beads.

5.6) Leave inverted plates at room temperature for 3-4 days. As colonies appear, patch onto new YPD + antibiotic plates.

6) Genomic DNA Isolation for PCR

Note: This is a modified version using reagents from a DNA purification kit (See Table of Materials).

6.1) Grow a 5 mL culture of each of the *C. neoformans* transformants in YPD liquid at 30 °C shaking at 250 RPM overnight.

6.2) Pellet 3 mL of cells at 900 x g, and resuspend in 600 μ L of nuclei lysis solution.

6.3) Add the suspension to a new 1.5 mL microcentrifuge tube with 200 μ L of 0.5 mm acid washed glass beads.

6.4) Homogenize for 45 sec in a mini beadbeater at ambient temperature, cool tube on ice, and repeat.

6.5) Allow sample to settle on ice for 2 min and transfer supernatant to a new 1.5 mL tube. Add 200 μ L of protein precipitation solution to each tube, (100 μ L for every 600 μ L of supernatant recovered) and vortex vigorously for 20 sec.

- 6.6) Allow samples to settle on ice for 5 min, and centrifuge at 11,000 x g for 3 min.
- 6.7) Transfer the supernatant to a clean 1.5 mL tube containing 300 μ L of room temperature isopropanol. Gently mix by inversion.
- 6.8) Centrifuge samples at 11,000 x g for 2 min, carefully remove the supernatant, and drain the tubes onto paper towels.
- 6.9) Add 300 μ L of room temperature 70% ethanol to each tube, and gently invert to wash the pellet.
- 6.10) Centrifuge samples at 11,000 x g for 2 min, and carefully remove all of the ethanol.
- 6.11) Drain the tube onto clean paper towels, and allow the pellet to air dry for 10 - 15 min.
- 6.12) Add 50 μ L of DNA rehydration solution and 1.5 μ L of RNase solution to each pellet and vortex.
- 6.13) Centrifuge samples for 5 sec to remove all of the liquid from the cap.
- 6.14) Incubate samples at 37 °C for 15 min.
- 6.15) Rehydrate the DNA by incubating the samples at 65 °C for 1 hour.

6.16) Quantify DNA spectrophotometrically by measuring the absorbance at 260 nm (an A_{260} reading of 1.0 is equivalent to ~ 50 $\mu\text{g/ml}$ double-stranded DNA), and use up to 200 ng in each PCR reaction.

7) RNA Isolation for Reverse Transcriptase-PCR.

7.1) Using a RNA purification kit (See Table of Materials), follow the manufacturer's instructions to isolate RNA from yeast cells using a minibeadbeater.

7.2) Quantify the concentration of the RNA by measuring the absorbance at 260 nm (an A_{260} reading of 1.0 is equivalent to ~ 40 $\mu\text{g/ml}$ single-stranded RNA).

7.3) Using an RT-PCR kit (See Table of Materials), follow the manufacturer's instructions to set up RT-PCR reactions with approximately 1 μg of RNA. For the results obtained in this study, use the primers listed in **Table 2.1**.

III. Representative Results

A successful biolistic transformation of *C. neoformans* can be obtained by following this protocol scheme (**Figure 2.1**). With biolistic transformation, a successful shoot of the coated gold beads is indicated by a gold ring visible on the plate after the DNA is shot (**Figure 2.2a**). Colonies should appear within 4 to 5 days when left at room temperature after plating the recovered cells from the YPD + 1M sorbitol plates onto selective media. Transforming 2 μ g of DNA should result in 20 to 30 colonies (**Figure 2.2b**). When colonies appear, they should be restreaked on selective media for individual colonies.

The individual colonies can be grown in YPD media, and both DNA and RNA can be isolated from these cells and analyzed through PCR and RT-PCR to confirm proper integration and expression. If this protocol is used for tagged gene fusion, as in this example, the primers would need to anneal within the coding region of the gene of interest (primer 2) and within the 3' noncoding region of the gene of interest (primer 4) (**Figure 2.3a**). With this construct, the DNA amplified from the PCR reaction was sequenced for another confirmation that the mCherry tag was fused in frame to the *ACK* gene. A positive PCR confirmation would be a larger PCR product from the DNA isolated from the transformed cells compared to the DNA isolated from the wild type cells. Another PCR reaction would also need to be conducted utilizing the primer set (primers 2 & 5) where one primer anneals outside of the construct and within the surrounding genome (primer 5) to confirm the correct recombination into the desired locus (primer 7 in **Table 1**) (**Figure 2.3b**). RT-PCR will be used to make sure that both the gene of interest and the tag are both being expressed (**Figure 2.3c**). Sequencing of the RT-PCR fusion product indicates that the tag is properly fused to the gene at the RNA level.

If this protocol is utilized to knock out a gene of interest, primer sets for PCR should be designed such that one primer anneals to a genome sequence outside of where the construct should recombine into the genome, and the other primer anneals either in the coding region of the gene or in the selective marker. A positive confirmation that the construct has successfully and correctly recombined into the genome would be the presence of the correct size product for the primer set that anneals within the marker but not with the primer set that anneals to the gene of interest. Another primer set should be made that has one primer that anneals outside of the designed construct, which is used with PCR to confirm that the recombination event occurred at the correct locus. In the same design to create a knockout, RNA is isolated from both the transformed cells and wild type (WT) cells, and RT-PCR is performed to confirm that no expression of the gene of interest is observed from the transformed cells.

Because a fluorescent tag was fused to the *ACK* gene, another confirmation that recombination was a success into the desired locus and that RNA is being translated into protein is through fluorescent microscopy (**Figure 2.4**). Ideally, conditions have already been established where it is known that the protein of interest is being expressed. However, if the fluorescent signal is too low to observe, there is a possibility that successful recombination still occurred, but growth conditions need to be altered in the chance that optimal conditions have not been met for sufficient expression, which would lead to a low fluorescent signal. This would need to be confirmed through other methods such as a western blot.

IV. Discussion

Utilizing this protocol, biolistic transformation can be accomplished in which linear DNA is integrated into a desired locus in the *Cryptococcus neoformans* genome by homologous recombination. Certain steps in the protocol can have a dramatic effect on the effectiveness/efficiency of the transformation. For a successful transformation, it is imperative that the DNA utilized in the shoot has a concentration of at least 1 μg . However, the volume of DNA added to the gold beads can be increased in the chance the DNA yield is lower than 1 μg (Step 3.4).

Another important step is in the DNA coating of the gold beads. Insufficient numbers of beads in the DNA preparation sample, due to an error in the preparation, leads to a decreased amount of DNA shot onto the plate. After the DNA has been loaded onto the gold beads, they are pipetted onto the biolistic disc and allowed to dry. When dry, a visible gold circle about 1 cm in diameter should be present on the disc. The absence of this circle suggests that the concentration of the gold beads is not high enough. Another clue that the gold bead concentration is too low is following the shoot. There should be a gold ring visible on the plate (**Figure 2.2a**), and if no gold ring is visible and the rupture disc burst, this could indicate that the concentration of gold beads used in the preparation was not high enough.

The typical yield using the biolistic transformation method is 20-30 colonies. Fewer colonies may indicate that the technique or gene gun set-up is not 100% efficient. One reason for the fewer colonies may be the amount of cells scraped off from step 5.2. Depending on the size of the pellet in step 5.3 and the number of colonies that appear from the previous experiments, the volume the pellet is resuspended in, in step 5.4, may need to be altered. From these colonies, DNA should be isolated, and PCR conducted to confirm a larger size gene product compared to WT, indicating the presence of the tag. RNA should be isolated and RT-PCR performed to

confirm that there are transcripts of the gene product being made, and if a fluorescent tag was inserted into the genome, then microscopy should be used to observe whether the tag is being expressed.

The main limitation to this protocol is the requirement for specialized equipment such as a gene gun and a fluorescent microscope. However, biolistic transformation is the best choice for introduction of linear DNAs for gene knockouts versus electroporation, which is used for introduction of episomes or *Agrobacterium tumefaciens* mediated transformation, which has been used for random insertional mutagenesis (12). Biolistics may also prove to be a suitable method for rapid introduction of a wide variety of vital dyes into *Cryptococcus*. Lipophilic dyes are used to stain extracellular vesicles and the capsule of *C. neoformans* (13). Biolistic delivery of gold particles coated with lipophilic dye that imbed into the membranes of cells and organelles has been used to study the interconnection of neighboring cells (14). Therefore, biolistics may be a less time-consuming technique to visualize extracellular vesicles and organelles.

V. Acknowledgments

This work was supported by awards from the National Science Foundation (Award# 0920274) and the South Carolina Experiment Station Project SC-1700340. This paper is Technical Contribution No. 6283 of the Clemson University Experiment Station. The authors thank Dr. Lukasz Kozubowski for his helpful advice in development of this final protocol and Dr. Cheryl Ingram-Smith, Katie Glenn, and Grace Kisirkoi for their critical reading of the manuscript.

VI. References

1. Price MS, Betancourt-Quiroz M, Price JL, Toffaletti DL, Vora H, Hu G, Kronstad JW, Perfect JR. 2011. *Cryptococcus neoformans* requires a functional glycolytic pathway for disease but not persistence in the host. *mBio* **2**:e00103-00111.
2. Bubb WA, Wright LC, Cagney M, Santangelo RT, Sorrell TC, Kuchel PW. 1999. Heteronuclear NMR studies of metabolites produced by *Cryptococcus neoformans* in culture media: identification of possible virulence factors. *Magnetic resonance in medicine : official journal of the Society of Magnetic Resonance in Medicine / Society of Magnetic Resonance in Medicine* **42**:442-453.
3. Himmelreich U, Allen C, Dowd S, Malik R, Shehan BP, Mountford C, Sorrell TC. 2003. Identification of metabolites of importance in the pathogenesis of pulmonary cryptococcoma using nuclear magnetic resonance spectroscopy. *Microbes and infection / Institut Pasteur* **5**:285-290.
4. Wright L, Bubb W, Davidson J, Santangelo R, Krockenberger M, Himmelreich U, Sorrell T. 2002. Metabolites released by *Cryptococcus neoformans* var. *neoformans* and var. *gattii* differentially affect human neutrophil function. *Microbes and infection / Institut Pasteur* **4**:1427-1438.
5. Hu G, Cheng PY, Sham A, Perfect JR, Kronstad JW. 2008. Metabolic adaptation in *Cryptococcus neoformans* during early murine pulmonary infection. *Molecular microbiology* **69**:1456-1475.
6. Ingram-Smith C, Martin SR, Smith KS. 2006. Acetate kinase: not just a bacterial enzyme. *Trends Microbiol* **14**:249-253.
7. Davidson RC, Cruz MC, Sia RA, Allen B, Alspaugh JA, Heitman J. 2000. Gene disruption by biolistic transformation in serotype D strains of *Cryptococcus neoformans*. *Fungal Genet Biol* **29**:38-48.
8. Toffaletti DL, Rude TH, Johnston SA, Durack DT, Perfect JR. 1993. Gene transfer in *Cryptococcus neoformans* by use of biolistic delivery of DNA. *J Bacteriol* **175**:1405-1411.

9. Edman JC, Kwon-Chung KJ. 1990. Isolation of the URA5 gene from *Cryptococcus neoformans* var. *neoformans* and its use as a selective marker for transformation. *Mol Cell Biol* **10**:4538-4544.
10. Chang YC, Kwon-Chung KJ. 1994. Complementation of a capsule-deficient mutation of *Cryptococcus neoformans* restores its virulence. *Mol Cell Biol* **14**:4912-4919.
11. Del Poeta M, Toffaletti DL, Rude TH, Dykstra CC, Heitman J, Perfect JR. 1999. Topoisomerase I is essential in *Cryptococcus neoformans*: role in pathobiology and as an antifungal target. *Genetics* **152**:167-178.
12. McClelland CM, Chang YC, Kwon-Chung KJ. 2005. High frequency transformation of *Cryptococcus neoformans* and *Cryptococcus gattii* by *Agrobacterium tumefaciens*. *Fungal Genet Biol* **42**:904-913.
13. Nicola AM, Frases S, Casadevall A. 2009. Lipophilic dye staining of *Cryptococcus neoformans* extracellular vesicles and capsule. *Eukaryot Cell* **8**:1373-1380.
14. Gan WB, Grutzendler J, Wong WT, Wong RO, Lichtman JW. 2000. Multicolor "DiOlistic" labeling of the nervous system using lipophilic dye combinations. *Neuron* **27**:219-225.

Table 3.1. PCR and RT-PCR Primers.

Primer #	Primer Name	Primer Sequence
1	KI003	5' – GTA GCG AGG TCT GGA AGC CAC – 3'
2	ACKmChRT-F	5'- GCT TTG GCC GGT ACT ACC AAC -3
3	ACKmChRT-R	5'- GAC AGC TTC AAG TAG TCG GGG -3'
4	KI004	5' – GAC TTG GGG AAG AGG AAT TC – 3'
5	KI0032	5' – CGG GGT ACC ATC AAT AAA AGC TTT CTT CAC TCC - 3'
6	Actin 1	5'- CGC TAT CCT CCG TAT CGA TCT TGC -3'
7	Actin 2	5'- CAG CTG GAA GGT AGA CAA AGA GGC -3'

Protocol Scheme

1. Plate *C. neoformans* onto YPD + 1M sorbitol and allow to grow for 3-4 hours at ambient temperature.
2. Observe under a microscope for thorough distribution of cells.
3. Wash and aliquot gold beads.
4. Coat the gold beads with the DNA that is to be transformed.
5. Prepare macrocarriers with gold beads coated with DNA.
6. Using the gene gun, transform DNA into *C. neoformans*
7. Allow cells to recover by incubating plates for 3-4 hours at room temperature.
8. Scrape recovered *C. neoformans* cells onto selective media.
9. Allow cells to grow on the selective media until colonies appear.
10. Restreak each colony onto a freshly made YPD + antibiotic plate to ensure individual colonies.
11. Isolate DNA and RNA from those individual colonies, and perform PCR and RT-PCR analysis to confirm a successful recombination event.
12. Examine cells under a fluorescent microscope to confirm fluorescently tagged fusion protein is being expressed.

Figure 3.1. Protocol Scheme.

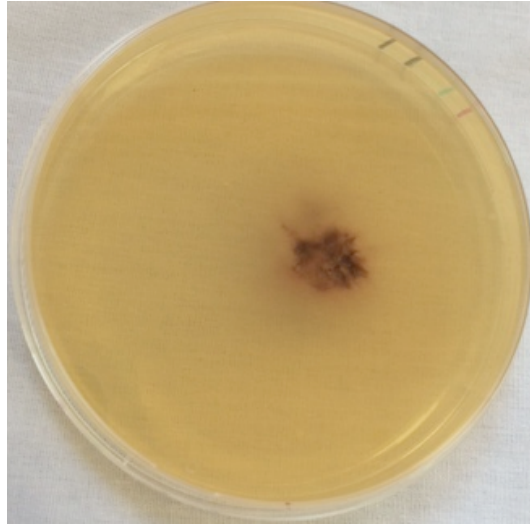


Figure 3.2a. DNA-coated Gold Beads Successfully Shot Onto a YPD + 1M Sorbitol Plate.

An orange patch seen in the center of the YPD + 1M sorbitol plate is due to the DNA-coated gold beads, indicating proper gold preparation, as well as a successful shoot.

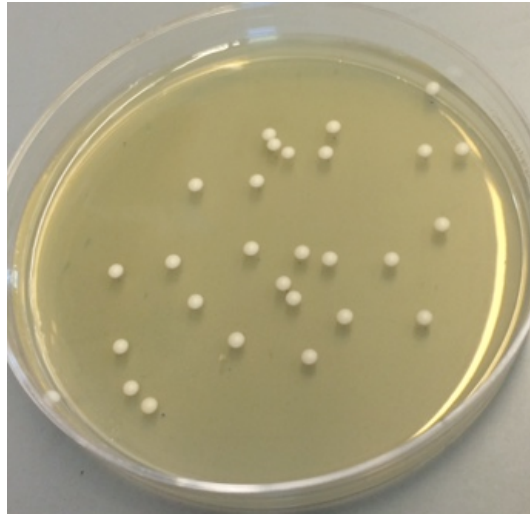


Figure 3.2b. Transforming 2 μg of DNA Results in 20-30 Colonies per Plate. If the cells were diluted as mentioned in the protocol, approximately 20-30 colonies are expected prior to plating on selective media.

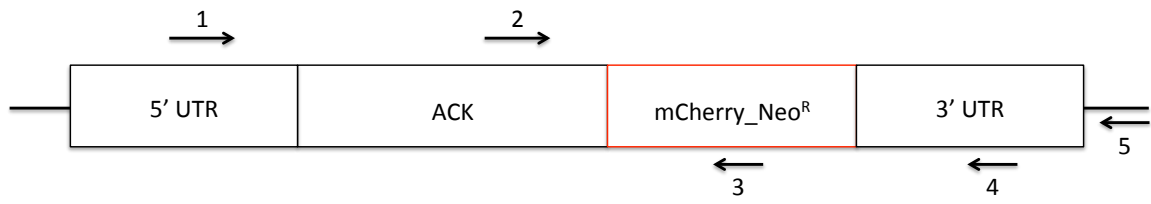


Figure 3.3a. Schematic of the ACK:mCherry:Neo Construct and Primer Design.

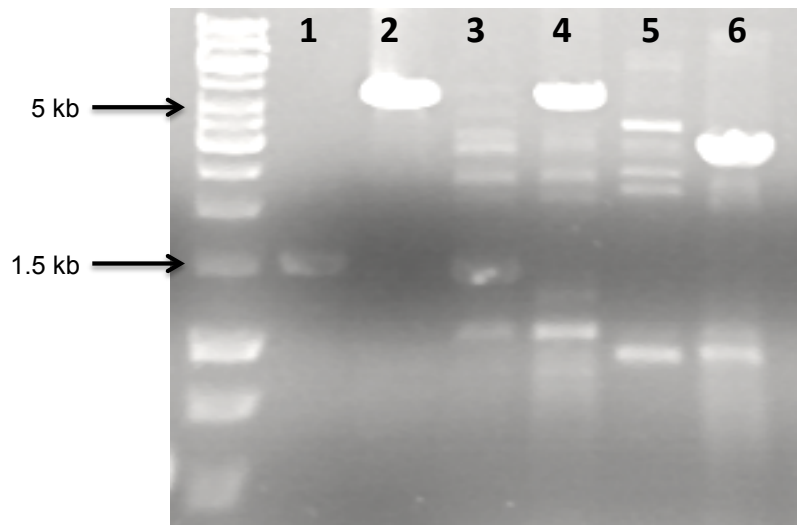


Figure 3.3b. PCR Used to Confirm Successful Homologous Recombination. Lanes 1 and 2: PCR products obtained using primers 2 and 5 (Table 1) with genomic DNA from wild type *C. neoformans* H99 (lane 1) and the ACK:mCherry transformed strain, (lane 2). Expected sizes are 1511 and 5622 bp, respectively. Lanes 3 and 4 are the DNA products of the *C. neoformans* H99 (expected size 1443 bp) and the ACK:mCherry (expected size 5552 bp) strains, respectively, using primers 2 and 4 in Table 1. Lanes 5 and 6 are the DNA products of the *C. neoformans* H99 (should not anneal) and ACK:mCherry (expected size 3016 bp) strains, respectively, using primers 1 and 3.

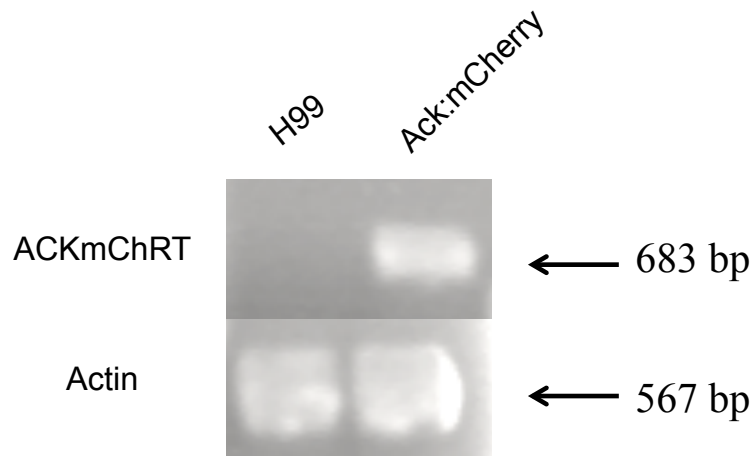


Figure 3.3c. RT-PCR Confirmation of Expression of the mCherry Tag. The top lanes are the cDNA products of the ACKmCherry fusion product (expected size 683 bp) amplified from the *C. neoformans* H99 and the ACK:mCherry strains using primers 2 and 3 in Table 1. The actin gene was included as a control and was amplified under the same conditions as ACKmCherry (expected size 567 bp) using primers 6 and 7 in Table 1.

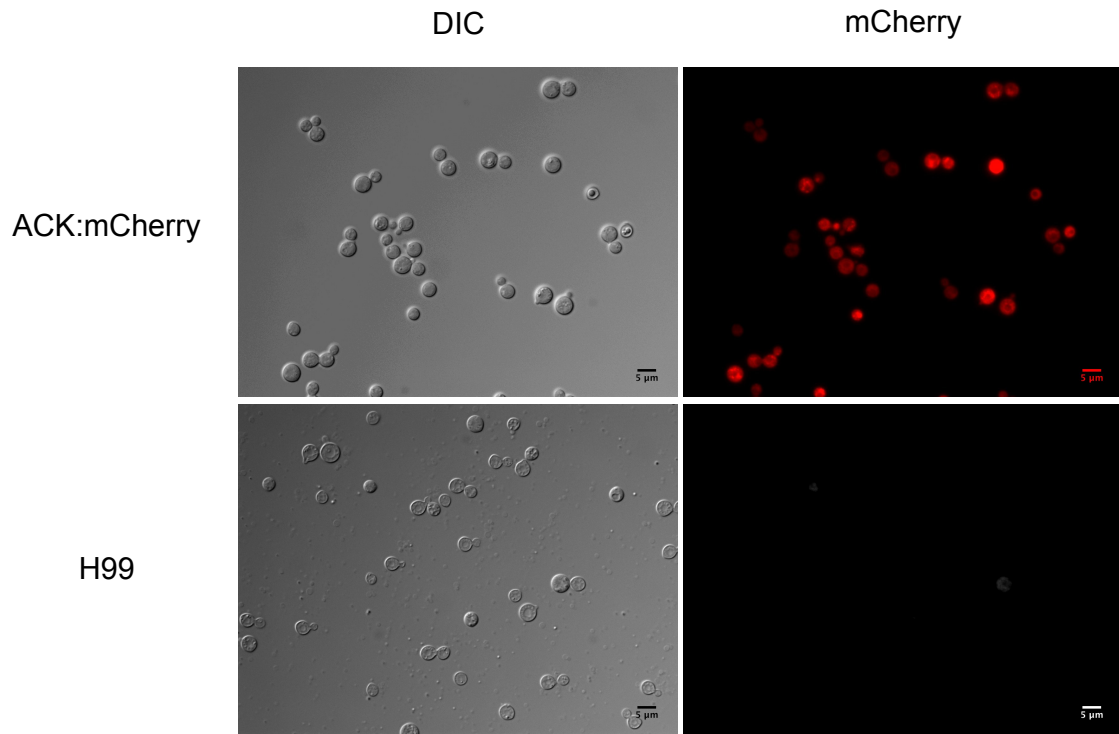


Figure 3.4. Fluorescence of the mCherry tagged Ack. Microscopic analysis of strains producing Ack fused to a mCherry tag with an excitation optimum at 587 nm and an emission optimum at 610 nm.

CHAPTER FOUR

The Investigation into the Metabolic and Physiological Role of the Ack-Xfp Pathway in *Cryptococcus neoformans*

Tonya Taylor, Indrani Bose, Taylor Luckie, and Kerry Smith

Abstract

Cryptococcus neoformans, an invasive opportunistic pathogen of the central nervous system, is the most frequent cause of fungal meningitis resulting in more than 625,000 deaths per year worldwide. Acetate has been shown to be a major fermentation product during cryptococcal infection, and genes encoding enzymes from two putative acetate-producing pathways and two putative acetate transporters have been shown to be upregulated during infection. This suggests that acetate production and transport may be a necessary and required part of the pathogenic process; however, the significance of this is not yet understood. One possible source of acetate in *C. neoformans* is the xylulose 5-phosphate/fructose 6-phosphate phosphoketolase (Xfp) - acetate kinase (Ack), a pathway previously thought to be present only in bacteria, and like most other fungi, *C. neoformans* has two ORFS with sequence identity to Xfp, designated as Xfp1 and Xfp2.

To investigate the metabolic and physiological role of the Ack-Xfp pathway in *C. neoformans*, we have generated single *XFPI*, *XFP2*, and *ACK* knockouts through a 3-step overlap PCR technique, as well as a double *XFPI/XFP2* knockout. If Ack and Xfp do indeed partner together, then the phenotypes observed in the *in vitro* and *in vivo* assays described below would be expected to be similar for the *xfp* or *ack* knockout mutants. The mutants do not have a discernable phenotype when grown on YNB media containing alternative carbon sources (2% and 0.2%) or under a variety of stresses. However, when the wild type and mutants were grown in YNB with very low glucose concentrations (as low as 0.001%), growth of the $\Delta xfp2$ mutant was

impaired. A measurable increase in growth was seen for the $\Delta xfp1$ mutant, while an intermediate phenotype was observed for the $\Delta xfp1/xfp2$ mutant. Macrophage-killing assays suggest the $\Delta xfp1$, $\Delta xfp2$, and $\Delta xfp1/xfp2$ mutants are more susceptible to killing than both the wild type and Δack mutant, suggesting a role for both Xfp1 and Xfp2 in survival in the macrophage. Overall, our results suggest that Ack and Xfp may have separate functions in the physiology and metabolism of *C. neoformans*.

I. Introduction

Cryptococcus neoformans is an opportunistic, fungal pathogen and the leading cause of fungal meningitis, killing approximately 625,000 people per year globally (1). This basidiomycetous yeast gains access into the respiratory tract through inhalation of its fungal spores and can disseminate throughout the body of immunocompromised individuals causing infection. *C. neoformans*, the most common fungal infection of the central nervous system, has a predilection for the central nervous system (CNS), where it causes fungal meningitis (2).

Acetate and ethanol are two main metabolites produced by *Cryptococcus* during infection and in glucose-fed cultures (3, 4); however, the significance of this is not yet understood. We have identified two potential pathways for acetate metabolism in *C. neoformans* (**Figure 1**). The pyruvate decarboxylase (Pdc; EC 4.1.1.1) – acetaldehyde dehydrogenase (Ald; EC 1.2.1.10) pathway, that converts pyruvate to acetate, is found in yeast and fungi. The second pathway is the xylulose-5-phosphate/fructose-6-phosphate phosphoketolase (Xfp) and acetate kinase (Ack) pathway, which is also present in other eukaryotic and basidiomycete fungi (5). Heterofermentative bacteria such as *Lactobacillus* use Xfp-Ack as part of a modified form of the pentose phosphate pathway for the breakdown of pentoses and hexoses (11). Xfp catalyzes the formation of acetyl phosphate from the pentose phosphate pathway products xylulose 5-phosphate (X5P; $X5P + P_i \leftrightarrow \text{acetyl phosphate} + \text{glyceraldehyde 3-phosphate}$; EC 4.1.2.9) and fructose 6-phosphate (F6P; $F6P + P_i \leftrightarrow \text{acetyl phosphate} + \text{erythrose 4-phosphate}$; EC 4.1.2.2). Ack then converts the acetyl phosphate product of the Xfp reaction to acetate and ATP ($\text{acetyl phosphate} + \text{ATP} \leftrightarrow \text{acetyl phosphate} + \text{ADP}$; EC 2.7.2.1) (5). Many fungi, including *C. neoformans*, have two Xfp ORFs each belonging to one of two distinct clades, designated as Xfp1 and Xfp2, for the fungal Xfps (6).

Most *Aspergillus* species have two *XFP* genes, but *Aspergillus nidulans* has only one, that belongs to the Xfp1 sub-family. When the *A.nidulans ACK* and *XFP* were overexpressed in *Saccharomyces cerevisiae*, which lacks this pathway, an increase in acetate production was observed in batch cultivations (12); this experiment suggests that at least in *A. nidulans*, this pathway works in the direction of acetate production. The identification of the genes encoding the enzymes of the pentose phosphate pathway in *Cryptococcus* (4), along with the presence of *ACK* and *XFP*, suggest these eukaryotes might utilize a modified pentose phosphoketolase pathway for acetate production.

The biochemical and kinetic characterization of Ack and Xfp2 support a role for acetate production. The *C. neoformans* Ack functions in both directions of acetate metabolism; however, kinetic characterization of *C. neoformans* reveals a higher k_{cat} in the acetate-forming direction (C. Ingram-Smith, T. Dang, A. Guggisberg, S. Henry, J. Welch, K. Laws, A. Mattison, A. Bizhanova, and K. Smith, manuscript in preparation) (13). The presence of two putative *XFP* ORFs and the minimal (39%) identity between Xfp1 and Xfp2 suggests possible differences in the physiological/metabolic roles for these two enzymes in *C. neoformans*. Xfp has been biochemically and kinetically characterized from several bacterial species, including *Lactobacillus plantarum* (14, 15), *Bifidobacterium* spp. (16, 17), *Lactococcus lactis* (18), *Leuconostoc mesenteroides* (18), *Pseudomonas aeruginosa* (18), and *Anabaena* sp. PCC 7120 (19). However, the characterization of Xfp from a eukaryote had not been reported until the recent description of Xfp2 from *C. neoformans*. Xfp2 is allosterically regulated by key metabolic intermediates, such as ATP, PEP and OAA (20), and although slight differences are observed between organisms, allosteric regulation is a general property of both eukaryotic and bacterial phosphoketolases (21). The Xfp2 enzyme is fairly well characterized, however, there is no report on the biochemical investigation of an Xfp1.

Although the role of the Xfp-Ack pathway in *C. neoformans* has not yet been investigated, several studies examining gene expression during infection or under conditions that the fungus is expected to experience during infection (e.g., oxidative stress and hypoxia) suggest this pathway is active during *C. neoformans* infection. An early microarray study of *C. neoformans* gene expression by Fan et al. (7) indicated *ACK* is expressed during murine macrophage infection; however, *XFP1* and *XFP2* were not included in the microarray. Serial analysis of gene expression on cells recovered from the lungs of infected mice uncovered elevated transcripts of *XFP2* (8). A global transcriptome profile of *C. neoformans* treated with hydrogen peroxide revealed induction of *XFP1* in response to oxidative stress (9). In addition, Chun et al. (10) executed a genome wide microarray study that revealed both *ACK* and *XFP2* are induced under hypoxic conditions.

To investigate the role of the Xfp-Ack pathway in *C. neoformans*, we have taken a genetic approach by generating single *XFP1*, *XFP2* and *ACK* knockouts, as well as the double *XFP1/XFP2* knockout, through a three-step overlap PCR technique. Our *in vitro* experiments suggest that Ack and Xfp2 may partner together in low glucose environments, and possibly under low iron conditions. In addition, we have also shown that Xfp1 and Xfp2 play a mammalian-specific role in the survival of *C. neoformans* within murine macrophages. This work provides the first investigation into the role of Ack and Xfp in *C. neoformans*, which indicates that although these enzymes may partner together, they also may operate individually under certain conditions.

II. Materials and Methods

Materials

Chemicals were purchased from Sigma-Aldrich, VWR, Fisher Scientific, Becton Dickinson and Company, and Gold Biotechnology. Oligonucleotide primers were purchased from Integrated DNA Technologies. *C. neoformans* strains were grown in Yeast Extract Peptone Dextrose (YPD) medium (yeast extract 1%, peptone 2%, dextrose 2%) or Yeast Nitrogen Base (YNB) broth supplemented with a carbon source.

Disruption of *ACK*, *XFP1*, and *XFP2* mutants

The Δ ack:Neo was generated in the congenic *C. neoformans* KN99a strain and the Δ xfp1:Hyg and Δ xfp2:Neo were generated in the KN99a strain. The three-step overlap PCR technique, previously described (22), was used to generate the null mutant constructs. Primer sequences used for construction of the gene deletions are listed in Table 1. Deletion constructs were generated by joining approximately 1000 bp of non-coding genomic sequence 5' to the targeted gene, the neomycin resistance (Neo^r) or hygromycin resistance (Hyg^r) cassette (amplified from pMH12-T and pHYG7KB1 vectors, respectively (23), and approximately 1000 bp of non-coding genomic sequence 3' to the targeted gene. The final gene deletion constructs were created through overlap PCR using all three amplified regions, and the resultant PCR products were confirmed through sequencing. The constructs were transformed using biolistic delivery of gold microcarrier beads (0.6 μ m; Bio-Rad) into the serotype A strains as described previously (22). YNB medium + 0.2% glucose containing either G418 (300 μ g/mL) or hygromycin B (300 μ g/mL) was used for the screening of stable transformants.

Confirmation of successful homologous integration occurred through the use of PCR, RT-PCR and Southern blot. Genomic DNA was isolated using a modified version of protocol from the Wizard Genomic DNA Isolation Kit (Promega) (50). The following primers from Table 2, 5'XFP1ext/3'HYGintcoding, 5'HYGintcoding/3'XFP1ext, 5'XFP2ext/3'NEOintcoding, 5'NEOintcoding/3'XFP2ext primers and 200 ng of genomic DNA from the wild type and putative knockouts were used in each PCR reaction; the KOD Hot Start polymerase kit (EMD Millipore) was used for each reaction.

RNA isolation was performed by the manufacturer's instructions for the RNeasy Mini kit (Qiagen). The following primers from Table 2, XFP1F-RT/ XFP1R-RT, XFP2F-RT/ XFP2R-RT, ACTIN-1/ACTIN-2 and 1 µg of RNA were used to set up the RT-PCR reactions using the One-step RT-PCR kit (Qiagen).

Genomic DNA for Southern blots was isolated following the CTAB midi prep protocol (51, 52). Genomic DNA isolated from both the WT and knockout strains was restricted overnight at 37°C. Genomic DNA from strains with the neomycin resistance cassette was restricted with *EcoRI*, while DNA from strains with the hygromycin resistance cassette was restricted with *PvuII*. Restriction of the pMH12-T and pHYG7KB1 plasmids was used as controls. The Biotin Chromogenic Detection kit (Thermo Scientific) was used to detect biotinylated nucleic acid probes: (Neo) 5' TGC CGA ATA TCA TGG TGG AAA ATG GCC GCT 3' and (Hyg) 5' CGC GAT TGC TGA TCC CCA TGT GTA TCA CTG 3'.

Stress and drug response assays

C. neoformans WT and knockout strains were grown overnight in YPD at 30°C, washed three times and were diluted in PBS to 1×10^4 cells. Five microliters of ten-fold serial dilutions were spotted onto plates with different carbon sources or chemicals that induce a stress response.

Plates were incubated at both 30°C and 37°C to determine the response of each *C. neoformans* strain. For alternative carbon sources, cells were plated and growth was monitored on YNB agar with one of the following carbon sources: 0.2% glucose, 2% glucose, 2% arabinose, 2% xylose, 2% glycerol, 2% galactose, 2% ethanol, 0.2% acetate, and 1.5% acetate.

In addition, growth was monitored in liquid synthetic medium (6.7g/L Sigma Yeast Nitrogen Base with 2% glucose, 2% agar, and 1x amino acid stock mix) supplemented with no glucose, 0.001% glucose, 0.01% glucose, and 0.1% glucose for both the WT and knockout strains (Andrew Alspaugh, Duke University, personal communication). Cells were incubated at 30°C and shaking at 250 RPM in an Incubating Microplate Shaker (Fisher Scientific). Absorbance measurements were taken at 0, 9, and 30 hours using the Epoch Multi-volume Microplate Reader (BioTek Instruments, Inc.).

The response to hypoxia was tested using YES media (0.5% yeast extract, 2% glucose, and 225 µg/ mL of each: uracil, adenine, leucine, histidine, and lysine) supplemented with 0.7 mM CoCl₂ (25). To test osmotic stress, the cells were plated and growth was monitored on YPD supplemented with either 1.2 M KCl or 1.5 M NaCl. Cells were plated on YPD supplemented with 0.5 mM H₂O₂ for oxidative stress and with 8 mM NaNO₂ for nitrosative stress. YPD with the addition of 0.1% SDS or 0.5 mg/mL Congo Red analyzed the cell wall integrity of each strain.

To test sensitivity to fluconazole, *C. neoformans* WT and knockout cells were grown overnight in YPD at 30°C. Cells were diluted 1:10 into YPD and grown for another 3 hours. Cells were diluted to 0.07 OD in 0.9% NaCl, and cotton swabs were used to plate each strain onto a YPD or YNB + 0.2% glucose plate. One fluconazole Etest Strip (BioMérieux, Inc.) was gently placed down the center of each plate and plates were incubated at 30°C for two days. The minimal inhibitory concentration (MIC) for each was determined in µg/mL by the ellipse that intersected the strip.

Capsule formation and melanin production

Melanin production was assayed using YNB media with 0.1% glucose and 1 mM L-Dopamine. Cells were washed three times and diluted in PBS to 1×10^4 cells, and five microliters of ten-fold serial dilutions were spotted onto the L-Dopamine media. The polysaccharide capsule formation was tested by growing the WT and mutant cells overnight under iron limiting conditions at 30°C using YNB liquid supplemented with 100 μ M bathophenanthroline disulfonate (BPS). The cells grown under low iron were washed and diluted to 2×10^3 cells, and visualized microscopically using India ink as described previously (24).

Virulence assays

C. neoformans WT and mutant cultures were grown in YPD at 30°C, washed three times and diluted to 1.5×10^5 cells in sterile phosphate-buffered saline (PBS). *Galleria mellonella* (wax moth) larvae (Vanderhorst, Inc.) were weighed (330 ± 25 mg in weight) and inspected for any discoloration. Ten larvae per strain were chosen at random and disinfected using alcohol wipes before each inoculation. Hamilton syringes were used to inject 10 μ L aliquots of each diluted culture into the bottom, left proleg of each larva. PBS was injected into the larvae within one group to monitor death due to injury. As a negative control, WT cells were also heat killed at 60°C for 1 hour, and the Δ acs knockout strain (kindly provided by Dr. James Kronstad, University of British Columbia) was used as a control. Two sets of larvae were inoculated for each strain; one set was incubated at 30°C and the other at 37°C. The larvae were monitored daily and scored for death when they no longer were able to roll over. Each assay was repeated three times. Kaplan-Meier survival analysis was conducted using GraphPad Prism version 4.0 software.

Survival of *C. neoformans* cells in J774A.1 cells

Phagocytosis and fungal killing assays were conducted using J774A.1 macrophages (kindly provided by Jeff Anker, Clemson University) as previously described (26). Approximately 1×10^5 J774A.1 macrophage-like cells per well were cultured in complete Dulbecco's modified Eagle medium (DMEM) and incubated at 37°C, 5% CO₂ overnight. *C. neoformans* cells were grown overnight in YPD at 30°C, washed three times and diluted in PBS. *C. neoformans* cells were opsonized with 1 µg/mL MAb 18B7 (kindly provided by Arturo Casadevall, Albert Einstein College of Medicine of Yeshiva University) and added to 10 nM phorbol myristate acetate (PMA) - activated macrophages in a 1:1 ratio. The macrophages and fungal cells were co-incubated for one hour at 37°C, 5% CO₂. Each well was carefully washed to remove extracellular fungi and left overnight at 37°C, 5% CO₂. The macrophages were lysed, the cell suspension diluted 1:100 and plated onto YPD, where the killing index was determined (# of fungal cells added/# of cells recovered). Each strain had three replicates per assay, and the assay was repeated three times. Analysis of variance was calculated using Graph Pad online software QuickCalcs (<http://www.graphpad.com/quickcalcs/>).

Fluorescence microscopy

For confocal microscopy, cells expressing Ack:Neo:mCherry (27, 50) were grown overnight in synthetic medium at 30°C and shaking at 250 RPM; cells were diluted five-fold and grown for an additional two hours. Prior to microscopy, cells were washed and resuspended in PBS. Z-stack images were collected on a DeltaVision Elite Deconvolution microscope (Olympus)

using a 100x oil immersion objective with the mCherry/AF594 575/25 filter. Images were processed using Fiji (ImageJ).

Molecular organelle dyes (Life Technologies) were used to label the cells to further delineate the localization of Ack. Ack:mCherry cells were grown overnight at 30°C in YPD and shaking and then diluted five - fold and grown for an additional two hours before the addition of the following dyes. Manufacturer's instructions were followed for all dyes. The Nuc Blue Live Cell Reagent is Hoechst 33342 nuclear stain that when bound to DNA and excited by the DAPI 365/50 filter emits blue fluorescence. The yeast vacuole membrane marker, MDY-64, which stays sequestered in the lumen of the vacuole, the FM1-43 dye, which partitions into the lipid bilayer of the membranes of endocytic vesicles and the plasma membrane, and the Mitotracker Green Stain, which crosses the mitochondrial membrane where it interacts with thiol groups on other proteins and stays sequestered within the organelle, all emit green fluorescence when excited using the GFP/FITC 470/40 filter. The ER-tracker Blue-White dye is a lipophilic dye that selectively stains the ER and emits blue fluorescence when excited by the DAPI 365/50 filter. Images were taken on an Axiovert Inverted Microscope (Zeiss). Images were processed using Zeiss software and Fiji (Image J).

Western blot analysis

A 10 mL culture of Ack:Neo:mCherry H99 was grown overnight at 30°C and shaking at 250 RPM. Five milliliters of culture was centrifuged for five minutes at 900 x g at 10°C. The pellet was resuspended in 500 µL of lysis buffer (1% TritonX-100, 50 mM Tris, pH 7.5, 150 mM NaCl, 0.5 mM EDTA) and cells were lysed using glass beads with eight passages through a mini-beadbeater (Biospec Products, Inc.) at RT with one minute rests on ice. The debris was pelleted by centrifugation and the lysate collected. Lysate samples were diluted 1:1 with sample buffer

containing 0.4% SDS and 1% β -mercaptoethanol, denatured at 95°C for ten minutes, and then electrophoresed on a 10% SDS-PAGE gel. The gel was transferred to nitrocellulose membrane at 12V for 1.5 hours using the Trans-Blot SD Semi-Dry Transfer Cell (Biorad Laboratories, Inc.), followed by incubation for 2 hours at RT in blocking solution, 5% non-fat dry milk in 50 mL of 1x TBS/Tween (2 mM Tris-HCl, pH 7.6/13.7 mM NaCl/0.5% Tween). The membrane was rinsed in 1x TBS Tween before adding the anti-mCherry monoclonal antibody (Abcam) at a 1:2000 dilution in blocking buffer overnight at 4°C to detect the ACK:Neo:mCherry. The secondary antibody was a goat anti-mouse HRP-conjugated antibody (ImmuneChem) used at a 1:6000 dilution in blocking buffer at RT for 1 hour.

III. Results

Disruption of the *ACK*, *XFP1* and *XFP2* genes in the *C. neoformans* serotype A strain through biolistic transformation

To characterize the role of the Xfp-Ack pathway in the physiology and metabolism of *C. neoformans*, constructs for the gene disruptions of *ACK*, *XFP1* and *XFP2* were generated (**Figure 2**) using both the neomycin resistance gene (2.7kb) and the hygromycin resistance gene (2.9 kb), and then introduced into *C. neoformans* using biolistic transformation. The double $\Delta xfp1:Hyg/\Delta xfp2:Neo$ was generated by transforming the $\Delta xfp2:Neo$ construct into $\Delta xfp1:Hyg$ cells. Attempts to create a double $\Delta ack:Neo/\Delta xfp1:Hyg$ through both biolistic transformation and mating were not successful.

The validation of a successful homologous recombination event into the proper locus occurred through the use of PCR with two independent primers sets: one set that annealed within the selective marker and a second set that annealed within the coding region of the gene. If the *XFP1* coding region were present, a PCR product of 2173 bp would be expected. If the hygromycin resistance gene had replaced the *XFP1* coding region, a PCR product of 1612 bp would be generated. The 1612 bp band observed confirmed the *XFP1* knockout (**Figure 3a**). If the *XFP2* coding region were intact, a PCR product of 1850 bp would be amplified. If the neomycin resistance gene had replaced the *XFP2* coding region, a PCR product of 1535 bp would be generated. The 1535 bp band observed confirmed the *XFP2* knockout (**Figure 3b**).

As further confirmation that the coding region of *XFP1* and *XFP2* were indeed disrupted RNA was isolated from the wild type (WT) and knockout mutants for cDNA analyses. The *XFP1* primers amplified the 5' region of the *XFP1* transcript, and would produce a cDNA product approximately 410 bp in size (**Figure 4a**). The *XFP2* primers amplified the 5' region of the *XFP2*

transcript and would produce a cDNA product approximately 567 bp in size (**Figure 4b**). The RT-PCR products were of the expected size, which is conclusive of successful homologous recombination and that the RNA isolation was not contaminated with genomic DNA. Amplification of the 3' portion of the actin transcript was used as a positive control for each RT-PCR reaction (**Figure 4c**).

To confirm a single integration event into the appropriate locus and that the construct had also not illegitimately recombined elsewhere in the genomes, a Southern blot was performed. *EcoRI* cuts one time within the neomycin resistance gene, downstream from where the biotinylated neomycin probe would anneal. The *PvuII* cuts one time within the hygromycin resistance gene, downstream from where the biotinylated hygromycin probe would anneal. The detection of single bands indicated that only a single integration event occurred for each of the knockout strains (data not shown).

Ack and Xfp may influence growth under low glucose and low iron conditions

The availability of glucose as the sole carbon source is limiting in some environments of the mammalian host during infection (28, 29). To test whether the *ACK* and *XFP* mutants could adapt and utilize other carbon sources during limiting conditions, the *C. neoformans* WT and mutants were grown on media supplemented with glucose, acetate, ethanol, xylose, galactose, arabinose or glycerol (**Figure 5**). The WT and mutants displayed similar growth to one another on all media tested, and under both 30°C and 37°C.

Environments of infection are usually low in available glucose (28, 30); therefore, we conducted growth curves of the *ACK* and *XFP* mutants in low concentrations of glucose, 0.001%, 0.01%, and 0.1% glucose, to observe any differences (**Figure 6**). Under all conditions tested, the $\Delta xfp1$:Hyg experienced an average of 8.7% increase in growth compared to WT by 30 hours,

whereas the $\Delta\text{ack}:\text{Neo}$ and the $\Delta\text{xfp}2:\text{Neo}$ grew slightly less than the WT by 10.6% and 9.1%, respectively, by 30 hours. The $\Delta\text{xfp}1:\text{Hyg}:\Delta\text{xfp}2:\text{Neo}$ had an increase in growth as glucose increased. By 30 hours at 0.001% glucose, the double knockout was 17.9% below WT absorbance, at 0.01%, it was 16.7% below WT absorbance, and at 0.1% glucose, it reached WT absorbance.

C. neoformans has three main virulence factors: the presence of a polysaccharide capsule, the production of melanin, and the ability to grow at 37°C. The effect of these mutants on polysaccharide capsule production was observed by growing the cells under low iron conditions. The $\Delta\text{xfp}1:\text{Hyg}$ produced cells with capsule that were similar to WT whereas the $\Delta\text{xfp}2:\text{Neo}$ was primarily microcells (**Figure 7a**). However, a pleiotropic effect was observed with the $\Delta\text{ack}:\text{Neo}$ in which microcells, macrocells, and cells with and without capsule were observed. A melanin deficiency was tested on media supplemented with L-Dopamine; both the WT and the mutants were able to produce melanin at a similar level (**Figure 7b**). The growth of the WT and mutants on various carbon sources were also performed at 37°C. No growth defect was observed at 37°C (Data not shown).

***C. neoformans* Xfp-Ack pathway may play a role in stress response towards azole drugs**

To determine whether the mutants of the Xfp-Ack pathway display an increased sensitivity to stress conditions, all strains were tested for a response to osmotic, nitrosative, and oxidative stresses. When the mutants and WT were grown on YNB medium supplemented with the different compounds that mimic stressful conditions, no significant differences were observed (**Figure 8**). Changing the growth to mammalian body temperature did not alter the effect of the stress response.

Next, we determined whether the Xfp-Ack pathway might play a role in stress response towards azole drugs by testing the effect of fluconazole, which is used to inhibit fungal growth in mammals, on the mutants and wild type. Fluconazole Etest strips (**Figure 9**) were used to determine the MIC₅₀ for the WT and the *ACK* and *XFP* mutants (**Table 3**). Since the mutants were originally isolated on YNB + 0.2% glucose plates, both 0.2% and 2% glucose plates were used to determine sensitivity to fluconazole. At 0.2% glucose, the Δ ack:Neo and Δ xfp1:Hyg: Δ xfp2:Neo displayed sensitivity to fluconazole with a MIC₅₀ of 10 μ g/mL and 8 μ g/mL, respectively, compared to the WT with a MIC₅₀ of 12 μ g/mL. The Δ xfp1:Hyg and Δ xfp2:Neo displayed more resistance to fluconazole with MIC₅₀ values of 32 μ g/mL and 16 μ g/mL, respectively. At 2% glucose, no difference was observed in MIC₅₀ values compared between Δ xfp2:Neo, Δ xfp1:Hyg: Δ xfp2:Neo and WT at 8 μ g/mL. However, the Δ ack:Neo and Δ xfp1:Hyg exhibited slight resistance compared to WT with a MIC₅₀ of 12 μ g/mL.

The *XFPI*, *XFP2*, and *XFPI/XFP2* knockout mutants displayed reduced survival in J774A.1 macrophages

To investigate the role of this acetate-producing pathway in the virulence of *C. neoformans*, the Ack and Xfp mutants were injected into the model, the wax moth larvae *Galleria mellonella*. All of the mutants killed the larvae at the same rate as the WT cells, at both 37°C and 25°C, with no significant difference observed (**Figure 10**). The median days of survival at 37°C for the PBS control was 4.74 \pm 1.09, the WT was 3.30 \pm 1.20, the Δ ack:Neo was 2.41 \pm 0.62, the Δ xfp1:Hyg was 3.22 \pm 0.52, Δ xfp2:Neo was 3.02 \pm 0.44, and the Δ xfp1:Hyg: Δ xfp2:Neo was 3.37 \pm 0.89. The median days of survival at 25°C for the PBS control was 10.87 \pm 2.96, the WT was 6.43 \pm 2.39, the Δ ack:Neo was 6.70 \pm 2.79, the Δ xfp1:Hyg was 6.90 \pm 2.48, Δ xfp2:Neo was 6.63 \pm 2.25, and the Δ xfp1:Hyg: Δ xfp2:Neo was 6.80 \pm 2.16.

Although insect immunity is similar to mammalian immunity (31), we tested the survival of the *ACK* and *XFP* knockout strains within alveolar macrophages. The *C. neoformans* mutant cells were co-cultured with J774A.1 macrophage-like cells and analyzed for defects in survival within macrophages (**Figure 11**). There was no significant difference in survival between the WT ($67.9 \pm 22.5\%$) compared to the $\Delta\text{ack}:\text{Neo}$ ($67.8 \pm 24.8\%$). In contrast, all three *XFP* mutants displayed a significant decrease in survival. The $\Delta\text{xfp1}:\text{Hyg}$ had a recovery of $45.2 \pm 18.4\%$ ($p < 0.05$). The $\Delta\text{xfp2}:\text{Neo}$, and $\Delta\text{xfp1}:\text{Hyg}:\Delta\text{xfp2}:\text{Neo}$ had a significance with a p-value less than 0.001 with a recovery of 35.4 ± 7.3 and 32.8 ± 3.8 , respectively.

***C. neoformans* AckmCherry localizes to punctate structures when grown in synthetic complete medium and to the cytoplasm when grown in YPD.**

To further address the role of Ack in physiology and virulence, we studied the localization of Ack. The AckmCherry fusion construct was integrated into the *ACK* locus where it is under the control of its native promoter. The resulting strain lacked any morphological abnormalities when grown in low iron media and visualized with India ink as the $\Delta\text{ack}:\text{Neo}$ indicating that the AckmCherry is functional. A Western blot conducted with antisera to mCherry demonstrated that full length AckmCherry is expressed. Cleaved mCherry would have been expected to approximately 26.7 kDa, whereas full length AckmCherry is 74 kDa (**Figure 12**).

When AckmCherry cells were grown and refreshed in synthetic complete medium, confocal microscopic analysis revealed the mCherry to be localized to punctate vesicles (**Figure 13**). To identify these punctate structures, co-localization experiments using organelle dyes were conducted. We used Nuc Blue Live Cell Stain to identify the nucleus, Yeast Vacuole Membrane Marker to visualize vacuoles (**Figure 14**), Mitotracker to identify the mitochondria (**Figure 15**), FM1-43 to stain endosomes/lysosomes (**Figure 16**), and ER-tracker to visualize the endoplasmic

reticulum (**Figure 17**). Throughout all of the co-localization experiments, the AckmCherry continued to display a pattern consistent with cytoplasmic staining when the cells were grown in YPD.

IV. Discussion

Across all three domains of life, acetate is found to be a predominant metabolite excreted from the cell that can be used as both a carbon and energy source (32). The study of *E. coli* growth on multiple acetogenic carbon sources, has led to the observation that a “switch” occurs that allows the cells to adapt to their varying nutritional status; when acetate evolution and activation come to equilibrium with one another, bacterial cells execute what is known as the “acetate switch” (33, 34). During acetate evolution, the TCA cycle operates through a branched route, which provides precursor metabolites but lacks the production of high-energy molecules. Therefore, in *Escherichia coli*, ATP pools regenerate through glycolysis or through the Pta-Ack pathway when acetate concentrations are high (35, 36).

A highly diverse group of eukaryotic microbes evolved ways to produce acetate as a metabolic end product when supplied glucose but little oxygen through anaerobic metabolism (37). One pathway previously thought to be only found in bacteria, Xfp-Ack, is found in some fungi and may provide ATP under conditions when the TCA cycle or oxidative phosphorylation is not functioning at levels as when both glucose and oxygen are available. In *C. neoformans*, acetate production by the Xfp-Ack pathway could play a role in virulence by reducing the pH of the external environment. This can result in the inhibition of chemotaxis of neutrophils, increased apoptosis of neutrophils, and lowering the generation of superoxides (4). Expression studies in *C. neoformans* have shown that genes encoding enzymes of this pathway are upregulated during infection (8) and under conditions the microbe may experience in the mammalian host, such as growth in macrophages (7) or in environments that induce hypoxic (24) and oxidative stress (9).

The presence of both Xfp and Ack, combined with the presence of genes encoding all of the other enzymes of the pentose phosphate pathway in *Cryptococcus* suggested Xfp-Ack might

function as a modified pentose phosphoketolase pathway for acetate production (4). Comparing the mutant strains to the WT, there is not a significant defect on acetate production when grown on glucose (G. Kisirkoi and K. Smith, unpublished), indicating the Pdc-Ald pathway maybe the principal route of acetate production *in vitro*. Also, the acetate may never leave the cell but instead, be utilized by Acs, which converts the acetate to acetyl-CoA (1). However, this does not rule out a role for Ack-Xfp1/Xfp2 pathways in acetate production during infection.

The lack of phenotype for both mutants under certain *in vitro* conditions suggests that although Xfp and Ack may partner, they may not always partner together. The individual knockouts of *ACK*, *XFPI*, and *XFP2* could be constructed, along with the double *XFPI/XFP2* knockout; however, attempts to generate a double knockout of *ACK* and *XFPI* have thus far been unsuccessful. If these enzymes partnered together under all circumstances, the individual knockouts, as well as the *XFPI* and *XFP2* double knockout, would be expected to show a phenotype similar to the double *ACK* and *XFPI* knockout. Therefore, this genetics approach suggests the enzymes may function in two separate pathways, but we also question the possibility of another partner enzyme that interacts with either Xfp and/or Ack that can use and produce acetyl phosphate. Genes encoding other known acetyl phosphate-producing enzymes are absent from the *C. neoformans* genome. Two possibilities to explain this are: (1) a novel or evolutionarily distinct class of known acetyl phosphate-producing enzyme is present in fungi with Ack, or (2) a previously uncharacterized or undiscovered acetyl phosphate-generating enzyme is present in fungi with Ack

In each fungal genome that possesses an *ACK*, at least one *XFP* ORF has been identified. In many cases, like *C. neoformans*, two ORFS have sequence identity to *XFP* (5). A phylogenetic analysis of Xfp sequences revealed two distinct fungal Xfp clades, designated as Xfp1 and Xfp2. This is the first study that investigates the physiological role of this pathway in a fungus that has

two Xfps. Sanchez et al. (6) conducted a phylogenetic analysis that grouped the Xfps into three groups. Group 1 includes fungal and bacterial phosphoketolases from *Cryptococcus*, *Aspergillus*, *Bifidobacteria*, and *Lactobacillus* species. Group 2 and 3 include phosphoketolases mainly from proteobacteria and cyanobacteria; however, Group 3 does include the fungal Xfp1 clade (19). Several experimental studies on Xfp2 enzymes from Group 2 have been reported (19, 21). Until recently, the only biochemical data available on an Xfp came from bacterial Xfps, but Glenn et al. (20) characterized the Xfp2 from *C. neoformans* in the acetyl phosphate-producing direction and did not report characterization of the phosphoketose-forming direction.

The Group 3 Xfps include the Xfp1 enzymes from *C. neoformans*, *A. nidulans*, and *Schizosaccharomyces pombe*. Characterization of a fungal Xfp1 has not been reported. Prior attempts to express and purify these three fungal Xfps from *E. coli* have resulted in the production of inactive protein when assayed with F6P (Taylor, Nguyen and Smith, unpublished data). In addition, the Group 3 Xfp from *Anabaena* lacks activity with either X5P or F6P as the substrate, whereas both Group 1 Xfps could use both substrates (19). The Xfp1 enzymes could possibly be functioning in the opposite direction or catalyzing a different reaction, since they all possess a TPP-binding domain and little activity when assayed with either F6P or X5P (19). However, a phosphoproteomic study conducted in *S. pombe* (38) indicates that a conserved serine residue is phosphorylated, within all of the fungal Xfp1 enzymes, which is a glycine residue in the Group 1 Xfps: the fungal Xfp2s and the bacterial Xfps (Taylor, Guggisberg, and Smith, unpublished). Therefore, post-translational modification may be needed in order for these enzymes to be active.

Furthermore, the question is also raised whether Xfp1 and Xfp2 are redundant enzymes in *C. neoformans*. This could be an additional reason for why the individual *XFPI* and *XFPII*

knockouts survive. However, if they aren't redundant, one of the Xfps could partner with Ack to catalyze the phosphoketose-forming direction, and under certain conditions, one of the Xfps could play a role in generating glyceraldehyde 3-phosphate to shuttle back into the pay-off phase of glycolysis to by-pass the consumption of ATP in the beginning of glycolysis under stressful conditions (12). If glyceraldehyde 3-phosphate is the main product, then acetyl phosphate is a by-product, and Ack could be present to regulate the acetyl phosphate pools of the cell.

The low glucose growth experiments (**Figure 6**) suggest that Ack and Xfp2 may function together under low glucose environments. The $\Delta xfp1$:Hyg grew 8.7% better than WT under all conditions tested. Ack and Xfp2 would still be present in this knockout, but in both the Δack :Neo and $\Delta xfp2$:Neo, growth was less than observed in WT under all three conditions tested. In this scenario, Ack and Xfp2 could be functioning to produce acetate to be used as a carbon source since glucose is limiting, along with ATP. If Xfp1 is using another phosphoketose such as sedoheptulose 7-phosphate or ribose 5-phosphate, it may be removing metabolites from important pathways such as the pentose phosphate pathway or the synthesis of nucleotides. However, certain fungi, such as *A. nidulans* and *S. pombe*, only have one Xfp that falls within the Xfp1 clade suggesting that Xfp1 may partner with Ack under certain growth conditions within these fungi.

To investigate the role of the Xfp-Ack pathway in *C. neoformans* virulence, *in vivo* studies were conducted with the *ACK*, *XFPI*, and *XFP2* mutants using the invertebrate *Galleria mellonella* (wax moth larvae). *G. mellonella* is an excellent model for studying fungal pathogenesis due to the larvae's size, cost effectiveness, and survival at RT, removing any temperature effects in the experiment (39). In addition, the larvae are an easy method to study the interactions of the fungus with the immune system, which is similar to the mammalian innate

immune system (40). The immune system of the larvae is organized by hemocytes, which are very similar to mammalian neutrophils. This model system is excellent when observing mutants that may be defected in capsule or melanin production (40). Although insect hemocytes can phagocytose and kill invading cells, they more closely resemble human neutrophils than macrophages, especially through their oxidative burst pathways (41).

No significant difference was observed in the phenotype between WT and mutants (**Figure 10**). The disparity that insect immunity displays compared to mammalian immunity (42) may be an explanation for why no difference is seen among the mutants and the WT, when *G. mellonella* was used as the *in vivo* model .

Macrophage survival assay indicates that Xfp1 and Xfp2 each play important roles in fungal survival in J774A.1 cells (**Figure 11**). Furthermore, this data suggests that Xfp1 and Xfp2 may not be partnering with Ack within the macrophage in the mammalian host, since the survival for the $\Delta\text{ack}:\text{Neo}$ is similar to WT and that of $\Delta\text{xfp1}:\text{Hyg}$, $\Delta\text{xfp2}:\text{Neo}$, and $\Delta\text{xfp1}:\text{Hyg}:\Delta\text{xfp2}:\text{Neo}$ are all statistically reduced from the WT. The acetyl phosphate produced by these enzymes could still be hydrolyzed to acetate in the absence of Ack. We hypothesize these mutants will also be less virulent than wild type in the murine model, since experimental results produced in macrophage studies predict the results acquired when using mice as an *in vivo* model (43). Additional experimental evidence suggesting Ack and Xfp2 may work together is when the cells were grown in low iron media and imaged with India ink as both the $\Delta\text{ack}:\text{Neo}$ and $\Delta\text{xfp2}:\text{Neo}$ mutants displayed different cell wall and cell size effects (**Figure 7a**).

Ack localizes to punctate structures within the cell (**Figure 13**), which is similar to the localization previously reported for both Kic1 and Cbk1 (44). Kic1 and Cbk1 are both serine threonine kinases that localize to punctate structures within *C. neoformans* that function within the RAM signaling pathway that plays a role in morphogenesis (44). Homologs of both of these

proteins have been studied in *Drosophila melanogaster*, *Neurospora crassa*, *Caenorhabditis elegans*, and humans (44). These homologs play some role in morphology such as hyphal elongation in fungi, wing hair development in the fruit fly, neuronal cell shape in *C. elegans*, and tumor suppression in humans (44). These punctate structures are thought to be recycling endosomes, which are an intermediate between the Golgi and the plasma membrane and are thought to be a hub for the biosynthesis or modification of plasma membrane proteins (44). These data suggests that Ack may play a structural role within *C. neoformans*. Little is known about the sorting of proteins to the cell surface in eukaryotic organisms, but there is some evidence that sorting occurs in endosomes (45, 46).

The punctate structures in the confocal microscopy are absent in the fluorescence microscopy (**Figures 14-17**), and the fluorescence pattern is consistent with Ack localizing to the cytoplasm (47). Therefore, the FM1-43 dye used to determine co-localization to the plasma membrane and recycling endosomes does not co-localize with the AckmCherry pattern. This difference could possibly be due to the YPD media the cells were grown prior to the fluorescence microscopy versus the synthetic complete media the cells were grown in prior to the confocal microscopy. The punctate structures seen in Figure 13, which were observed in cells grown in synthetic complete medium, could be a difference in localization due to the surrounding environment (48).

Localization studies of Xfp1 from *S. pombe* indicate that this enzyme is found in both the cytoplasm and the nucleus (49). If Xfp1 and Ack function together at some point during metabolism, then it would be reasonable that Ack would also be found in the cytoplasm. In addition, if there were instances these two enzymes did not work together, then the localization of Ack to these punctate structures within the cell would also be plausible, along with Xfp1

localizing to the nucleus. Even though many questions remain unanswered, the Xfp-Ack pathway(s) is far more complex in fungi than in heterofermentative bacteria.

Our data indicates that Xfp1 and Xfp2 play a role in macrophage survival during *C. neoformans* pathogenesis, and that Ack and Xfp2 possibly partner together under low glucose and low iron environments. Although Ack does not seem to play a role in virulence, it does have a role under specific growth conditions. Further studies need to be conducted to elucidate the partnership of Ack and Xfp1 or Xfp2, as well as whether both Xfp enzymes use the same phosphoketose substrates or if a second partner enzyme is present. Additionally, more rigorous mating experiments with the $\Delta\text{ack}:\text{Neo KN99a}$ and $\Delta\text{xfp1}:\text{Hyg KN99}\alpha$ cells needs to be conducted, since attempts to generate an *ACK/XFP1* double mutant by both biolistic transformation and preliminary mating experiments have been unsuccessful. The creation of a $\Delta\text{xfp2}:\text{Hyg}$ construct would allow generation of a *ACK/XFP2* double mutant through biolistic transformation or mating. The inability to create a double mutant of either pathway (Xfp1-Ack or Xfp2-Ack) would clarify if one or both pathways are indeed essential and indicate whether the functioning of both enzymes is necessary.

Ma et al. have previously demonstrated that experimental results generated with macrophage studies are strong predictors to the results using mice as an *in vivo* model. Therefore, inhalation and/or tail-vein injection experiments need to be conducted in the murine model with the different mutants since we have observed an *in vivo* phenotype within mouse macrophages with both the *XFP1* and *XFP2* mutants. These experiments would be expected to provide more information about the mammalian specific role these enzymes are playing within *C. neoformans*.

V. Acknowledgments

The authors thank Dr. Lukasz Kozubowski for his helpful advice in the advancement of this work and Dr. James Morris and Dr. Meredith Morris for their insight and recommendations on the microscopy work. Awards from the National Institutes of Health (GMO84417-01A1), the National Science Foundation (Award # 0920274), and the South Carolina Experiment Station Project SC-1700340 supported this work.

IV. References

1. Price MS, Betancourt-Quiroz M, Price JL, Toffaletti DL, Vora H, Hu G, Kronstad JW, Perfect JR. 2011. *Cryptococcus neoformans* requires a functional glycolytic pathway for disease but not persistence in the host. *mBio* **2**:e00103-00111.
2. Lin X, Heitman J. 2006. The biology of the *Cryptococcus neoformans* species complex. *Annu Rev Microbiol* **60**:69-105.
3. Himmelreich U, Allen C, Dowd S, Malik R, Shehan BP, Mountford C, Sorrell TC. 2003. Identification of metabolites of importance in the pathogenesis of pulmonary cryptococcoma using nuclear magnetic resonance spectroscopy. *Microb Infect / Institut Pasteur* **5**:285-290.
4. Wright L, Bubb W, Davidson J, Santangelo R, Krockenberger M, Himmelreich U, Sorrell T. 2002. Metabolites released by *Cryptococcus neoformans* var. *neoformans* and var. *gattii* differentially affect human neutrophil function. *Microb Infect* **4**:1427-1438.
5. Ingram-Smith C, Martin SR, Smith KS. 2006. Acetate kinase: not just a bacterial enzyme. *Trends Microbiol* **14**:249-253.
6. Borja Sanchez MZ, Fernando Gonzalez-Candelas, Clara G. de los Reyes-Gavilan, and Abelard Margolles. 2010. Bacterial and Eukaryotic Phosphoketolases: Phylogeny, Distribution and Evolution. *J Mol Microbiol Biotechn* **18**:37-51.
7. Fan W, Kraus PR, Boily MJ, Heitman J. 2005. *Cryptococcus neoformans* gene expression during murine macrophage infection. *Eukaryot Cell* **4**:1420-1433.
8. Hu G, Cheng PY, Sham A, Perfect JR, Kronstad JW. 2008. Metabolic adaptation in *Cryptococcus neoformans* during early murine pulmonary infection. *Mol Microbiol* **69**:1456-1475.
9. Upadhy R, Campbell LT, Donlin MJ, Aurora R, Lodge JK. 2013. Global transcriptome profile of *Cryptococcus neoformans* during exposure to hydrogen peroxide induced oxidative stress. *PLoS One* **8**:e55110.

10. Chun CD, Liu OW, Madhani HD. 2007. A link between virulence and homeostatic responses to hypoxia during infection by the human fungal pathogen *Cryptococcus neoformans*. PLoS Pathog **3**:e22.
11. Kleijn RJ, van Winden WA, van Gulik WM, Heijnen JJ. 2005. Revisiting the ¹³C-label distribution of the non-oxidative branch of the pentose phosphate pathway based upon kinetic and genetic evidence. FEBS J **272**:4970-4982.
12. Papini M, Nookaew I, Siewers V, Nielsen J. 2012. Physiological characterization of recombinant *Saccharomyces cerevisiae* expressing the *Aspergillus nidulans* phosphoketolase pathway: validation of activity through ¹³C-based metabolic flux analysis. Appl Microbiol Biotechnol **95**:1001-1010.
13. Thaker TM, Tanabe M, Fowler ML, Preininger AM, Ingram-Smith C, Smith KS, Iverson TM. 2013. Crystal structures of acetate kinases from the eukaryotic pathogens *Entamoeba histolytica* and *Cryptococcus neoformans*. J Struct Biol **181**:185-189.
14. Glenn K, Smith KS. 2015. Allosteric regulation of *Lactobacillus plantarum* xylulose 5-phosphate/fructose 6-phosphate phosphoketolase (Xfp). J Bacteriol **197**:1157-1163.
15. Yevenes A, Frey PA. 2008. Cloning, expression, purification, cofactor requirements, and steady state kinetics of phosphoketolase-2 from *Lactobacillus plantarum*. Bioorg Chem **36**:121-127.
16. Meile L, Rohr LM, Geissmann TA, Herensperger M, Teuber M. 2001. Characterization of the D-xylulose 5-phosphate/D-fructose 6-phosphate phosphoketolase gene (*xfp*) from *Bifidobacterium lactis*. J Bacteriol **183**:2929-2936.
17. Suzuki R, Katayama T, Kim BJ, Wakagi T, Shoun H, Ashida H, Yamamoto K, Fushinobu S. 2010. Crystal structures of phosphoketolase: thiamine diphosphate-dependent dehydration mechanism. J Biol Chem **285**:34279-34287.
18. Petrareanu G, Balasu MC, Vacaru AM, Munteanu CV, Ionescu AE, Matei I, Szedlaczek SE. 2014. Phosphoketolases from *Lactococcus lactis*, *Leuconostoc mesenteroides* and *Pseudomonas aeruginosa*: dissimilar sequences, similar

- substrates but distinct enzymatic characteristics. *Appl Microbiol Biotechnol* **98**:7855-7867.
19. Moriyama T, Tajima N, Sekine K, Sato N. 2014. Characterization of three putative xylulose 5-phosphate/fructose 6-phosphate phosphoketolases in the cyanobacterium *Anabaena* sp. PCC 7120. *Biosci Biotechnol Biochem* doi:10.1080/09168451.2014.993357:1-8.
 20. Glenn K, Ingram-Smith C, Smith KS. 2014. Biochemical and kinetic characterization of xylulose 5-phosphate/fructose 6-phosphate phosphoketolase 2 (Xfp2) from *Cryptococcus neoformans*. *Eukaryot Cell* **13**:657-663.
 21. Glenn K, Smith KS. 2015. Allosteric Regulation of *Lactobacillus plantarum* Xylulose 5-phosphate/Fructose 6-phosphate Phosphoketolase (Xfp). *J Bacteriol* doi:10.1128/JB.02380-14.
 22. Davidson RC, Blankenship JR, Kraus PR, de Jesus Berrios M, Hull CM, D'Souza C, Wang P, Heitman J. 2002. A PCR-based strategy to generate integrative targeting alleles with large regions of homology. *Microbiology* **148**:2607-2615.
 23. Hua J, Meyer JD, Lodge JK. 2000. Development of positive selectable markers for the fungal pathogen *Cryptococcus neoformans*. *Clin Diagn Lab Immunol* **7**:125-128.
 24. Chun CD LO, Madhani HD. 2007. A link between virulence and homeostatic responses to hypoxia during infection by the human fungla pathogen *Cryptococcus neoformans*. *PLoS Pathog* **3**:e22.
 25. Lee H, Bien CM, Hughes AL, Espenshade PJ, Kwon-Chung KJ, Chang YC. 2007. Cobalt chloride, a hypoxia-mimicking agent, targets sterol synthesis in the pathogenic fungus *Cryptococcus neoformans*. *Mol Microbiol* **65**:1018-1033.
 26. Nicola AM, Robertson EJ, Albuquerque P, Derengowski Lda S, Casadevall A. 2011. Nonlytic exocytosis of *Cryptococcus neoformans* from macrophages occurs *in vivo* and is influenced by phagosomal pH. *MBio* **2**.

27. Budden B. 2013. Characterization of putative acetate kinase in the pathogenic yeast *Cryptococcus neoformans*. Master of Science Western Carolina.
28. Perfect JR, Lang SD, Durack DT. 1980. Chronic cryptococcal meningitis: a new experimental model in rabbits. *Am J Pathol* **101**:177-194.
29. Bahn YS, Xue C, Idnurm A, Rutherford JC, Heitman J, Cardenas ME. 2007. Sensing the environment: lessons from fungi. *Nat Rev Microbiol* **5**:57-69.
30. Barelle CJ, Priest CL, Maccallum DM, Gow NA, Odds FC, Brown AJ. 2006. Niche-specific regulation of central metabolic pathways in a fungal pathogen. *Cell Microbiol* **8**:961-971.
31. Dubovskiy IM, Krukova NA, Glupov VV. 2008. Phagocytic activity and encapsulation rate of *Galleria mellonella* larval haemocytes during bacterial infection by *Bacillus thuringiensis*. *J Invertebr Pathol* **98**:360-362.
32. Smith KS, Ingram-Smith C. 2007. *Methanosaeta*, the forgotten methanogen. *Trends Microbiol* **15**:150-155.
33. Wolfe AJ. 2005. The acetate switch. *MMBR* **69**:12-50.
34. Wolfe AJ. 2010. Physiologically relevant small phosphodonors link metabolism to signal transduction. *Curr Opin Microbiol* **13**:204-209.
35. Brown TD, Jones-Mortimer MC, Kornberg HL. 1977. The enzymic interconversion of acetate and acetyl-coenzyme A in *Escherichia coli*. *J Gen Microbiol* **102**:327-336.
36. Rose IA, Grunberg-Manago M, Korey SF, Ochoa S. 1954. Enzymatic phosphorylation of acetate. *J Biol Chem* **211**:737-756.
37. Tielens AG, van Grinsven KW, Henze K, van Hellemond JJ, Martin W. 2010. Acetate formation in the energy metabolism of parasitic helminths and protists. *Int J Parasitol* **40**:387-397.

38. Beltrao P, Trinidad JC, Fiedler D, Roguev A, Lim WA, Shokat KM, Burlingame AL, Krogan NJ. 2009. Evolution of phosphoregulation: comparison of phosphorylation patterns across yeast species. *PLoS biology* **7**:e1000134.
39. Fuchs BB, O'Brien E, Khoury JB, Mylonakis E. 2010. Methods for using *Galleria mellonella* as a model host to study fungal pathogenesis. *Virulence* **1**:475-482.
40. Arvanitis M, Glavis-Bloom J, Mylonakis E. 2013. Invertebrate models of fungal infection. *Biochim Biophys Acta* **1832**:1378-1383.
41. Bergin D, Reeves EP, Renwick J, Wientjes FB, Kavanagh K. 2005. Superoxide production in *Galleria mellonella* hemocytes: identification of proteins homologous to the NADPH oxidase complex of human neutrophils. *Infect Immun* **73**:4161-4170.
42. Tojo S, Naganuma F, Arakawa K, Yokoo S. 2000. Involvement of both granular cells and plasmatocytes in phagocytic reactions in the greater wax moth, *Galleria mellonella*. *J Insect Physiol* **46**:1129-1135.
43. Ma H, Hagen F, Stekel DJ, Johnston SA, Sionov E, Falk R, Polacheck I, Boekhout T, May RC. 2009. The fatal fungal outbreak on Vancouver Island is characterized by enhanced intracellular parasitism driven by mitochondrial regulation. *Proc Natl Acad Sci U S A* **106**:12980-12985.
44. Walton FJ, Heitman J, Idnurm A. 2006. Conserved elements of the RAM signaling pathway establish cell polarity in the basidiomycete *Cryptococcus neoformans* in a divergent fashion from other fungi. *Mol Biol Cell* **17**:3768-3780.
45. Proszynski TJ, Klemm RW, Gravert M, Hsu PP, Gloor Y, Wagner J, Kozak K, Grabner H, Walzer K, Bagnat M, Simons K, Walch-Solimena C. 2005. A genome-wide visual screen reveals a role for sphingolipids and ergosterol in cell surface delivery in yeast. *Proc Natl Acad Sci U S A* **102**:17981-17986.
46. Alvarez-Vasquez F, Riezman H, Hannun YA, Voit EO. 2011. Mathematical modeling and validation of the ergosterol pathway in *Saccharomyces cerevisiae*. *PLoS One* **6**:e28344.

47. O'Meara TR, Norton D, Price MS, Hay C, Clements MF, Nichols CB, Alspaugh JA. 2010. Interaction of *Cryptococcus neoformans* Rim101 and protein kinase A regulates capsule. PLoS Pathog **6**:e1000776.
48. Sophianopoulou V, Diallinas G. 1995. Amino acid transporters of lower eukaryotes: regulation, structure and topogenesis. FEMS Microbiol Rev **16**:53-75.
49. Matsuyama A, Arai R, Yashiroda Y, Shirai A, Kamata A, Sekido S, Kobayashi Y, Hashimoto A, Hamamoto M, Hiraoka Y, Horinouchi S, Yoshida M. 2006. ORFeome cloning and global analysis of protein localization in the fission yeast *Schizosaccharomyces pombe*. Nat Biotechnol **24**:841-847.
50. Taylor T, Bose I, Luckie T, Smith K. 2015. Biolistic Transformation of a Fluorescent Tagged Gene into the Opportunistic Fungal Pathogen *Cryptococcus neoformans*. J.Vis. Exp. **97**.
51. Lee S, Milgroom M, and Taylor J. 1988. A rapid, high yield mini-prep method for isolation of total genomic DNA from fungi. Fungal Genet Newsl **35**: 23–24.
52. Wu Z, Wang T, Huang W, and Qu Y. 2001. A simplified method for chromosome DNA preparation from filamentous Fungi. Mycosystema **20**: 575–577.

Table 1. Primers Used in Creating the Deletion Constructs.

No	Primer Name	Primer Sequence
1	5' XFP1 out:	5' CAGTGCAATTTTCAGGGAAAC 3'
2	5' XFP1 in:	5' GAAGATATTGTCAGCCTGCTACTGCG 3'
3	5' XFP1-selec	5' GTCAGCTGAACGCTCATAAACAGGAAACAGCTATGACCATG 3'
4	selec-5' XFP1	5' CATGGTCATAGCTGTTTCCTGGTTTATGAGCGTTCAGCTGAC 3'
5	selec-3' XFP1	5' CACTGGCCGTCGTTTTACAACGGTCCAGTCACTGGAATAAT 3'
6	3' XFP1- selec	5' ATTATTCCAGTGACTGGACCGTTGTAAAACGACGGCCAGTG 3'
7	3' XFP1 in	5' CGTCTTCTCCCTTTCGACCATCCGAG 3'
8	3' XFP1 out	5' CAGATTTGGGCAGCAGTGAGC 3'
9	5' XFP2 out:	5' CGTCGGTGACCGATTATTAAG 3'
10	5' XFP2 in:	5' CAAGGTTCAAGGGGAAACAAGGCGGC 3'
11	5' XFP2-selec	5' CACTCAATACAACCTCTCAGCCAGGAAACAGCTATGACCATG 3'
12	selec-5' XFP2	5' CATGGTCATAGCTGTTTCCTGGCTGAGAGTTGTATTGAGTG 3'
13	selec-3' XFP2	5' CACTGGCCGTCGTTTTACAACCGAATAGGGTAGGGTACAGTC 3'
14	3' XFP2- selec	5' GACTGTAACTACCCTATTCGGTTGTAAAACGACGGCCAGTG 3'
15	3' XFP2 in	5' GTCCTACTGCTCTTCCCATGTC 3'
16	3' XFP2 out	5' CGGACAGCTCAGGCGAGACG 3'
17	K101	5' TTCTGAAAGACAGAAGGAGCCCACC 3'
18	K102	5' GCTTTCTTCACTCCCGATGGATTTCG -3'
19	K103	5' GTAGCGAGGTCTGGAAGCCAC 3'
20	K104	5' GACTTGGGGAAGAGGAATTC 3'
21	K105	5' CATCACCAAGTACTGACTGCCAGGAAACAGCTATGACCATG 3'
22	K106	5' CATGGTCATAGCTGTTTCCTGGGCAGTCACTACTTGGTGATG 3'
23	K107	5' CACTGGCCGTCGTTTTACAACATTTACTACGAAGCCAACATTC 3'
24	K108	5' GAAATGTTGGCTTCGTAGTAAATGTTGTAAAACGACGGCCAGTG 3'

Table 2: PCR and RT-PCR Confirmation Primers

Primer Name	Primer Sequence
5'XFP1ex	5' – CCAGTATCCGGCCCTCATCTGGTC – 3'
3'HYGintcoding	5' – GCCGATGCAAAGTGCCGATAAACA – 3'
5'HYGintcoding	5' – TGTTTATCGGCACTTTGCATCGGC – 3'
3'XFP1ext	5' – CCGACGTTCTTACCAGGGCCTTGG – 3'
5'XFP2ext	5' – GCCGCTCGATGAATTTGTGGCCTC – 3'
3'NEOintcoding	5' – CTGCAGTTCATTACAGGGCACCGGA – 3'
5'NEOintcoding	5' – TCCGGTGCCCTGAATGAACTGCAG – 3'
3'XFP2ext	5' – TCTGGCTTCTTCCCTGATCAGGAC – 3'
XFP1F-RT	5' – GGTCTCATTGCTTTCCAGAGGGTAGCC – 3'
XFP1R-RT	5' – CCACCTTCATGAAGCGCACCGGG – 3'
XFP2F-RT	5' – CATCTCAAGGCTCGTCTTTTGGGTCACTGG – 3'
XFP2R-RT	5' – GGCTTCCAGCCATAGCCAACGAAGAG – 3'
ACTIN-1	5' – CGCTATCCTCCGTATCGATCTTGC – 3'
ACTIN-2	5' – CAGCTGGAAGGTAGACAAAGAGGC – 3'

Table 3. The Effect of Fluconazole Determined Through Etest.

	2% Glucose	0.2% Glucose
WT	8 µg/mL	12 µg/mL
Δack	12 µg/mL	10 µg/mL
Δxfp1	12 µg/mL	32 µg/mL
Δxfp2	8 µg/mL	16 µg/mL
Δxfp1Δxfp2	8 µg/mL	8 µg/mL

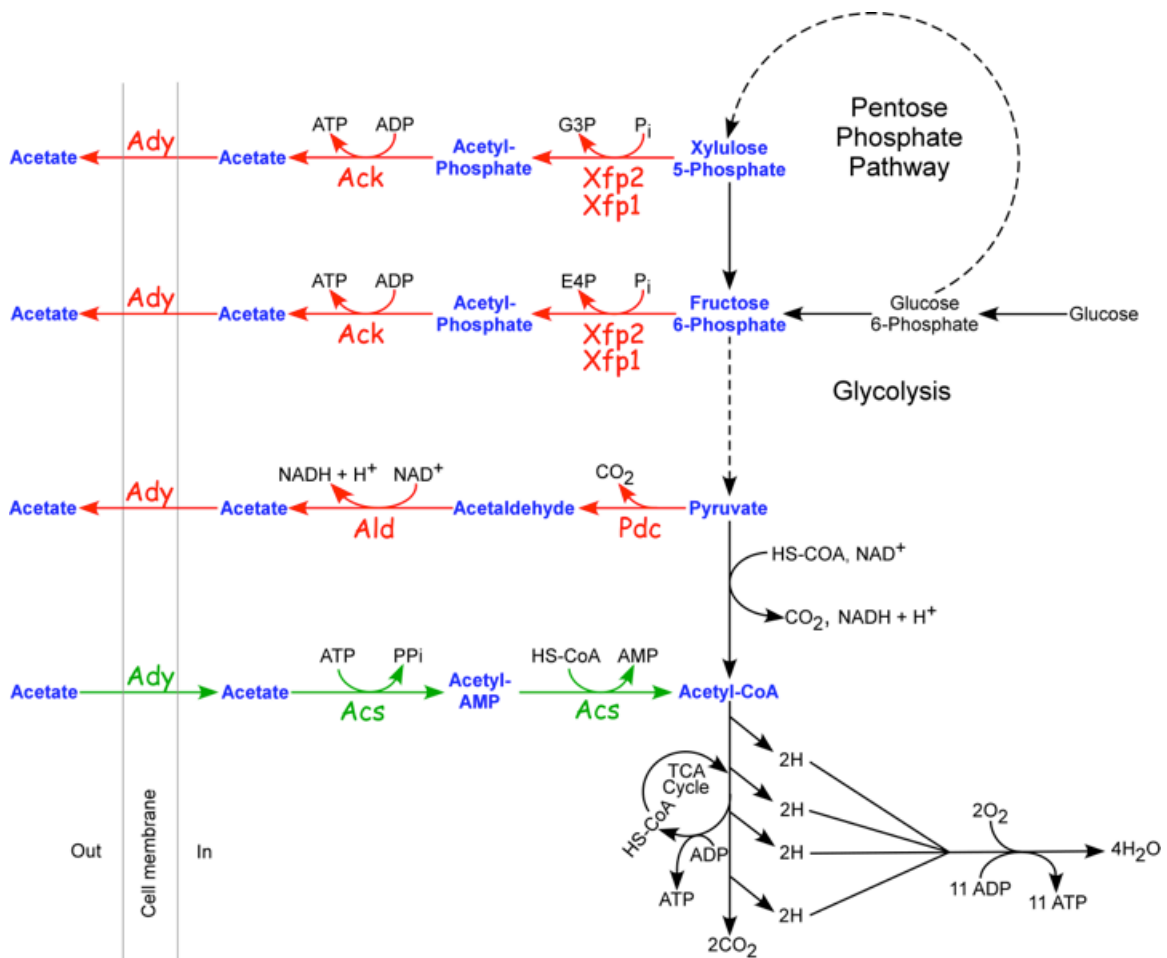


Figure 1. Two putative pathways in *C. neoformans* for acetate production. Two pathways for the production of acetate in *C. neoformans* are highlighted in red. Acs (in green) utilizes acetate transported into the cell and converts it into acetyl-CoA. Enzyme abbreviations are designated in the text. (Unpublished data; permission granted for the reuse of this figure by K. Smith).

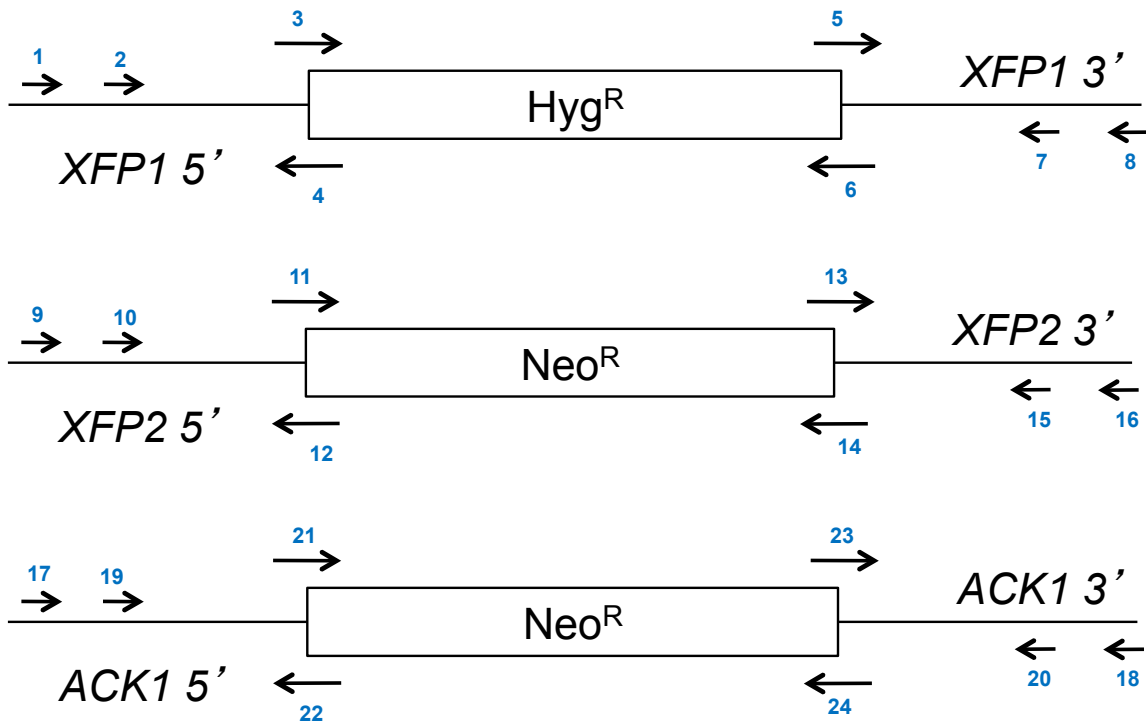


Figure 2. Strategy for generating *XFP1*, *XFP2*, and *ACK* deletion knockouts. The final deletion constructs with either the Neomycin or Hygromycin selectable marker were created by three-step overlap PCR. Using the Xfp1 schematic as an example, the first PCR would include amplification of the 5' non-coding region, with primers 1 and 4, and the 3' non-coding region, with primers 5 and 8 from genomic DNA. The second PCR would include amplification of the selectable marker using primers 3 and 6 from the respective plasmids. The third PCR would use the overlap strategy of this method and amplify all 3 pieces with nested primers 2 and 7.

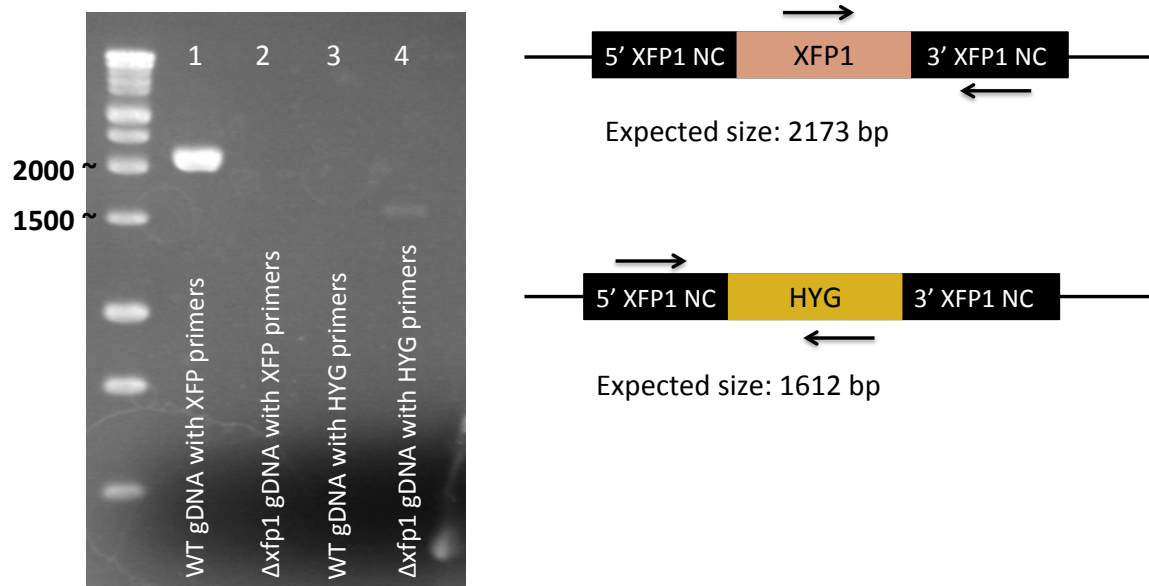


Figure 3a. Δ xfp1 KN99 α knockout mutant gDNA confirmation. gDNA was amplified with primers that would anneal within the XFP1 coding region and the 3' non-coding region. This results in an expected size product of 2173 bp for WT gDNA (Lane 1) and would not amplify the Δ xfp1 KN99 α gDNA (Lane 2). gDNA was also amplified with primers that would anneal within the 5' non-coding region and the hygromycin resistance gene. This would not amplify the WT gDNA (Lane 3) and results in the expected size product of 1612 bp for the Δ xfp1 KN99 α gDNA (Lane 4).

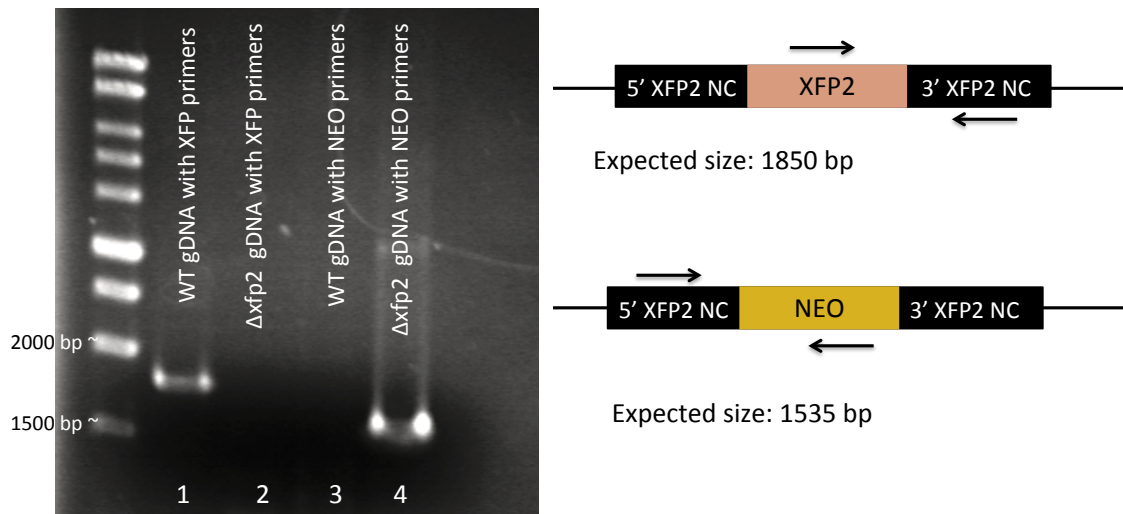


Figure 3b. $\Delta xfp2$ KN99 α knockout mutant gDNA confirmation. gDNA was amplified with primers that would anneal within the *XFP2* coding region and the 3' non-coding region. This results in the expected size product of 1850 bp for WT gDNA (Lane 1) and would not amplify the $\Delta xfp2$ KN99 α gDNA (Lane 2). gDNA was also amplified with primers that would anneal within the 5' non-coding region and the neomycin resistance gene. This would not amplify the WT gDNA (Lane 3) and results in the expected size product of 1535 bp for the $\Delta xfp2$ KN99 α gDNA (Lane 4).

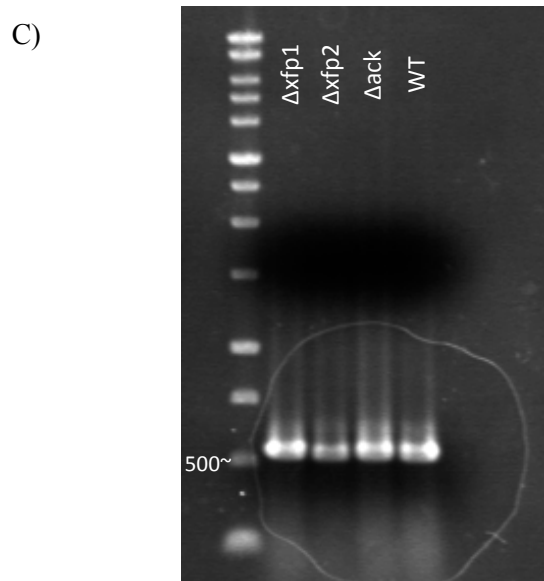
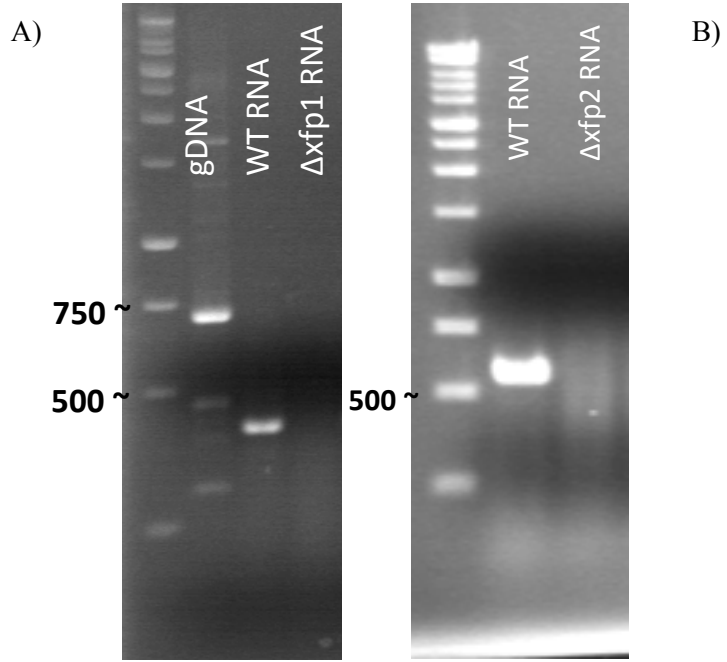


Figure 4. Confirmation of knockout mutants using RT-PCR. (a) ***Δxfp1* KN99α knockout mutant verification.** Isolated RNA from both WT and the *Δxfp1* KN99α, grown in YPD at 30°C, was used for cDNA analysis. Amplification of WT gDNA results in a size of 695 bp (Lane 1). WT RNA produced a cDNA with a size of 410 bp (Lane 2), and the primers would not amplify the *Δxfp1* KN99α RNA (Lane 3). (b) ***Δxfp2* KN99α knockout mutant verification.** Isolated RNA from both WT and the *Δxfp2* KN99α was used for cDNA analysis with primers that amplified across 2 introns of *XFP2*. The amplification of WT RNA produces a cDNA with a size of 567 bp (Lane 1), and the primers would not amplify the *Δxfp2* KN99α RNA (Lane 2). (c) **Actin RNA controls.** As confirmation of RNA stability, primers were used to amplify the 3' portion of the actin gene. This results a 543 bp band for *Δxfp1* (Lane 1), *Δxfp2* (Lane 2), *Δack* (Lane 3), and WT (Lane 4).

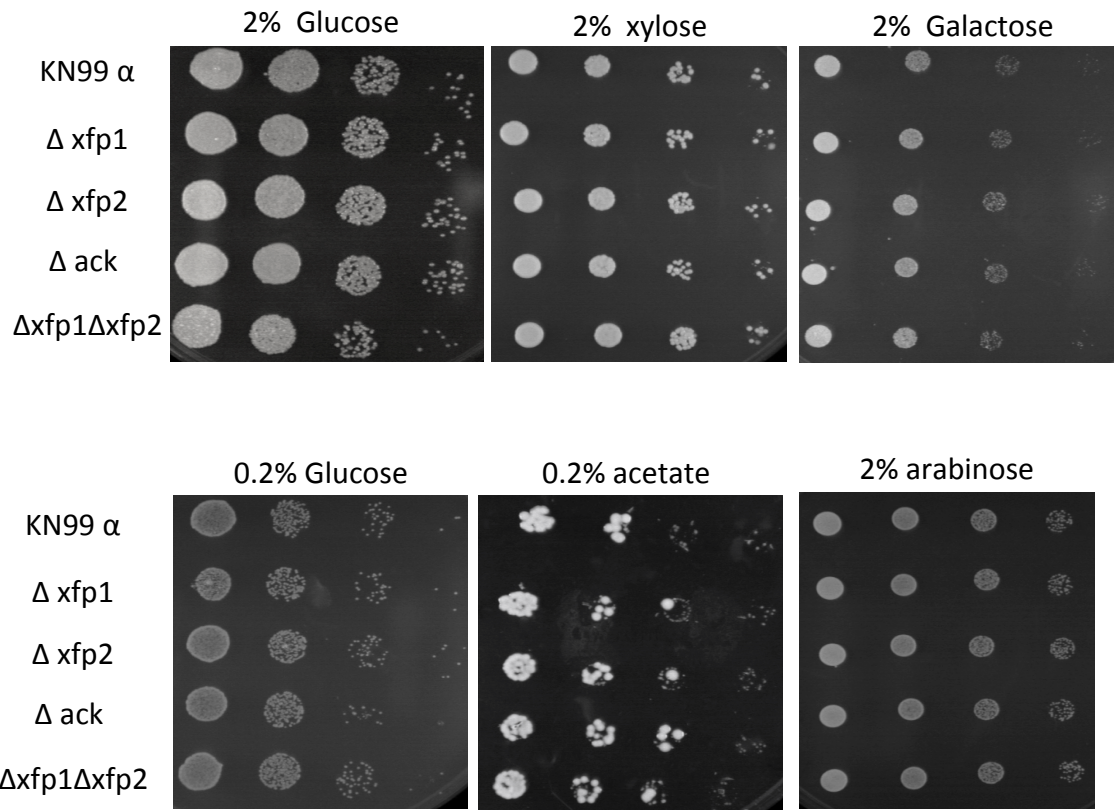
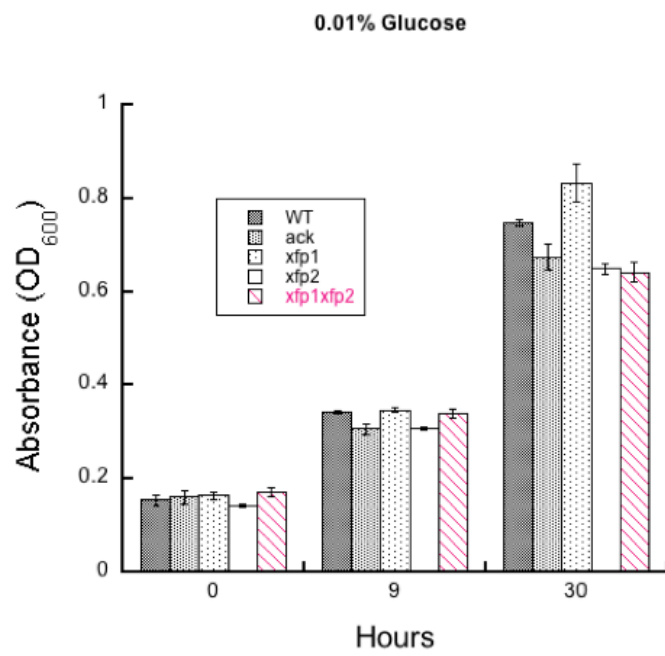
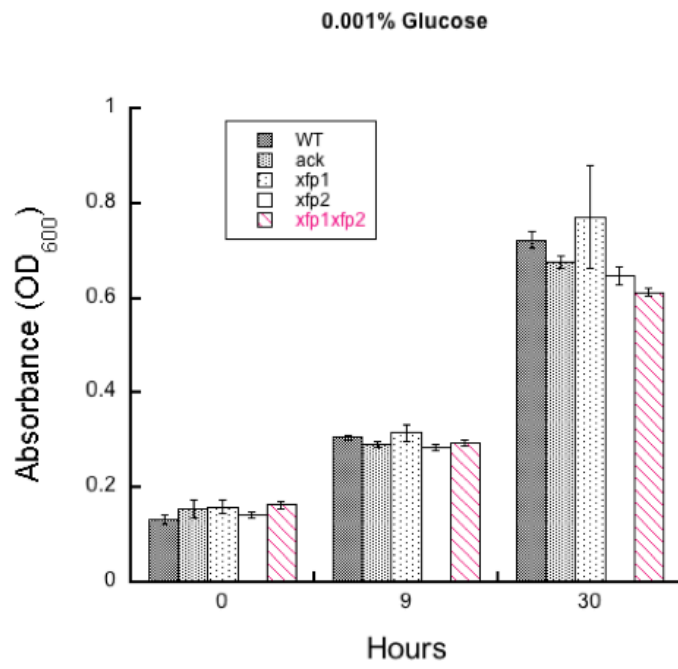


Figure 5. Xfp-Ack knockouts lack a growth phenotype on all carbon sources. Cells were diluted in water to 1×10^4 cells, and then diluted serially 10-fold. Five microliters of each dilution was spotted onto YNB plates. Similar results were seen at both 30°C and 37°C.



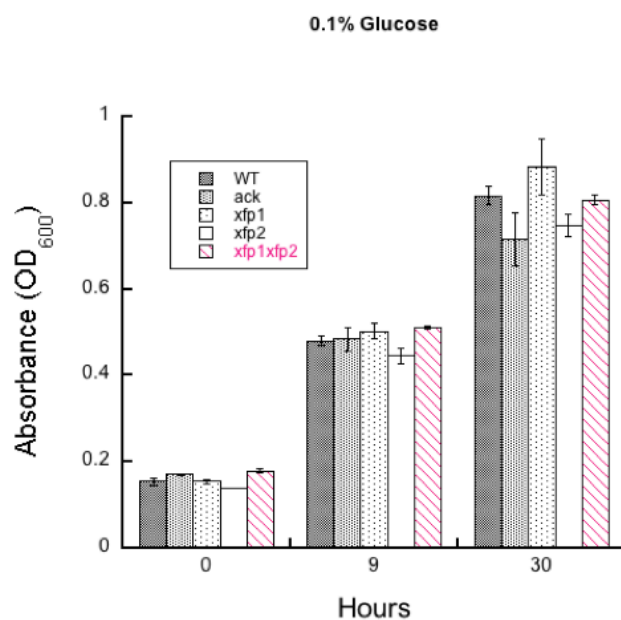


Figure 6. Growth differences observed with the Xfp-Ack knockouts when grown in low glucose. Growth in YNB + Glucose (0.001%, 0.01% and 0.1%) at 30°C. Growth was monitored at OD₆₀₀ from zero to thirty hours. Data shown are three different independent assays per strain and error bars represent standard deviations.

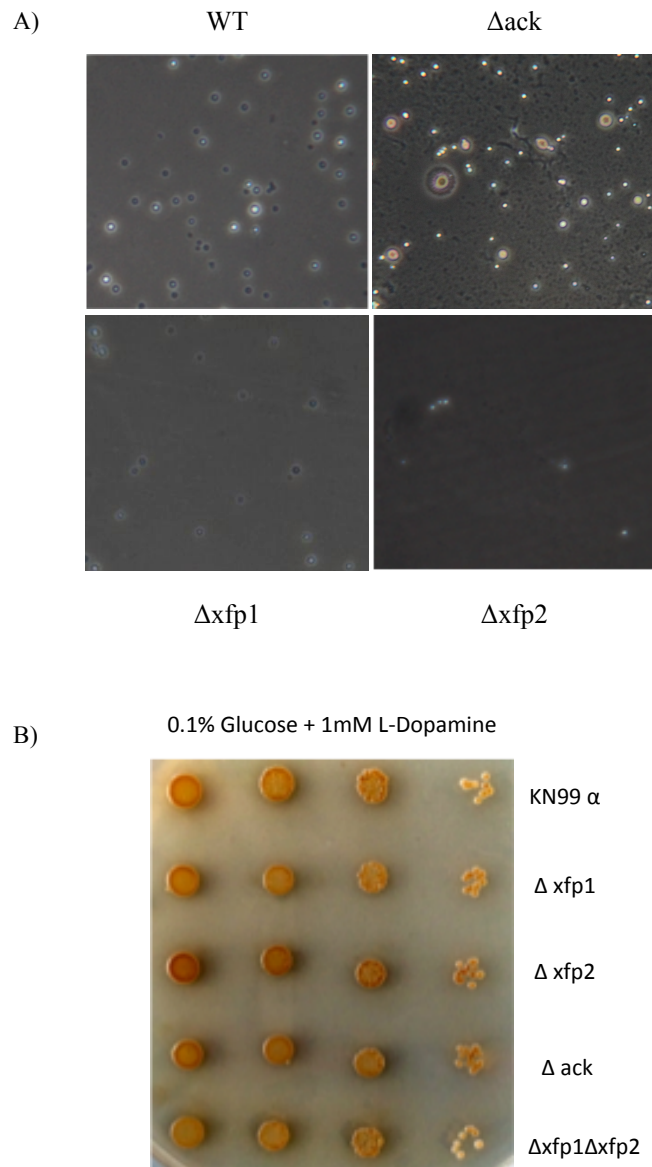


Figure 7. The effect of the *ACK* and *XFP* mutants on virulence factors. (a) Cells were grown in low iron conditions at 30°C and visualized microscopically using India Ink at 40x magnification. (b) Cells were resuspended in water to 1×10^4 cells and diluted serially 10-fold. Five microliters of each dilution was spotted onto 0.1% Glucose + 1mM L-Dopamine plates to test melanin production.

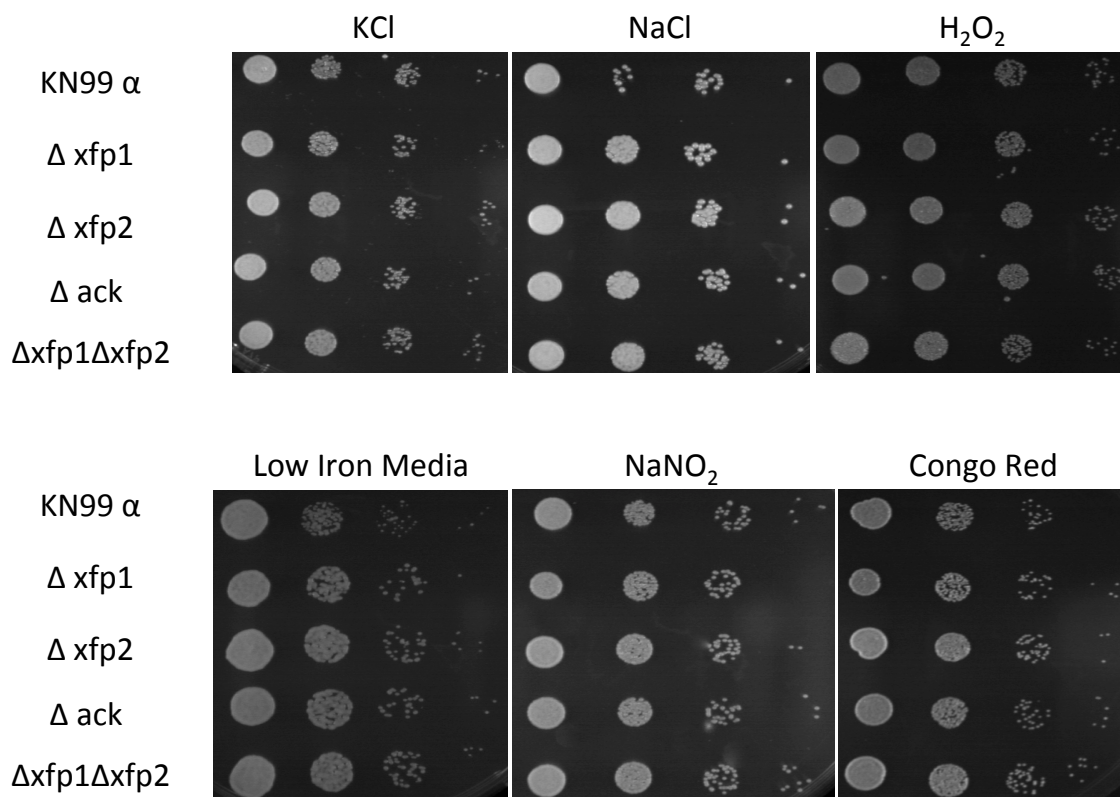


Figure 8. Knockouts lack a stress response phenotype on all compounds tested. Cells were resuspended in water to 1×10^4 cells, and then diluted serially 10-fold. Five microliters of each dilution was spotted onto YPD plates.

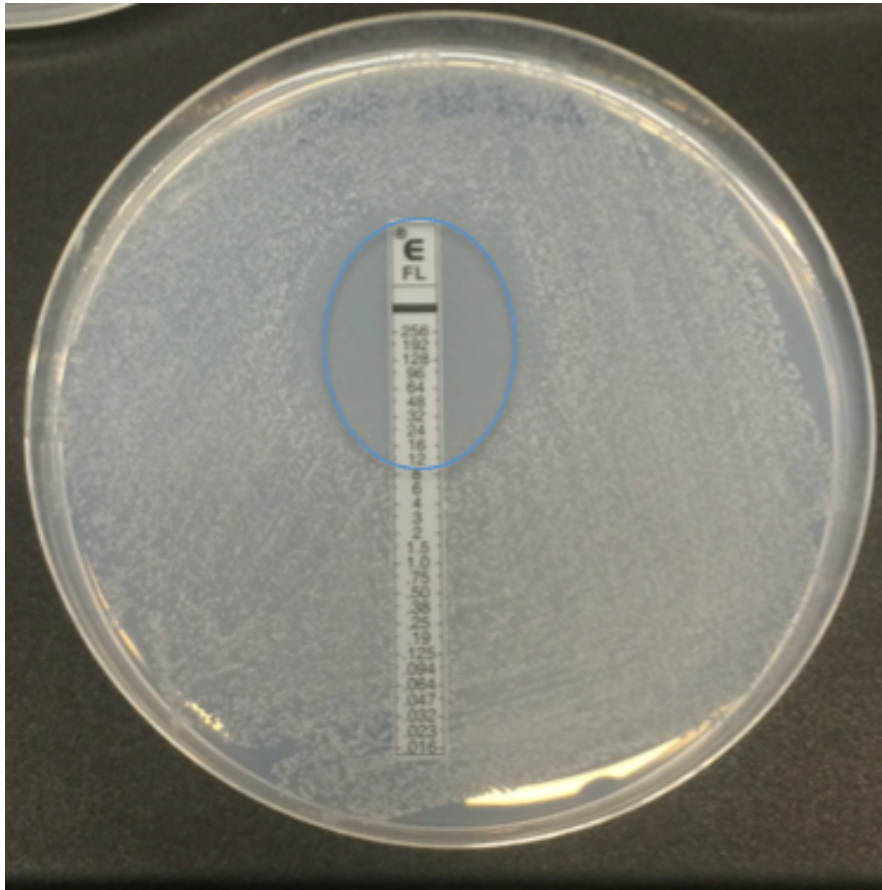


Figure 9. A representation of the fluconazole Etest. WT and mutant cells were diluted to 0.07 OD in 0.9% NaCl and plated onto a YPD or YNB + 0.2% glucose plate. One fluconazole Etest Strip (BioMérieux, Inc., Durham, NC) was gently placed at the center of each plate and the plate was incubated at 30°C 2-3 days. The MIC₅₀ for each strain was determined by the zone of killing.

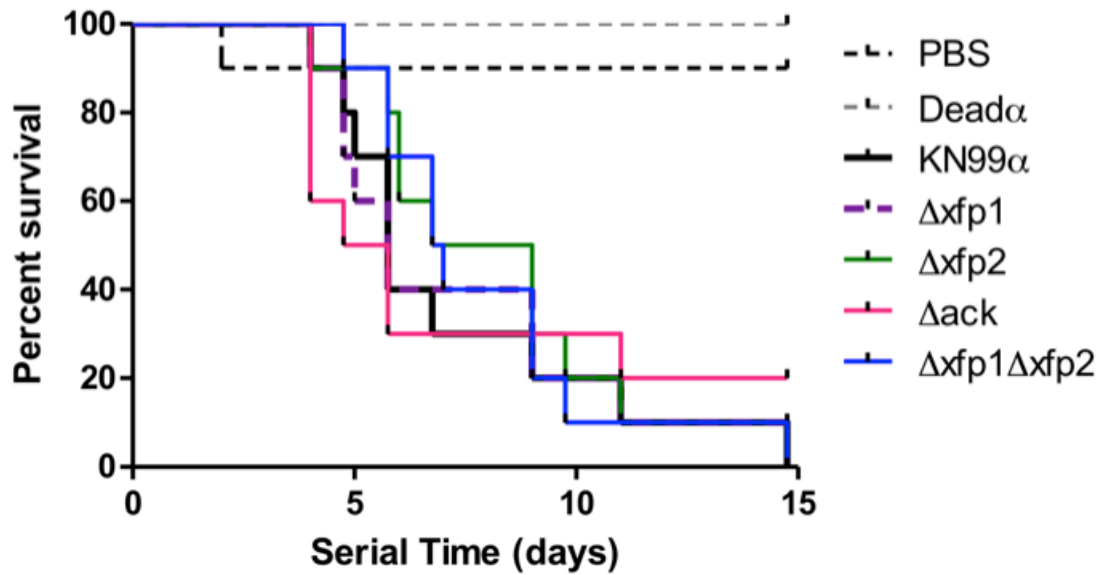


Figure 10. The *ACK* and *XFP* mutants are as virulent as WT *C. neoformans* in *Galleria mellonella* model. Kaplan-Meier plots of WT and mutant strains injected into *G. mellonella* larvae. The larvae were incubated at both 25°C and 37°C. PBS and heat-killed WT cells were used as controls.

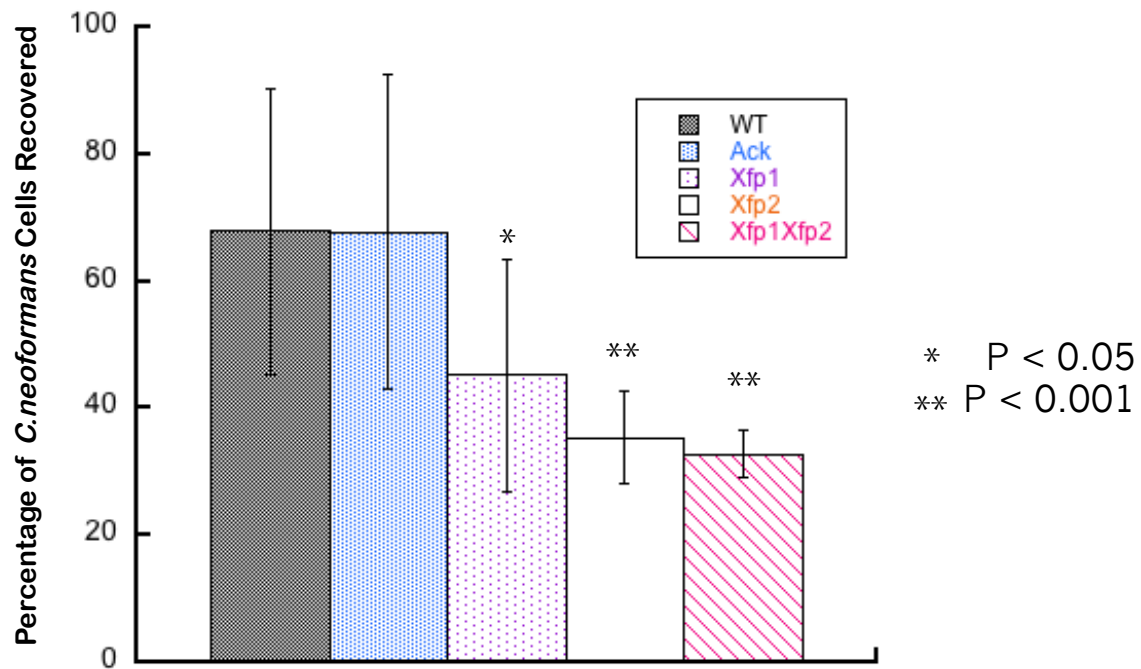


Figure 11. Xfp1 and Xfp2 play a role in the survival of *C. neoformans* in macrophages. WT and mutant strains were co-incubated in a 1:1 ratio with J774A macrophages, and incubated at 37°C, 5% CO₂. The mean numbers of cells recovered (%) ± SD are reported. Three biological replicates and three assay replicates were conducted for each strain.

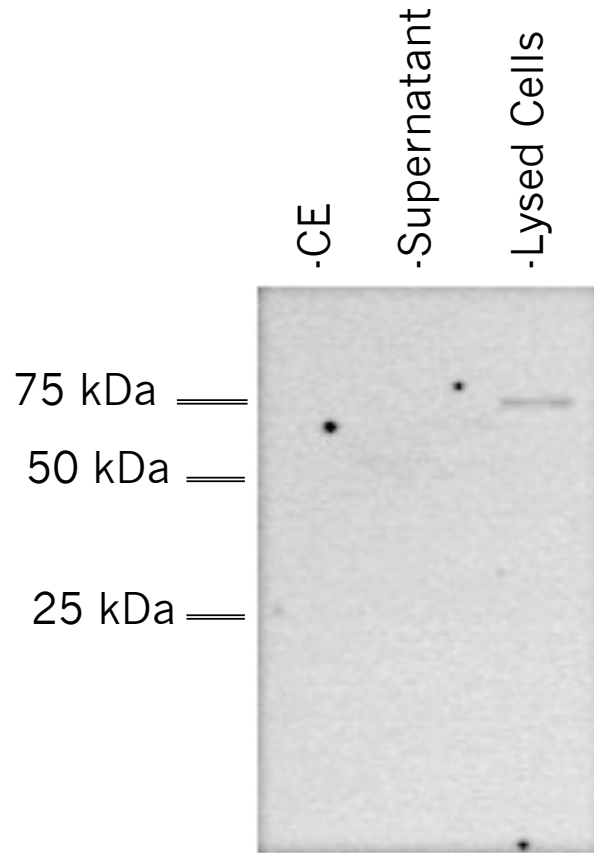


Figure 12. Only full length AckmCherry detected in cell lysate. An anti-mCherry monoclonal antibody was used to detect the full-length ACK:Neo:mCherry in cell extract, supernatant and the cell lysate of *C. neoformans* cells grown on YPD.

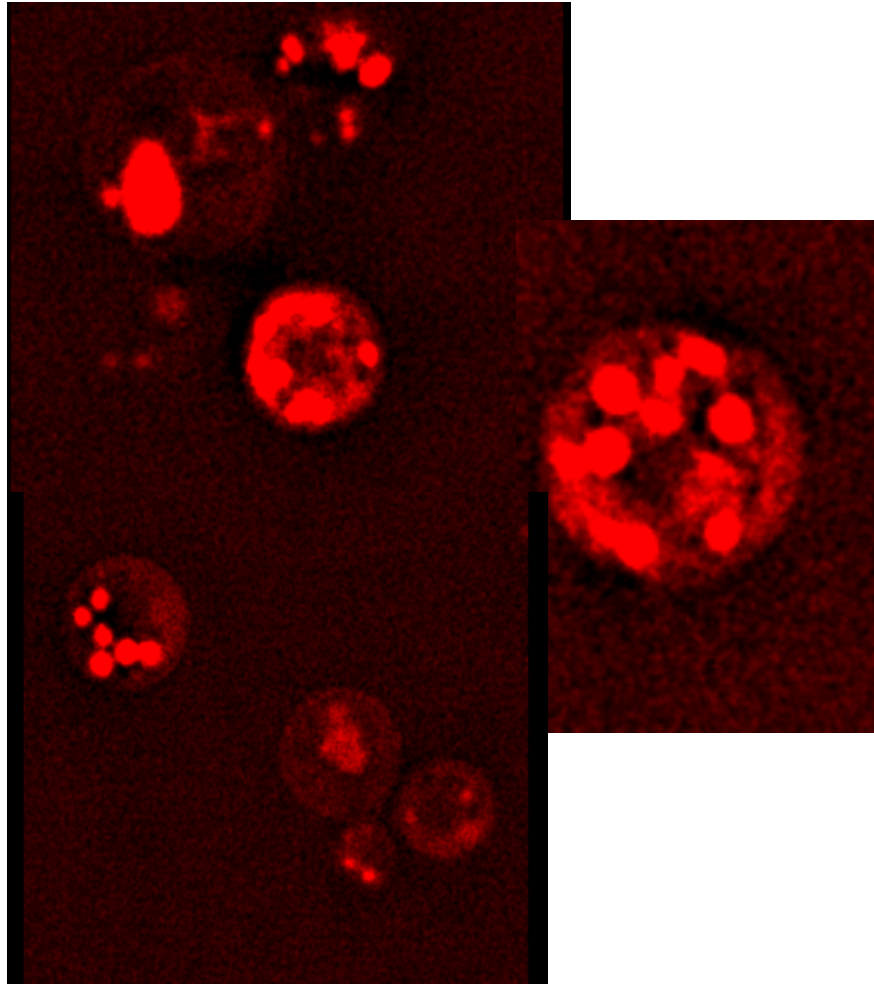


Figure 13. AckmCherry confocal microscopy localizes to punctate structures within the cell.

A strain expressing AckmCherry under its native promoter was grown at 30°C in synthetic complete medium. Z-stack images were collected using a 100x oil immersion objective with the mCherry/AF594 575/25 filter.

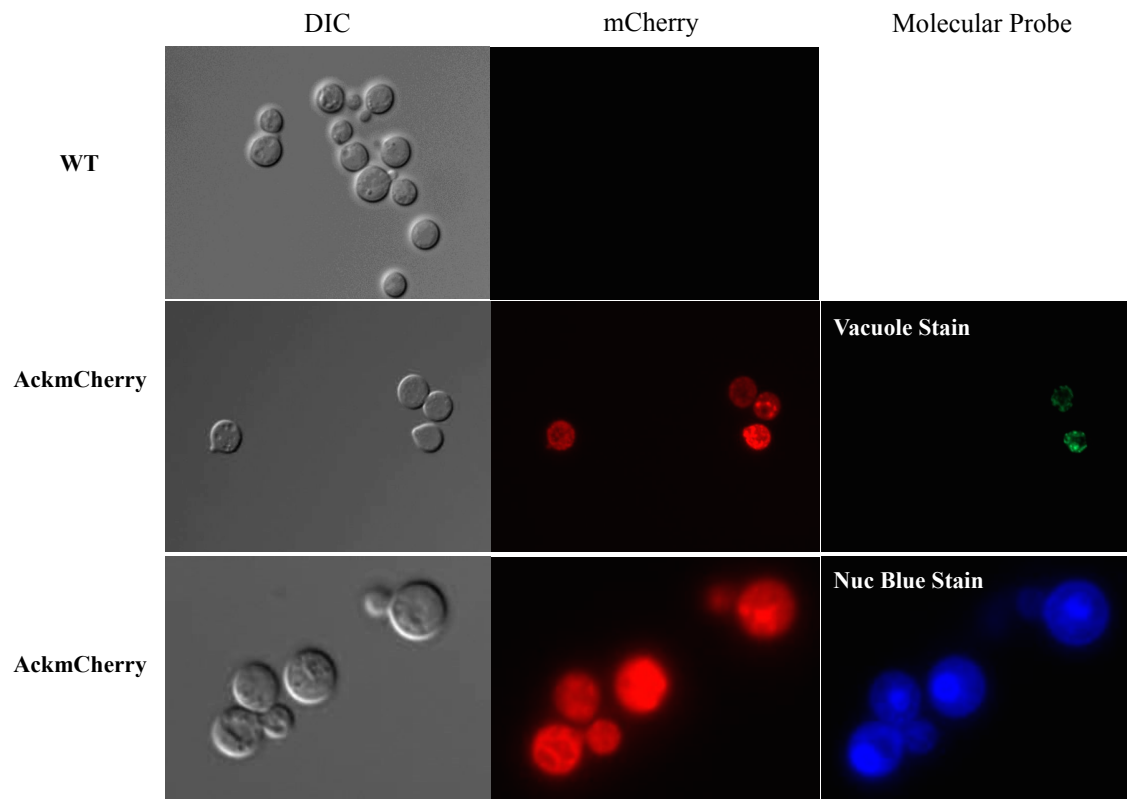


Figure 14. AckmCherry does not localize to the vacuolar membrane or the nucleus. Images were taken using a fluorescent microscope at a magnification of 100x. AckmCherry cells were stained with the vacuole organelle dye and the nuc blue stain.

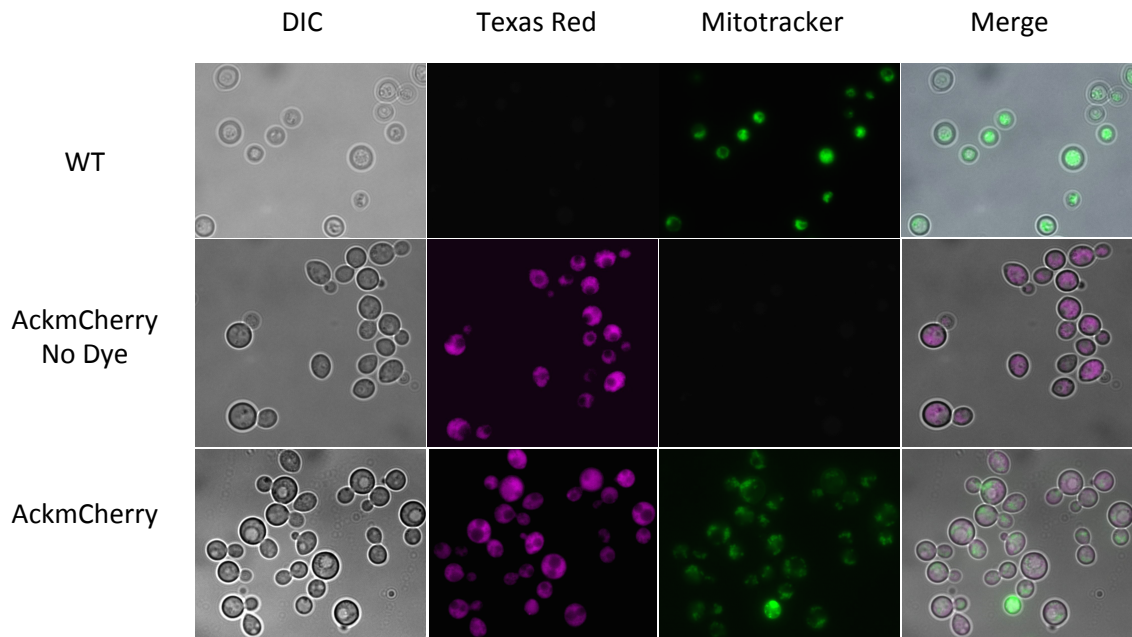


Figure 15. AckmCherry does not localize to the mitochondria. Images were taken using a fluorescent microscope at a magnification of 100x. AckmCherry cells were stained with the mitotracker organelle dye, while another population of AckmCherry cells that lacked stain was used as a control for interference due to the dyes.

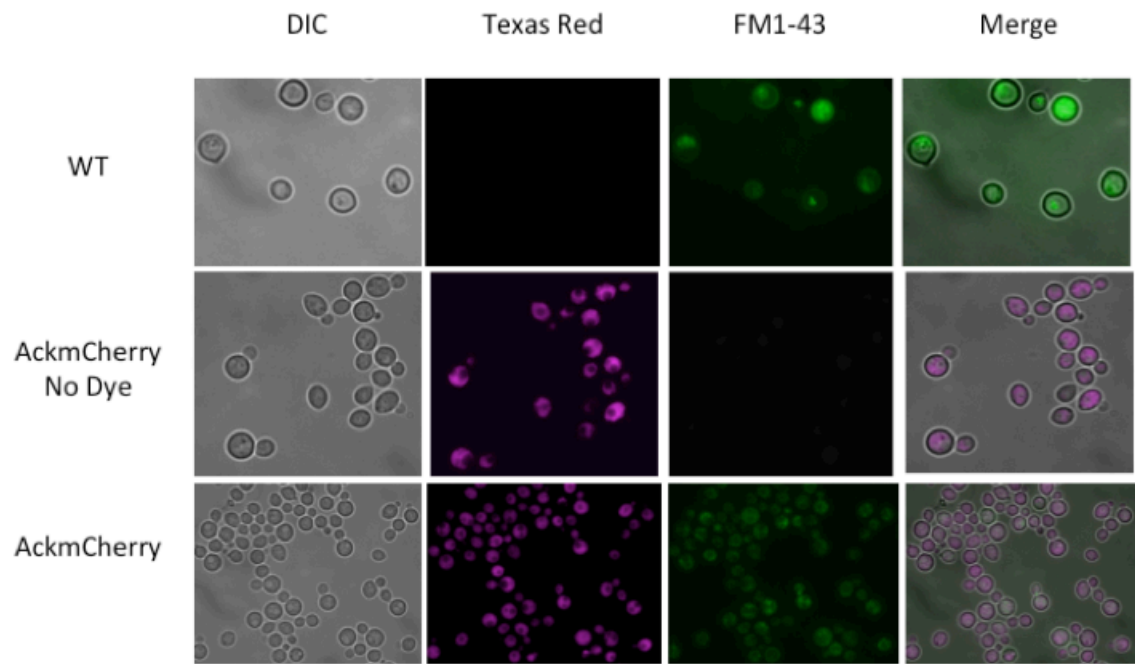


Figure 16. AckmCherry does not localize to endosomes. Images were taken using a fluorescent microscope at a magnification of 100x. AckmCherry cells were stained with the FM1-43 organelle dye, while another population of AckmCherry cells that lacked stain was used as a control for interference due to the dyes.

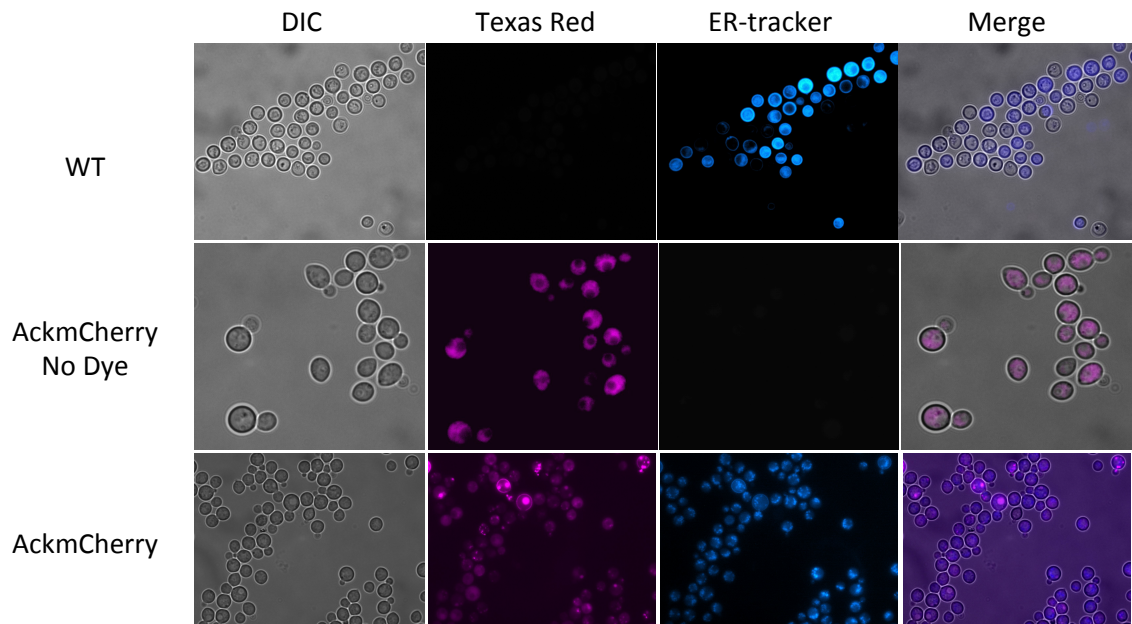


Figure 17. AckmCherry does not appear to co-localize with the ER-tracker. Images were taken using a fluorescent microscope at a magnification of 100x. AckmCherry cells were stained with the ER-tracker organelle dye, while another population of AckmCherry cells that lacked stain was used as a control for interference due to the dyes.

CHAPTER FIVE

Conclusions and Future Works

Acetate assimilation and dissimilation pathways and the regulation of the enzymes in these pathways have received far less attention in eukaryotic microbes than in bacteria. This dissertation is comprised of two studies that provide details on the partner enzymes of acetate kinase (Ack) in eukaryotic pathogens and the roles that the two different pathways may play in metabolism.

The first major study is the biochemical and kinetic characterization of the *Phytophthora ramorum* Pta^{II} enzyme, which functions primarily to convert acetyl phosphate and CoA to acetyl-CoA and P_i. This work highlights significant differences and similarities between bacterial and eukaryotic Pta enzymes, including the two previously characterized bacterial Pta^{II} enzymes from *Escherichia coli* and *Salmonella enterica*. A comparison of the bacterial and eukaryotic enzymes and the phylogenetic diversity across the domains suggests that the N-terminal domain and its regulatory role have evolved throughout the Bacteria and the Eukarya. We discovered that the Pta^{II} enzyme family is more complex than previously thought. Four subtypes of Pta^{II} are found based on the presence and absence of the P-loop and DRTGG subdomains within the N-terminus regulatory domain. We also demonstrate that a conserved Gly residue (Gly-300 in *P. ramorum* Pta1^{II}) in the N-terminal regulatory domain of both the bacterial and eukaryotic Pta enzymes influences the regulation of the Pta enzyme in how it responds to pyruvate as an allosteric effector.

Future studies for the *P. ramorum* Pta project should include the biochemical and kinetic characterization of the PrPta2^{II} from *P. ramorum*. This would provide information on whether PrPta1^{II} and PrPta2^{II} are redundant enzymes within the organism, such as both enzymes only

working in the acetyl-CoA-forming direction, or if they play two separate roles, such as PrPta2^{II} working in either direction or only the acetyl phosphate-forming direction. In addition, it would be interesting to know whether PrPta2^{II} is allosterically regulated in a similar manner to PrPta1^{II} or through a different type of regulation.

Within *C. reinhardtii*, the Pat1-Ack2 pathway is found in the mitochondria, whereas the Pat2-Ack1 pathway is found within the chloroplast (1). Utilizing predicted subcellular localization software, PrPta1^{II} is predicted to localize to the cytoplasm but also has a chloroplast targeting sequence, whereas PrPta2^{II} is only predicted to localize to the cytoplasm. Would the *P. ramorum* and *C. reinhardtii* enzymes be similar in their localization and biochemical role? Are the differences seen between the bacterial and eukaryotic enzymes restricted between the two domains or would we see differences among the eukaryotes as well? Due to the presence and absence of the two subdomains, differences in allosteric regulation would be expected among all of the Type II subtypes. The characterization of the other Pta subtypes would allow us to establish the role of the P-loop and DRTGG subdomains.

We have provided purified PrPta1^{II} protein to a crystallographer collaborator; however, crystal growth has been problematic. If a structure were solved in the presence of an effector molecule, the molecular basis for allostery could be directly investigated. A structure in the absence of effectors would allow us to utilize molecular modeling to assist in the identification of allosteric effector binding pockets. Pta^{II} structures would provide information on other residues within both the N-terminus and C-terminus that would answer more questions about the differences between the Pta^I and Pta^{II} enzymes, along with the differences among Bacteria, Eukarya and Archaea Pta enzymes.

The second focus of my dissertation is the characterization of the Ack-Xfp1/Xfp2 pathway in the opportunistic fungal pathogen *Cryptococcus neoformans*. We generated single

ACK, *XFPI* and *XFP2* knockouts, as well as the double *XFPI/XFP2* knockout to investigate the metabolic and physiological role of this pathway in *C. neoformans*. When acetate production was assayed for both the WT and mutants, no significant defect was observed, which led us to hypothesize that this, at least *in vitro*, may not be the main acetate fermentation pathway in *C. neoformans*. Our results suggest that Ack and Xfp2 most likely partner together under low glucose and possibly low iron environments, and that Xfp1 and Xfp2 play a role in the survival of *C. neoformans* within macrophages. Although these two enzymes partner together in lactic acid bacteria, they may serve separate functions in eukaryotic fungi, especially in the role of survival of *C. neoformans* within macrophages.

Future work should be focused on trying to further elucidate the partnership of Ack and Xfp1 or Xfp2 and the roles each enzyme or pathway plays. Attempts to generate an *ACK/XFPI* double mutant by both biolistic transformation and preliminary mating experiments have been unsuccessful. A more rigorous mating experiment with the Δ ack:Neo KN99a and Δ xfp1:Hyg KN99a cells needs to be conducted. The inability to create a double mutant would clarify that this pathway is indeed essential and indicate that the functioning of both enzymes is necessary. The creation of a Δ xfp2:Hyg construct would allow generation of a *ACK/XFP2* double mutant through biolistic transformation or mating.

Since the *XFPI*, *XFP2* and *XFPI/XFP2* mutants have an *in vivo* phenotype within mouse macrophages, inhalation and/or tail-vein injection experiments need to be conducted in the murine model. These experiments would be expected to provide more information about the mammalian specific role these enzymes are playing within *C. neoformans*. Ma et al. have previously demonstrated that experimental results generated with macrophage studies are strong predictors to the results using mice as an *in vivo* model (2).

Lastly, localization studies of Ack, Xfp1 and Xfp2 will continue to answer questions about the physiological role of these enzymes. The Xfp1 and Xfp2 fluorescent-tagged constructs should be created with the coding regions fused with GFP; this will allow for co-localization studies with the AckmCherry construct. Once all of the constructs are generated and transformed into *C. neoformans*, studies can be conducted to look at the localization of these enzymes when the cells are grown under different growth conditions. If co-localization occurs, this may further address when Ack may partner with Xfp1 and/or Xfp2. Co-localization under only certain growth conditions could uncover the role of the Ack-Xfp1/Xfp2 pathway. This could lead to protein-protein interaction studies, such as pull down assays with cell extract to further characterize these interactions.

This is the first substantial study into the two major partner enzymes of Ack in eukaryotic pathogenic microbes. The phylogenetic analysis of the Pta enzymes from both bacterial and eukaryotic organisms has filled a major gap in this field by identifying four different subtypes of the regulated Pta enzyme by the absence and presence of the DRTGG and P-loop subdomains within the N-terminal regulatory domain. This work indicates there is a complexity in the regulation of the Pta enzyme across the Bacteria and Eukarya, and although we have biochemically characterized only one of the two Pta^{Ia} enzymes from *P. ramorum*, this information along with further characterization of other enzymes of different subtypes, such as the bacterial pathogen *Mycobacterium*, will provide further advancement in the field where testable hypotheses can be proposed about the metabolic and physiological role of these enzymes and their regulation.

In addition, the investigation into the metabolic and physiological role of the Xfp-Ack pathway in *C. neoformans*, has led us to conclude that environmental conditions play a role in the localization and partnering of these enzymes. It also indicates that the Xfp-Ack pathway in fungi

is more complex than it is in heterofermentative bacteria. In this work, we indicate a role for Xfp in the survival of *C. neoformans* within the macrophage, which may open up a new, unappreciated target that could be exploited in drug development.

References

1. Yang W, Catalanotti C, D'Adamo S, Wittkopp TM, Ingram-Smith CJ, Mackinder L, Miller TE, Heuberger AL, Peers G, Smith KS, Jonikas MC, Grossman AR, Posewitz MC. 2014. Alternative Acetate Production Pathways in *Chlamydomonas reinhardtii* during Dark Anoxia and the Dominant Role of Chloroplasts in Fermentative Acetate Production. *Plant Cell* **26**:4499-4518.
2. Ma H, Hagen F, Stekel DJ, Johnston SA, Sionov E, Falk R, Polacheck I, Boekhout T, May RC. 2009. The fatal fungal outbreak on Vancouver Island is characterized by enhanced intracellular parasitism driven by mitochondrial regulation. *Proc Natl Acad Sci U S A* **106**:12980-12985.

Appendix A

Fungal Ack Structures Possess a Loop that is Non-Existent in Other Ack Enzymes

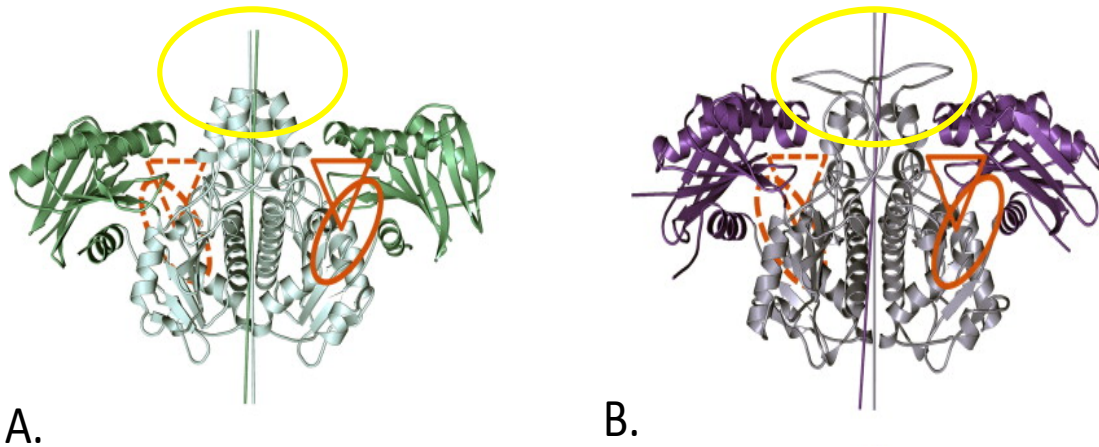


Figure A-1. The *E. histolytica* Ack (A) and *C. neoformans* Ack (B) Crystal Structures. The loop structure highlighted in yellow is present in fungal sequences only, and could possibly be a binding domain for another partner enzyme. Image is adapted from (Ch. 4, Ref 13) and permission was granted for the reuse of this figure.

	232	241	
Mtherm	CHLGNG-SSITAVEGGKSVETSMGFTPLEGLAMGTRCGSIDPAIVPFLMEKEGL-----		259
Bsubtilis	CHLGNG-ASIAAVEGGKSIDTSMGFTPLAGVAMGTRSGNIDPALIPYIMEKTGQ-----		257
Creinhardtii2	CHLGNG-SSVAAVRGGQCVDTSMGMTPLEGLLMGTRCGDIDPAVLHIQNQLGL-----		285
Creinhardtii1	CHLGNG-SSVAAVRGGQCVDTSMGLTPLEGLLMGTRCGDMDPAVLHIQNQCGL-----		267
Pramorum	CHLGNG-SSIAAISKGRCIDTSMGMTPLEGLVMGTRSGDIDPAIHAFCKELDM-----		287
Psojaj	CHLGNG-SSIAAIHKGRCIDTSMGMTPLEGLVMGTRCGDVDPALHAFCKELDM-----		332
EcoliK12	CHLGNG-GSVSAIGNGKCVDTSMGLTPLEGLVIGTRSGDIDPAIIFHLHDTLGM-----		261
Ehistolytica	CHLGTGGSSCCGIVNGKSFDTSMGNSTLAGLVMSTRCGDIDPTIPIDMIQQVG-----		249
Edispar	CHLGTGGSSCCGIVNGKSFDTSMGNSTLAGLVMSTRCGDIDPTIPIDMIQQVG-----		249
Einvadens	CHLGTGGSSCCAILNGKSYDTSMGNSTLAGLVMSTRCGDIDPSIPINIVEQIG-----		249
Anidulans	LHIGSG-ASVCAIKDGKSIDTSMGLTPLAGLPGATRSGDIDPSLVFHYTNEAGKLS ^{PAST}		270
Ncrassa	LHLGSG-ASACAIKGGKSLDNSMGLTPLAGLPGATRSGSVDPSSLVFHYASDVGKLS ^{PAST}		296
Pnodorum	LHLGSG-ASACVMNGKSHDTSMGLTPLAGLPGATRSGSIDPSLMFHFTHKAGKPS ^{RSSS}		273
Cneoformans	AHLGSG-SSSCKKNGKSVDTSMGLTPLEGLLGGTRSGTIDPTAIFHHTKDA--SDANV		275
Umaydis	LHLGSG-SSICSVVRGRSFDTSMGLTPLEGLPGGTRSGSVDPVLALHLSSATLPGGK ^{DGT}		304
	:.* .*	:*:. :.*.* :.* *:	.*.* :*
	283 285		
Mtherm	-----TTREIDTLMNKKSGVLGVSGLSNDFRDLDEAASKGN-----		R 296
Bsubtilis	-----TADEVLNLTNKKSGLLGISGFSSDLRDIVEATKEGN-----		E 294
Creinhardtii2	-----SASETDTLLNKKSGLLGLTG-SNDLR ^{AVIEGAGKGE} -----		P 321
Creinhardtii1	-----NVKETDTLLNKKSGLLGLTG-SNDLR ^{AVIEGAGKGE} -----		P 303
Pramorum	-----SIQEVDTMLNKKSGLLGICD-ESDIR ^{VIQDRVRAGDD} -----		P 324
Psojaj	-----TIQVDKMLNKQSGLLGICD-ESDIR ^{VIQDRVRAGND} -----		P 369
EcoliK12	-----SVDAINKLLTKESGLLGLTEVTSDCRYVEDNYATKE-----		297
Ehistolytica	-----IEKVDILNKKSGLLGVSELSSDMRDILHEIETRGPK-----		AK 288
Edispar	-----VERVVDILNKRSGLLGVSELSSDMRDILHEIETRGPK-----		AK 288
Einvadens	-----IQKTVDLLNKRSGLFGVSETSCDIR ^{DLLKEIKENGQK} -----		AE 288
Anidulans	^{KEMH} ----ISTAEIILNKKSGWKVLTG-TTDF ^{SQIAVEDPPS} -----		E 308
Ncrassa	^{KDLH} ----ISRAEEIILNKQSGWKALTG-TTNF ^{GTITAALDPSSDTTS} ----		HLSPEEVA 347
Pnodorum	^{EKLH} ----ITQAEIILNKNSGWSLTLG-TTDF ^{GKISSDRRE} -----		310
Cneoformans	^{GDFT} ----VSKAEIILNKNSGLKALAG-TTNF ^{GHI IQNLDPS} -----		KCSKEDHE 320
Umaydis	^{VEIADGIR} VSRAEVVLNKHSGFKAVAG-SSDF ^{AEIVQRNEFLQGR} TMGKHKEEERSKDR		363
	::*.* :	:	:

Figure A-2. Sequence Alignment of Ack Sequences. The residues found in the loop structure in Figure A-1, are highlighted in yellow and found only in fungal Ack sequences.